UNIVERSITY OF CALIFORNIA SAN DIEGO

Molecular Mechanisms of Meiotic Chromosome Assembly, Architecture, and Interhomolog Recombination

A dissertation submitted in partial satisfaction of the
requirements for the degree
Doctor of Philosophy

in

Biomedical Sciences

by

Sarah Nicole Ur

Committee in charge:

Professor Kevin Corbett, Chair
Professor Richard Kolodner
Professor Lorraine Pillus
Professor Elizabeth Villa Rodriguez
Professor Huilin Zhou

2021

The dissertation of Sarah Nicole Ur is approved, and it is acceptable in quality and form for publication on microfilm and electronically.

University of California San Diego

2021

DEDICATION

To:

To my family and friends. My success would not have been possible without your encouragement, support, and love. Thank you for all you've done and continue to do for me.

TABLE OF CONTENTS

LIST OF FIGURES

LIST OF TABLES

ACKNOWLEDGEMENTS

This thesis is the culmination of my graduate school career and represents my efforts to become and biochemist with an emphasis on structural biology. None of this work would have been possible without the support of my thesis advisor, Kevin Corbett. Kevin allowed me the freedom to explore the experimental methods and questions I wanted, while also creating an environment where I felt supported. I am grateful that Kevin truly cares about the people in his lab as more than just cogs in an academic machine, and sees us as people who he wants the best for. My success has also been made possible by members of the Corbett lab, specifically I've had many scientific discussions with and been mentored by Qiaozhen Ye, Namit Singh, Kanika Arora, Yajie Gu, and Scott Rosenberg. I genuinely value the time spent and the frozen yogurt eaten with Lisa Liang, Madison Lehmer, Sara Richey, Mark Jacob, Camilia Azimi and Scott Rosenberg. Outside of lab, I have been extremely lucky to have a community of wonderful friends to escape to the outdoors with. Particularly Athena Lau, Jessica Lawrence and the rest of the Women's Wednesday Climbing Crew, were always there to lend a helpful belay. However, most of all I'd like to thank my family for their unwavering support over the past 31 years. To my sister Becca, thank you for giving me a pristine example of someone to look up to, you have driven me to my proudest achievements. To Ian and Christine, thank you for reminding me how important family is, and showing me my capacity to love little humans. To all the fuzzy children, thank you for the snuggles and for always allowing me to pet you. Lastly to my parents Susan and Wilbur, thank you for making me who I am today, both from your genetic contributions and through how you raised me.

Chapter 2, in full, is a reprint of material as it appears in: **Ur, SN**, Corbett, KD. Ar-

chitecture and Dynamics of Meiotic Chromosomes. Annual Review of Genetics (2021). The dissertation author was first author of this paper.

Chapter 3, in part, is a reprint of material currently being prepared for submission for publication: **Ur, SU.***, Milano C*, Gu Y, Vale-Silva LA, Hochwagen A, Corbett K. A dual mechanism for meiotic chromosome axis assembly. *in preparation*. The dissertation author was the primary author.

VITA

2013	Bachelor of Science in Biomedical Engineering, California Polytechnic State University, San Luis Obispo
2013	Master of Science in Biomedical Engineering, California Polytechnic State University, San Luis Obispo
2021	Doctor of Philosophy in Biomedical Sciences, University of California San Diego

PUBLICATIONS

Ur, SN, Corbett, KD. Architechture and Dynamics of Meiotic Chromosomes. Annual Review of Genetics (2021).

West A.M.V., Rosenberg S.C., **Ur S.N.**, Lehmer M.K., Ye Q., Hagemann G., Caballero Munoz I., Uson I., Herzog F., Corbett K.D. (2019) The conserved molecular architecture and self-assembly mechanisms of the meiotic chromosome axis. Elife

Ye Q, **Ur SN**, Su TY, Corbett, KD. (2016) Structure of the Saccharomyces cerevisiae Hrr25:Mam1 monopolin subcomplex reveals a novel kinase regulator. EMBO J. 35(19):2139-51.

Rocca, CJ, Kreymerman A, **Ur SN**, Frizzi KE, Naphade S, Lau A, Tran T, Calcutt NA, Goldberg JL, Cherqui S. (2015) Treatment of Inherited Eye Defects by Systemic Hematopoietic Stem Cell Transplantation. Invest Opthalmol Vis Sci. 56(12):7214-23.

Hearon K, Wierzbicki MA, Nash LD, Landsman TL, Laramy C, Lonnecker AT, Gibbons MC, **Ur SN**, Cardinal KO, Wilson TS, Wooley KL, Maitland DJ. (2015) A Processable Shape Memory Polymer System for Biomedical Applications. Advanced Healthcare Materials. 4(9):1386-98.

Naphade S, Sharma J, Gaide Chevronnay HP, Shook MA, Yeagy BA, Rocca CJ, **Ur SN**, Lau AJ, Courtoy PJ, Cherqui S. (2015). Lysosomal cross-correction by hematopoietic stem cell-derived macrophages via tunneling nanotubes. Stem Cells. 33(1):301-9.

Rocca CJ, **Ur SN**, Harrison F, Cherqui S. (2014) rAAV9 combined with renal vein injection is optimal for kidney-targeted gene delivery: conclusion of a comparative study. Gene Therapy. 21(6):618-28.

ABSTRACT OF THE DISSERTATION

Molecular Mechanisms of Meiotic Chromosome Assembly, Architecture, and Interhomolog Recombination

by

Sarah Nicole Ur

Doctor of Philosophy in Biomedical Sciences

University of California San Diego, 2021

Professor Kevin Corbett, Chair

Meiosis, a hallmark of sexual reproduction, entails the division of one diploid parent cell into four haploid gamete daughter cells. To support proper chromosome segregation in two successive meiotic divisions, meiotic chromosomes must undergo dramatic structural changes in meiotic prophase to identify and pair with their corresponding homolog. This chromosomal structural rearrangement is accomplished through meiotic recombination, a process that inflicts double strand break damage on the chromosomes and necessitates their repair using their homologous sequence, in some cases forming an inter-homolog crossover. This work begins by

reviewing meiotic chromosome structure, and how it supports meiotic recombination. In order to understand the structural context of meiotic recombination I begin by reviewing higher-order data on how entire chromosomes are packaged and ordered during meiosis then zoom into well-known structures such as the chromosome axis, the synaptonemal complex, and their individual protein components. The chapters on my experimental work begin by examining a Chromatin Binding Region (CBR) in the yeast meiotic HORMAD Hop1, a component of the chromosome axis. I demonstrate how the CBR is responsible for a secondary mode of chromosome axis deposition through its capability to bind directly nucleosomes. This secondary mechanism functions alongside a previously defined cohesin dependent chromosome axis assembly mechanism, and I hypothesize that this second mode of axis assembly enables crossover formation in an as-yet unknown manner. I next examine the Msh4-Msh5 complex in an attempt to define its role in shuttling double strand DNA breaks towards a crossover fate. Through careful biochemistry, I demonstrate that the preferred DNA substrate of the *S. cerevisiae* Msh4-Msh5 is a Holliday junction, and I identify the critical regions in both Msh4 and Msh5 for this activity. My last study aims to examine meiotic recombination from a larger perspective. In order to determine how individual proteins interplay on the chromatin throughout the process of meiotic prophase I, I developed a mass spectroscopy protocol to assay a meiotic time-course of *S. cerevisiae* chromosomes. With this protocol I created a spatial and temporal atlas of chromatin associated proteins, which details how proteins assemble and disassemble throughout meiotic prophase I. As a whole this thesis provides an extensive review of the field of meiotic chromosome architecture, defines molecular mechanisms of individual protein assembly during meiosis, and demonstrates the proteomic context for interhomolog recombination.

Chapter 1

Introduction

1.1 Architecture and Dynamics of Meiotic Chromosomes

In sexually reproducing eukaryotes, two parents contribute equally to the genetic material of their offspring. To achieve this remarkable feat, parental cells must undergo a reduction in ploidy, or chromosome number, from two copies of each chromosome per cell (diploid) to one copy (haploid), generating specialized germ cells called gametes (in humans, sperm and egg cells). The fusion of haploid gametes from two parents reconstitutes the diploid state, completing sexual reproduction and creating offspring with an unique complement of genetic material. In order to create haploid gametes from a diploid cell, a parental cell first replicates its genome, then undergoes two consecutive cell divisions. In the first of these divisions, called meiosis I, each pair of homologous chromosomes must identify one another and physically associate via meiotic homologous recombination, enabling their segregation from one another in the meiosis I division to reduce ploidy. Errors in meiotic recombination can result in improper segregation of chromosomes and lead to aneuploidy, an incorrect number of chromosomes in the haploid

gamete and the resulting fertilized embryo (Hassold and Hunt, 2001)(Hassold et al., 2007). In humans, aneuploidy is a major cause of miscarriage and the source of developmental disorders like Turner Syndrome and Down Syndrome. To achieve accurate identification and recombination of homologous chromosomes, meiotic chromosomes must take on a specific architecture which is made possible by protein scaffolding. This scaffolding both organizes chromosomes as linear arrays of loops, and coordinates the recruitment of factors which eventually form a chiasmata between the two homologs, allowing them to be segregated. This scaffolding, or structure of meiotic chromosomes has been imaged in studies since the 1950's (Moses, 1956) and our understanding of how meiotic DNA is organized and what proteins are orchestrating meiotic recombination has grown exponentially in the last seven decades. We now know the key components of this scaffolding, which is divided into two major components termed the chromosome axis and the synaptonemal complex. Chapter 2 of this thesis is a review and compilation of the current knowledge in the field of meiotic chromosome structure.

1.2 A Dual Mechanism for Meiotic Chromosome Axis Assembly

During meiotic prophase, homologous chromosomes must physically associate through homologous recombination in order to be properly segregated into daughter cells. Among the proteins that facilitate the homolog pairing process, the meiotic HORMAD proteins are a highly conserved component of the chromosome axis. The *S. cerevisiae* meiotic HORMAD, Hop1 localizes to chromosomes in early meiosis and is one of the master regulators of meiotic recombination. Hop1 is a key part of the meiotic chromosome axis, which acts to organize chromosomes into linear loop arrays, recruit double strand break machinery, and promote use of the homolog as a repair template, as opposed to the sister chromosome. Pairing of homologs

requires the proper function of Hop1 to create double strand DNA breaks (DSBs) and inter-homolog crossovers. By investigating Hop1 from a structural and biochemical standpoint, we can advance our knowledge on how it acts as a master regulator of meiosis, and broaden our understanding of a process key to sexual reproduction, In Chapter 3, I report my work on a previously-unidentified chromatin binding region (CBR) in the central region of Hop1. I investigate the structure of this domain, how it mediates recognition of nucleosomal DNA, and its roles in chromosome architecture, DSB formation, and the formation of inter-homolog crossovers.

1.3 Biochemical Characterization of *S. cerevisiae* Msh4:Msh5

The highly-conserved Msh4-Msh5 complex plays a critical role in meiotic recombination and the segregation of homologous chromosomes during gamete/spore formation. Proper homolog segregation requires formation of inter-homolog crossovers, and the formation of crossovers is strongly reduced in mutants of Msh4 and Msh5 (Krishnaprasad et al., 2015). The current model for the Msh4-Msh5 complex's function is that it binds and stabilizes an early recombination intermediate, perhaps the D-loop product of initial strand invasion or alternatively a Holliday junction, and promotes the assembly of crossover-specific machinery. This machinery constitutes a "recombination nodule," a large assembly whose architecture is not known, but which is visible by low-resolution electron microscopy on meiotic chromosomes. From a biochemical standpoint, there remains much unknown in regards to the Msh4-Msh5 complex's binding mechanism to recombination intermediates and its roles in meiotic crossover formation. Chapter 4 features my work to reconstitute the *S. cerevisiae* Msh4-Msh5 complex, characterize its binding to artificial DNA structures mimicking recombination intermediates, and determine the structure of the complex bound to a favored intermediate. By researching the Msh4-Msh5

complex and its downstream partners, we will be able to make a leap in understanding the physical basis of crossover formation.

1.4 Creation of a Time Resolved Network of Meiotic Chromosome Associated Proteins

In order to accomplish the diploid-to-haploid transition, homologous chromosomes identify one another and physically associate through DNA recombination, before segregating from one another in the first meiotic division. Meiotic recombination initiates with programmed double strand DNA breaks (DSBs) on each chromosome, some of which are eventually resolved as inter-homolog crossovers. Many protein complexes are involved in meiotic chromosome organization and recombination, and their spatial and temporal interplay is critical to the proper segregation of chromosomes in Meiosis I. The proteinaceous chromosome axis and synaptonemal complex organize chromosomes and control their recombination, while other recombination complexes shepherd a subset of DSBs to the crossover fate. Previous studies have globally interrogated the timing of meiotic protein expression (Cheng et al., 2018) and indeed, many individual meiotic complexes have been studied in detail. However, a comprehensive view of meiotic proteins' chromosome localization and interactions has not been performed. In Chapter 5, I present a protocol to assess the localization of proteins to chromosomes throughout a synchronous *S. cerevisae* meiosis using a chromatin enriched purification process coupled with high-resolution tandem mass spectroscopy. I demonstrate the ability of this assay to identify proteins from critical meiotic complexes such as the chromosome axis, synaptonemal complex, ZMM family, recombination complexes, and proteins responsible for resolving key crossover in-

termediates. By disrupting individual proteins from these stratified groups, I elucidate how meiotic complexes work together to manipulate meiotic chromosomes and promote homolog pairing and segregation during Meiosis I. With this tool I have created a temporal atlas for meiotic proteins, and defined how protein complexes assemble and disassemble from chromosomes to coordinate meiotic recombination.

1.5 Outline of the dissertation

I will begin this thesis with a review of the state of the field in meiotic chromosome structure and dynamics (Chapter 2). This review sets the baseline for my other chapters, detailing the background of the structural components that organize chromosomes during meiosis. It details current knowledge of the dynamics of how those structural components assemble, interact with each other, and aid in the recruitment of various meiotic factors ultimately leading to the faithful segregation of homologous chromosomes in Meiosis I. Next, I will detail work that elucidated a novel mechanism for chromosome axis deposition on meiotic chromatin. Through careful structural studies I discovered how the chromatin binding region of the meiotic protein Hop1 orchestrates axis deposition by binding directly to nucleosomes (Chapter 3). Third, I elaborate on my attempts to examine the role of the signaling complex Msh4-Msh5 on the fate of chromosome crossovers (Chapter 4). Lastly, I describe a protocol I developed to create a spatial and temporal atlas of the protein present on meiotic chromatin (Chapter 5). This technology can be used to assay dependencies and the interconnectivity of all the key players in meiosis. Each section contains a structure within itself of an introduction, specific subject matter, and conclusion.

Chapter 2

Architecture and Dynamics of Meiotic Chromosomes

The specialized two-stage meiotic cell division program halves a cell's chromosome complement in preparation for sexual reproduction. This reduction in ploidy requires that in meiotic prophase, each pair of homologous chromosomes identify one another and form physical links through DNA recombination. Here, we review recent advances in understanding the complex morphological changes that chromosomes undergo during meiotic prophase, to promote homolog identification and crossing over. We focus on the SMC-family cohesin complexes and the meiotic chromosome axis, which together organize chromosomes and promote recombination. We then discuss the architecture and dynamics of the conserved synaptonemal complex, which assembles between homologous chromosomes and mediates local and global feedback to ensure high fidelity in meiotic recombination. Finally, we discuss exciting new advances including mechanisms for boosting recombination on particular chromosomes or chromosomal domains,

and the implications of a new “liquid crystal” model for synaptonemal complex assembly and structure.

2.1 Introduction

Sexual reproduction in eukaryotes depends on meiosis to divide a cell’s genome in half during production of germ cells or gametes, enabling the fusion of two gametes to reconstitute a full genome in the next generation. The reduction of chromosome number from diploid (two copies of each chromosome) to haploid (one copy) in meiosis is enabled by the identification, physical linkage, and separation of each pair of homologous chromosomes (homologs) through DNA recombination. In addition to physically linking homologs, meiotic recombination also shuffles gene combinations along each chromosome, driving genetic variation and evolution. Because meiotic recombination is critically important for accurate chromosome segregation in the meiotic divisions, errors in meiotic recombination can lead to aneuploidy, or an improper number of chromosomes in the resulting gamete (Hassold et al., 2007; Hassold and Hunt, 2001). In humans, aneuploidy is a major source of miscarriage and is the cause of developmental disorders like Down Syndrome and Turner Syndrome. To accommodate the specific identification and physical linkage of homologs through meiotic recombination, eukaryotes have evolved an extended meiotic prophase whose stages are named after the distinctive morphology of chromosomes at each stage (Figure 2.1a). Chromosomes are replicated prior to meiosis, resulting in a pair of sister chromosomes held together by ring-like cohesin complexes. In the first stage of meiotic prophase, termed leptotene (from the Greek for “thin threads”), chromosomes become organized as a linear array of DNA loops around a meiosis-specific structure called the chromosome axis (van Heemst and Heyting, 2000; Zickler and Kleckner, 1999). Next, the chromosome

axis recruits and controls proteins responsible for formation of programmed DNA double-strand breaks (DSBs) along each chromosome, and the repair of a subset of DSBs as inter-homolog crossovers (Carballo et al., 2008; Hollingsworth, 2010; Humphryes and Hochwagen, 2014; Kim et al., 2010; Lao et al., 2013; Lao and Hunter, 2010; Subramanian and Hochwagen, 2014; Zickler and Kleckner, 2015). In zygotene ("paired threads"), homologs physically associate at recombination sites and nucleate the synaptonemal complex, a proteinaceous assembly that juxtaposes homologs and promotes later steps of recombination. During leptotene and zygotene, many organisms' chromosomes undergo large-scale motions powered by the linkage of their telomeres through the nuclear envelope to molecular motors, which are thought to promote high-fidelity homolog recognition by disrupting weak or low-homology interactions (Chikashige et al., 2006; Ding et al., 2007; Horn et al., 2013; Morimoto et al., 2012; Sato et al., 2009). In pachytene ("thick threads"), the synaptonemal complex has fully assembled along paired homologs, and chromosomes have become thicker and shorter due to compaction of the chromosome axes coupled with extension of the associated chromatin loops (Page and Hawley, 2004; Rockmill et al., 1995; Sym et al., 1993). Finally, in diplotene ("two threads"), the synaptonemal complex disassembles after inter-homolog recombination has completed. Cells then enter diakinesis ("movement apart"), a stage roughly equivalent to mitotic prometaphase in which the chromosomes become individualized and compacted in preparation for chromosome segregation. After meiotic prophase, cells undergo two successive rounds of chromosome segregation, termed meiosis I and II (Figure 2.1 b-c). In metaphase of meiosis I, the kinetochores of each pair of linked homologs become attached to spindle microtubules in a bipolar manner, enabled by their physical linkage through crossovers and by the co-orientation or physical fusion of sister chromosomes' kinetochores (Nasmyth, 2015; Sarangapani et al., 2014). Once homologs are

properly aligned and attached to microtubules, chromosome segregation is initiated by cleavage of cohesin complexes along chromosome arms, releasing the physical links between homologs (Nasmyth, 2001). Critically, cohesin complexes are retained near each chromosome's centromere to maintain the physical association of sister chromosomes, which then align and segregate in the meiosis II division (Clift and Marston, 2011; Marston and Amon, 2004). The tightly-controlled series of chromosome morphological changes through meiotic prophase is absolutely crucial for the success of meiotic recombination and chromosome segregation. In this review, we focus on the molecular basis for meiotic chromosome architecture and dynamics, and on how the chromosome axis and synaptonemal complex serve as signaling hubs to control recombination and meiotic progression. Recent work has highlighted surprising conservation in the molecular underpinning of meiotic chromosome architecture and recombination control across diverse organisms, and we focus primarily on these broadly conserved principles. Where appropriate, we discuss unique features of meiotic chromosome architecture in specific model organisms, especially when these features reveal distinct and informative solutions to the problems of homolog pairing, recombination, and segregation in meiosis.

2.2 Meiotic Chromatin

Throughout the cell cycle, the genome is spatially organized to support important biological functions, including gene expression in interphase, chromosome segregation in the mitotic and meiotic divisions, and interhomolog recombination in meiotic prophase. At the lowest level, chromosomal DNA is packaged into nucleosomes comprising about 150 base pairs of DNA wrapped around an octamer of histone proteins (two copies each of histones H2A, H2B, H3, and H4) (Luger et al., 1997). Histones' N-terminal tails are substrates for extensive

post-translational modifications that serve as signals for chromatin remodelers, transcription machinery, and other regulatory apparatus (Rando, 2012; Strahl and Allis, 2000). Distinct patterns of these epigenetic marks divide the genome into two major chromatin types, euchromatin and heterochromatin. Euchromatin is gene-rich, transcriptionally active, and early-replicating, while heterochromatin is relatively gene-poor, transcriptionally inactive, and late-replicating. Historically, euchromatin and heterochromatin have been distinguished as so-called R bands and G-bands in stained mitotic metaphase chromosomes (Craig and Bickmore, 1993; Furey and Haussler, 2003; Lander et al., 2001). In more recent chromosome conformation capture (Hi-C) experiments, which use high-throughput sequencing to capture the spatial organization of chromosomes, euchromatin and heterochromatin are observed to self-associate into spatially distinct "compartments" (Falk et al., 2019; Lieberman-Aiden et al., 2009; Simonis et al., 2006). In meiotic prophase, cells must balance continuing transcriptional activity with the need to linearly organize and compact the genome to support the recombination-mediated homology search and inter-homolog crossover formation. Meiotic chromosomes retain most properties of interphase chromatin, including epigenetic marks on histone tails and the physical segregation of euchromatin and heterochromatin, even as the genome becomes organized as a linear array of loops around the chromosome axis (see Section 2.4) (Patel et al., 2019). Within this loop array, a hierarchical set of chromosome structural features determine the locations of DSBs. DSBs typically occur at so-called "hot spots along each chromosome, whose locations are determined by euchromatin/heterochromatin state, nucleosome occupancy, and a specific histone modification, trimethylation of histone H3 lysine 4 (H3K4me3) (Borde et al., 2009; Jin, 2021; Lichten and de Massy, 2011; Pan and Keeney, 2007). In budding yeast, H3K4me3 marks are enriched in promoter regions, which also tend to be nucleosome-free and hence accessible to

the Spo11 DNA break machinery (Lange et al., 2016; Pan et al., 2011). In most mammals, DSB hotspot locations are determined by H3K4me3 modifications introduced by PRDM9 (PR domain zinc finger protein 9), a DNA-binding histone methyltransferase (Baudat et al., 2010; Myers et al., 2010; Parvanov et al., 2010). In both cases, these H3K4me3 marks are recognized by chromatin reader proteins (Spp1 in S. cerevisiae, ZCWPW1 (Zinc finger CW-type and PWWP domain containing 1) in mammals) that promote DSB formation and control recruitment of DNA repair machinery to broken DNA ends (see Section 2.4) (Acquaviva et al., 2013; Huang et al., 2020; Mahgoub et al., 2020; Sommermeyer et al., 2013; Wells et al., 2020).

2.3 SMC complexes: The engines of chromosome organization

Beyond the nucleosome level, chromosomes are actively organized throughout the cell cycle by multi-protein complexes of the Structural Maintenance of Chromosomes (SMC) family (reviewed in (Yatskevich et al., 2019)). Eukaryotes possess three such complexes, termed cohesin, condensin, and the Smc5/6 complex. While Smc5/6 plays specialized and still poorly-understood roles in DNA repair (Aragon, 2018; Yu, 2021), the biological roles and molecular mechanisms of cohesin and condensin have become increasingly well understood in recent years. In interphase cells, cohesin complexes act as dynamic loop extruders, binding DNA and using the energy of ATP hydrolysis to create and processively expand a chromatin loop (Figure 2-6a) (Davidson et al., 2019; Kim et al., 2019; Yatskevich et al., 2019). The collective action of many such complexes gives rise to topologically associating domains (TADs), megabase-sized regions of each chromosome that tend to interact with themselves more than with surrounding sequences (Dixon et al., 2012; Rao et al., 2014). TAD boundaries are often marked by binding sites for the insulator protein CTCF, which captures cohesin through a direct protein-protein in-

teraction to halt loop extrusion and stabilize the loop/TAD boundary (Li et al., 2020). The role of TADs in regulating gene expression remains controversial: while TAD boundaries generally insulate genes from enhancers located across TAD boundaries, elimination of TADs by disrupting cohesin or CTCF function does not have a strong effect on overall gene expression patterns, at least in cultured cells (Nora et al., 2017; Rao et al., 2017b). Cohesin and condensin complexes play important and complementary roles in cell division. As cellular DNA is replicated prior to mitosis, a sub-population of cohesin complexes encircles both sister chromosomes to hold them together; this cohesin population is termed “cohesive” and is marked by acetylation of the Smc3 subunit, stabilizing its DNA binding (Beckouet et al., 2010; Borges et al., 2010; Ivanov et al., 2002; Skibbens et al., 1999; Toth et al., 1999). As cells approach mitosis, most cohesin is lost from chromosomes, and is replaced by condensin complexes. Similar to cohesin, condensin complexes possess processive loop-extrusion activity (Ganji et al., 2018; Terakawa et al., 2017), which in both the mitotic and meiotic cell divisions organizes chromosomes into a roughly linear array of nested chromatin loops (Gibcus et al., 2018; Kong et al., 2020; Naumova et al., 2013). This organization results in dramatic compaction and individualization of chromosomes, enabling chromosomes to properly attach to microtubules of the spindle. Chromosome segregation is triggered by separase-mediated cleavage of the kleisin subunit in the remaining chromosome-bound cohesin complexes, unlinking homologs (in meiosis I) or sisters (in meiosis II and mitosis) and allowing them to segregate to opposite spindle poles (Nasmyth, 2001). The need for alignment, physical engagement, and recombination of homologous chromosomes in meiotic prophase presents a significant organizational challenge. Cells meet this challenge by organizing meiotic prophase chromosomes as linear loop arrays, within which chromosomes retain most epigenetic marks and remain transcriptionally active throughout much of

meiotic prophase (Prakash et al., 2015; Zickler and Kleckner, 1999). The organization and compaction of meiotic chromosomes is achieved by modulation of cohesin complex function by the cohesin-associated chromosome axis (see Section 2.4), and by replacement of specific cohesin subunits with meiosis-specific variants. The active, loop-extruding cohesin complex in interphase cells comprises five subunits: two SMC-family ATPases (Smc1 and Smc3), a kleisin subunit (Scc1), and two HAWK (HEAT repeat proteins Associated With Kleisins) proteins, Scc2 and Scc3 (Figure 2-6b-c; See Figure 2.7 for cohesin proteins in major model organisms). Scc2 (NIPBL in mammals) is canonically a subunit of the Scc2:Scc4 "cohesin loader" complex, but in vitro biochemical experiments have shown that it is required for cohesin-mediated loop extrusion (Davidson et al., 2019; Kim et al., 2019). In meiosis, cohesin must accomplish two specialized tasks: first, to organize chromosomes as linear loop arrays with the meiotic chromosome axis; and second, to mediate proper bipolar orientation and segregation of homologs in meiosis I, and of sister chromosomes in meiosis II. The second task is accomplished by replacement of the cohesin kleisin subunit with a meiosis-specific variant, Rec8. In contrast to the mitotic kleisin Scc1/RAD21, a population of Rec8-containing cohesin near each chromosomes' centromere is protected through meiosis I by centromere-associated Shugoshin proteins, which recruit protein phosphatase 2A (PP2A) to dephosphorylate centromere-proximal Rec8 and stabilize it against separase-mediated cleavage (Ishiguro et al., 2010). Shugoshin and PP2A are lost from centromeres as cells enter meiosis II, enabling phosphorylation and separase-mediated cleavage of centromeric Rec8, and concomitant segregation of sister chromatids. The two-stage removal of cohesin in meiosis is absolutely critical for ploidy reduction in meiosis, and is highly conserved even in organisms that lack defined centromeres such as *C. elegans* (see Section2.6) (Ferrandiz et al., 2018). While the importance of Rec8 in the stepwise removal of cohesin complexes from

chromosomes in meiosis I and II is well established, the other critical function of cohesin complexes in meiosis is to associate with the chromosome axis, and extrude and constrain chromatin loops to organize meiotic chromosomes. While fungi possess only a single meiosis-specific cohesin complex, metazoans have evolved distinct complexes dedicated to cohesin's two major meiotic roles. In *C. elegans*, REC-8 containing cohesin complexes mediate sister chromosome cohesion during the meiotic divisions, while cohesin complexes containing the paralogous kleisin subunits COH-3/COH-4 mediate axis assembly and chromatin looping (Pasierbek et al., 2001; Severson et al., 2009; Woglar et al., 2020). *D. melanogaster* also has two distinct meiotic cohesin complexes, with sister chromosome cohesion mediated by a complex containing the meiosis-specific kleisin and HAWK proteins SOLO and SUNN, plus a putative meiosis-specific homolog of SMC ATPases (ORD) (Gyuricza et al., 2016; Krishnan et al., 2014; Webber et al., 2004; Yan and McKee, 2013). Meanwhile, axis assembly and chromatin looping is mediated by a distinct complex containing the kleisin protein C(2)M plus the Scc2 homolog Nipped-B (Manheim and McKim, 2003), which as noted above is crucial for cohesin's loop extrusion activity (Davidson et al., 2019; Kim et al., 2019). Finally, mammals also encode two meiosis-specific kleisin proteins, REC8 and RAD21L (Gutierrez-Caballero et al., 2011; Herran et al., 2011; Lee and Hirano, 2011). REC8 is solely required for maintaining sister chromosome cohesion into the meiotic divisions, consistent with its role in other organisms. Meanwhile, RAD21L is resident on chromosomes only from pre-meiotic S phase until mid-pachytene (Gutierrez-Caballero et al., 2011; Herran et al., 2011; Lee and Hirano, 2011) and deletion of RAD21L plus the meiosis-specific SMC1 protein (Novak et al., 2008; Revenkova et al., 2001; Revenkova et al., 2004) almost completely disrupts axis assembly (Biswas et al., 2016). These data support the idea that throughout metazoans, distinct cohesin complexes defined by different kleisin subunits me-

diate sister chromosome cohesion vs. axis assembly/chromatin looping. Mammals also encode a meiosis-specific HAWK subunit (SA3), which is required for proper meiotic chromosome architecture but whose specific roles are less well understood (Prieto et al., 2001; Winters et al., 2014).

2.4 The Chromosome Axis

The meiotic chromosome axis is a highly conserved proteinaceous scaffold that organizes meiotic chromosomes into a linear array of loops (van Heemst and Heyting, 2000; Zickler and Kleckner, 1999) and serves as the master regulator of meiotic recombination, controlling the formation of DSBs and their repair as inter-homolog crossovers. The axis includes three major sets of proteins: (1) DNA-binding and -looping cohesin complexes; (2) filamentous “axis core” proteins that likely capture cohesins and control assembly of the chromatin loop array; and (3) meiotic HORMAD proteins, which bind the axis core proteins and directly control DSB formation and downstream steps of recombination (See Figure 2.7 for chromosome axis proteins in major model organisms). Recent biochemical, genetic, and bioinformatics work on all three of these protein groups has led to an increasingly clear understanding of chromosome axis assembly, architecture, and function.

2.4.1. Axis core proteins

The foundation of the chromosome axis is made up of the axis core proteins (Moses, 1956), which are highly conserved across eukaryotes and include *S. cerevisiae* Red1 (Hollingsworth and Johnson, 1993; Rockmill and Roeder, 1990; Woltering et al., 2000), *S. pombe* Rec10/Rec27 (Lorenz et al., 2004; Tromer et al., 2021), mammalian SYCP2/SYCP3

(Yang et al., 2006; Yuan et al., 2002; Yuan et al., 2000), and plant ASY3/ASY4 (Chambon et al., 2018; Ferdous et al., 2012). Despite very low sequence identity between different organisms, these proteins share a common domain architecture with an N terminal globular domain, a central disordered region, and a short C-terminal coiled-coil domain (Figure 2-2a). The N-terminal domain, whose role remains mostly uncharacterized, comprises an Armadillo repeat (ARM) domain followed by a Pleckstrin Homology (PH) domain (Figure 2-2b) (Feng et al., 2017; Tromer et al., 2021). Immediately following the ARM/PH domain, axis core proteins possess a "closure motif" responsible for recruitment of meiotic HORMAD proteins to the chromosome axis (West et al., 2019; Woltering et al., 2000). Following an extended central disordered region, the C-terminal coiled-coil domain mediates large-scale self-assembly of the axis core proteins. In *S. cerevisiae*, the single axis core protein Red1 assembles into a coiled-coil homotetramer, and these homotetramers further associate in an end-to-end fashion to generate long filaments (West et al., 2019). Mammalian SYCP2 and plant ASY3 each assemble into 2:2 heterotetramers with short coiled-coil binding partners (SYCP3 and ASY4, respectively), which also associate end-to-end to form filaments (Figure 2-2c-f) (West et al., 2019; Yang et al., 2006). Recent bioinformatics analysis has revealed that the short coiled-coil axis proteins, including mammalian SYCP3, plant ASY4, and S. pombe Rec27, arose from multiple independent gene duplications of full-length axis core proteins through evolution (Tromer et al., 2021). While axis core proteins are broadly conserved across eukaryotes, these proteins have been lost from several eukaryotic lineages (Tromer et al., 2021). Axis core proteins are notably absent from *C. elegans* and *D. melanogaster*, both of which are prominent model organisms for the study of meiosis. In these organisms and potentially other lineages that have lost axis core proteins, the synaptonemal complex assembles independently of DSB formation and appears to shoulder the burden of

organizing chromosomes as compacted linear loop arrays (see Section 2.6).

2.4.2. Meiotic HORMADs

The meiotic HORMAD (HORMA Domain) proteins are named for their conserved N-terminal HORMA domain, which is shared by several families of signaling proteins in prokaryotes and eukaryotes (Figure 2-3a) (Aravind and Koonin, 1998; Rosenberg and Corbett, 2015; Tromer et al., 2019). The HORMA domain features a stable folded core and a flexible C-terminal region termed the "safety belt" (Figure 2-3b). HORMA domains bind 7-10 amino acid regions termed "closure motifs" in their protein binding partners. Closure motifs bind the folded core of the HORMA domain and are then enclosed by the safety belt to generate a highly stable complex. The topologically-closed nature of HORMA-closure motif complexes – with the HORMA domain wrapped entirely around the bound closure motif – lends both high stability and tight control, with disassembly of these complexes requiring energy input in the form of active unfolding by a regulatory ATPase, Pch2/TRIP13 (Figure 2-3d). Meiotic HORMAD-binding closure motifs are found in two sets of proteins: the axis core proteins, and in the meiotic HORMADs themselves. Emerging evidence in multiple organisms including fungi and plants suggests that the HORMADs' own C-terminal closure motifs bind their N-terminal HORMA domains in solution to form an auto-inhibited conformation (West et al., 2018). Active disassembly by Pch2/TRIP13 converts the "closed" auto-inhibited HORMADs to an "open" form competent to bind closure motifs in the axis core proteins, and thereby localize to the chromosome axis (Figure 2-3e) (Yang et al., 2020). Late in meiotic prophase, Pch2/TRIP13 again acts to disassemble HORMA-axis core protein complexes, in order to remove HORMADs from the axis to down-regulate recombination (see Section 2.5). All meiotic HORMADs possess an N-terminal HORMA domain and

a C-terminal closure motif. HORMAD proteins from *S. cerevisiae* (Hop1), *S. pombe* (Hop1), and plants (ASY1/PAIR2), also possess a conserved central region with less well-characterized roles. In *S. cerevisiae*, this region encodes a PHD finger domain and a winged helix-turn-helix (WHD) domain, which tightly associate with one another (Figure 2-3c). The PHD/WHD module specifically binds nucleosomes through a composite interface that recognizes the highly-bent nucleosomal DNA (Ur et al., 2021). This domain mediates cohesin-independent localization of Hop1 and Red1 to specific chromosome regions characterized by high nucleosome density, particularly the three smallest chromosomes (Ur et al., 2021). By boosting the level of chromosome axis proteins on these chromosomes, the Hop1 PHD/WHD may aid crossover formation on these chromosomes, whose small size otherwise puts them in danger of failing to receive enough DSBs to form crossovers (Ur et al., 2021). The conservation of this domain in fungi and plants suggests that these organisms may require a secondary means for axis protein localization to boost DSB formation and recombination levels on certain chromosome regions.

2.4.3 Chromosome axis assembly

The meiotic chromosome axis serves three major roles in meiotic prophase: (1) organization and compaction of each chromosome as a linear array of chromatin loops; (2) recruitment and control of DNA breakage and recombination machinery; and (3) integration into the synaptonemal complex as this structure's "lateral elements" (see Section 2.5). The first of these tasks is accomplished through the cooperative assembly of loop-extruding cohesin complexes with filamentous axis core proteins (Figure 2-4a). While the molecular basis of cohesin-axis core protein interactions are not yet understood, *S. cerevisiae* Red1 has been reported to physically associate with the meiotic cohesin complex (Sun et al., 2015), and high-resolution microscopy

in many organisms reveals that cohesin is closely associated with the axis core (Cahoon et al., 2017; Köhler et al., 2017; Xu et al., 2019). In *S. cerevisiae*, high-throughput methods including ChIP-Seq and Hi-C have revealed the organization of meiotic chromosomes at high resolution. In pachytene, cohesin complexes constrain chromatin loops averaging 26 kb in length, whose bases tend to be located at the ends of transcribing genes, particularly between convergent genes (Panizza et al., 2011; Schalbetter et al., 2019). These data suggest that transcribing RNA polymerase enzymes "push" axis-associated cohesin complexes along chromatin, resulting in a reproducible pattern of chromatin loops and axis attachment sites in this organism (Figure 2.6d-e). Compared to *S. cerevisiae*, mammalian cohesin complexes and chromosome axis proteins are distributed more evenly along chromosomes, and recent Hi-C analysis in *M. musculus* has revealed an overall lack of reproducible chromatin loop locations in meiotic prophase (Figure 2.6d-e) (Vara et al., 2019). This apparent inconsistency with *S. cerevisiae* may be partly a result of lower resolution in Hi-C analysis in *M. musculus*, but the much longer chromatin loops in this organism, ranging from 0.8-1 Mb in zygotene up to 1.5-2 Mb in pachytene, also likely result in less reproducible loop locations (Patel et al., 2019). Given earlier observations of an inverse relationship between loop lengths and overall chromosome axis lengths in certain cohesin mutants (Novak et al., 2008; Revenkova et al., 2004; Yuan et al., 2002), the observation that loop lengths in *M. musculus* extend by about two-fold between zygotene and pachytene suggests that cohesin complexes continue to extrude loops even after incorporation into the chromosome axis. More recent analysis of this same Hi-C data has shown that loop lengths also vary with chromatin state in *M. musculus*, with loops in euchromatic regions 2-3 fold shorter than those in heterochromatic regions (Jin, 2021). This difference may partially explain the relatively higher density of meiotic DNA breaks and crossovers that occur in euchromatin versus heterochro-

matin (Jin, 2021; Patel et al., 2019). Despite the dramatic differences in loop lengths between *S. cerevisiae* and *M. musculus*, the number of chromatin loops per unit length of chromosome axis is largely conserved, with 8.5 loops per μm of axis in *S. cerevisiae* compared to 10 loops per μm in *M. musculus* (Patel et al., 2019; Schalbetter et al., 2019). This finding is consistent with earlier observations that diverse organisms show a consistent number of chromatin loops per unit length of chromosome axis (Zickler and Kleckner, 1999) and point to a conserved underlying architecture of cohesin complexes and axis core proteins in these organisms. Localization of meiotic HORMADs to the chromosome axis is achieved in several ways. First, axis core proteins possess highly-conserved closure motifs that are critical for HORMADs' chromosome localization in many species (West et al., 2019; Woltering et al., 2000). As noted above, in many organisms Pch2/TRIP13 is important to disassemble an auto-inhibited conformation of these proteins, opening their HORMA domains to enable their axis localization (West et al., 2019; Woltering et al., 2000). The axis core proteins are likely not the only axis components with closure motifs, however: *C. elegans*, for example, lacks axis core proteins and its HORMAD protein HTP-3 appears to associate directly with meiotic cohesin complexes (Kim et al., 2014; Köhler et al., 2017). In mammals, HORMAD2 is likely recruited to the axis through an interaction with a closure motif on SYCP2 (West et al., 2019), but chromosome localization of HORMAD1 does not depend on SYCP2 and this protein instead associates directly with cohesin complexes (Fujiwara et al., 2020). Finally, meiotic HORMADs that contain the central PHD/WHD module can associate directly with nucleosomal DNA, providing a secondary pathway for axis-chromatin interactions at vulnerable regions (Ur et al., 2021).

2.4.4. Control of DSB formation and recombination by the axis

Once associated with the chromosome axis, meiotic HORMADs serve as the master regulators of meiotic recombination. HORMADs interact directly with a conserved three-protein complex termed RMM (Rec114, Mei4, Mer2) that binds meiotic chromosomes early in meiotic prophase and is required for Spo11 recruitment and DSB formation (Kumar et al., 2018; Li et al., 2006). Both *S. cerevisiae* Hop1 and mammalian HORMAD1 have been reported to interact directly with the RMM complex subunit Mer2/IHO1 (Kariyazono et al., 2019; Rousova, 2020; Stanzione et al., 2016). *S. cerevisiae* Mer2 also binds the chromatin reader protein Spp1, which in turn is thought to recognize the H3K4me3 marks on hotspot DNA in a chromatin loop and recruit it to the axis for cleavage (Acquaviva et al., 2013; Sommermeyer et al., 2013). Mer2 forms phase-separated condensates on DNA with its RMM complex partners Rec114 and Mei4, and these condensates also recruit the Spo11 core complex (Claeys Bouuaert, 2021; Tsai et al., 2020). Thus, the RMM complex serves as an organizational hub for DSB formation, assembling on the chromosome axis and bringing Spp1-associated hotspot DNA to the Spo11 core complex for cleavage (Figure 2-4b). The recruitment and assembly of multiple Spo11 complexes on the surface of an RMM complex condensate may explain the recent observation of Spo11 “double cuts” – closely-spaced DSBs in a single hotspot occurring with rough 10.5-bp periodicity (Johnson, 2019) (Franz Klein, personal communication). In mammals, the RMM complex subunit Rec114 also interacts with ANKRD31, which recruits the RMM complex to specific chromosome regions including the pseudo-autosomal region (PAR) and the X chromosome (Acquaviva et al., 2020; Boekhout et al., 2019; Papanikos et al., 2019). ANKRD31 thus likely represents a mechanism to boost DSB and crossover levels on chromosome regions particularly prone to recombination failure, similar to the Hop1 PHD/WHD module-mediated enrichment of

axis proteins on small chromosomes in S. cerevisiae (Ur et al., 2021). After assembly of RMM condensates on the chromosome axis and formation of DSBs by Spo11, the DNA damage response kinases ATR (Mec1 in S. cerevisiae) and ATM (Tel1 in *S. cerevisiae*) are recruited to these sites. In S. cerevisiae, Tel1/ATM suppresses the formation of DSBs within 70-100 kb (3-4 chromatin loops) of an existing DSB, in a process termed "DSB interference" (Carballo et al., 2013; Garcia et al., 2015; Zhang et al., 2011). Similar roles for Tel1/ATM have been identified in *S. pombe* (Fowler et al., 2018), *D. melanogaster* (Joyce et al., 2011), and *M. musculus* (Dereli et al., 2021; Lange et al., 2011), revealing that this kinase plays a conserved role in moderating the levels of DNA breaks along meiotic chromosomes (Cooper et al., 2014; Lukaszewicz et al., 2018). In *S. cerevisiae*, Mec1 and Tel1 also cooperate to phosphorylate the meiotic HORMAD protein Hop1 in its SQ/TQ Cluster Domain (SCD), located between its N-terminal HORMA domain and central PHD/WHD module (Carballo et al., 2008; Penedos et al., 2015). Phosphorylation of the Hop1 SCD, and in particular the conserved Thr318 residue, mediates recruitment and activation of another kinase, Mek1. Mek1 binds and stabilizes phosphorylated Hop1 Thr318 (Chuang et al., 2012; Xie et al., 2018) and locally inhibits recombination, thereby suppressing sister chromosome-templated repair to favor homolog invasion (Callender et al., 2016; Niu et al., 2007; Niu et al., 2009; Subramanian et al., 2016; Suhandynata et al., 2014). Hop1 phosphorylation and Mek1 activation are also required to enforce a checkpoint that delays meiotic progression in response to defective recombination and/or assembly of the synaptonemal complex (e.g. in *rad50S*, *dmc1*Δ or *zip1*Δ strains) (Carballo et al., 2008; Subramanian and Hochwagen, 2014). This checkpoint is mediated by Mek1-dependent suppression of Ndt80, a key transcription factor required for progression past pachytene in *S. cerevisiae* meiotic cells (Prugar et al., 2017; Tung et al., 2000). Thus, chromosome axis-associated meiotic HORMAD

proteins play a central role in coordinating meiotic recombination, recruiting DSB factors and controlling several overlapping signaling pathways controlling the fate of meiotic DSBs.

2.5 The Synaptonemal Complex

The synaptonemal complex (SC) was first observed over 60 years ago in electron micrographs of crayfish spermatocytes (Moses, 1956), yet this distinctive and highly conserved assembly has resisted detailed structural and functional analysis for decades. In recent years, light and electron microscopy of the intact SC has synergized with in vitro reconstitution and structural analysis of defined subcomplexes to yield an increasingly detailed picture of SC architecture and dynamics. Alongside these advances, the molecular mechanisms underlying the SC's important roles in meiotic recombination and checkpoint signaling are steadily becoming more clear.

2.5.1. Architecture of the Synaptonemal Complex

Electron micrographs of meiotic cells from diverse eukaryotes reveal the SC as a multilayered sandwich structure, bounded on either side by the chromosome axes of paired homologs (Carpenter, 1975; Moses, 1956). The edges of the SC are defined by the lateral elements (LEs), which are derived from the chromosome axes of the paired homologs and are spaced 100 nm apart in most organisms. Between the LEs lie two layers of transverse filaments (TFs), which are linked at the midline of the SC by the electron-dense central element (CE). The TFs and CE are sometimes collectively termed the "central region" of the SC, as distinguished from the chromosome axis-derived LEs. After nucleating at initial homolog engagement sites, the SC progressively extends along the entire length of each homolog pair to bring homologs into close

juxtaposition. The SC is required for the final stages of meiotic recombination and crossover formation, and also serves as a key signaling hub for multiple quality-control pathways in meiotic prophase.

2.5.1.1. Lateral elements

As noted above, the SC lateral elements are derived from the chromosome axes of each homolog pair. The organization of this structure, with filamentous axis core proteins capturing DNA-binding and -looping cohesin complexes, appears largely maintained as it becomes integrated into the SC. The most significant structural change to the axis upon SC assembly is the loss of most HORMAD proteins in a feedback pathway governing recombination levels, triggered by the recruitment of the Pch2/TRIP13 ATPase to the assembled SC (see Section 2.5.3).

2.5.1.2. Transverse filaments

The most distinctive feature of the SC is the TFs, which comprise long (800-1000 amino acid) proteins made up almost entirely of predicted coiled-coil domains (Figure 2-5a). Alpha-helical coiled coils are remarkably rigid structural elements in proteins, and the coiled-coil regions of TF proteins form a regular, three-dimensional network that spans the 50 nm gap from LE to CE. Interestingly, the coiled coil regions of most species' TF proteins are long enough to span nearly the entire 100 nm gap between LEs, yet each individual TF protein spans only half that distance, from one LE to the CE (Figure 2-5d-e). TF proteins from diverse organisms also adopt a common orientation within the SC, with their N-termini positioned at the SC midline with CE proteins, and their C-termini embedded in the LEs (Cahoon et al., 2017; Capilla-Perez et al., 2021; Dobson et al., 1994; Dong and Roeder, 2000; Hurlock et al., 2020; Liu et al., 1996; Page and Hawley, 2001; Schild-Prufert et al., 2011; Schmekel et al., 1996). In recent years, careful dissection and in vitro structural analysis of TF proteins, principally the mammalian TF protein

SYCP1, has yielded important information on their assembly mechanisms (Figure 2-5a-c). This protein's extreme N- and C-terminal domains are predicted to be intrinsically disordered, and likely interact with CE proteins and LE proteins in an as-yet undefined manner. The central coiled-coil region of SYCP1 is separated into four segments, beginning with a short segment that forms a parallel coiled-coil dimer and may form interdigitated interactions within the CE (Figure 2-5b,e). Following this is a segment that forms a parallel coiled-coil tetramer, then an extended segment of parallel coiled coil dimer. These two regions define the minimal SYCP1 oligomer as a homotetramer that splays open into a pair of dimeric coiled coils at its C-terminus (Fig. 2-5e) (Dunce et al., 2018). Finally, the C-terminal segment of the SYCP1 coiled-coil can form a parallel coiled-coil dimer or an antiparallel tetramer, suggesting that this segment could mediate interactions between neighboring SYCP1 tetramers to assemble the regular networks of TFs characteristic of the SC (Fig. 2-5c,e) (Dunce et al., 2018). While TF proteins in other organisms share little detectable sequence homology with SYCP1, their assembly mechanisms are likely to be broadly conserved. For example, *S. cerevisiae* Zip1 possesses disordered N- and C-terminal domains, and forms both dimers and tetramers in solution (Dunce et al., 2018). In *C. elegans*, mutation of the extreme N-terminus of the TF proteins SYP-1 results in failure of the SC to build a two-fold symmetric structure, consistent with the idea that TF proteins self-interact within the CE to bridge homologs and mediate pairing (Gordon et al., 2021).

2.5.1.3. The central element

The central element (CE) is an electron-dense structure positioned at the midline of the SC that is thought to help link the two layers of TF proteins extending inward from the LEs (Dunce et al., 2018). Like TF proteins, CE proteins from different organisms share no obvious sequence homology, making it difficult to comprehensively identify these proteins by

sequence and leaving unanswered the question of whether CE architecture is conserved across species. Like TF proteins, most CE proteins are predicted to assemble into multimeric -helical coiled coil structures. In *S. cerevisiae*, the CE comprises a complex of two proteins, Ecm11 and Gmc2, which associate with one another and stabilize assembly of the TF protein Zip1 on chromosomes (Humphryes et al., 2013). The mammalian CE is more complex, and includes at least five proteins (Figure2-7). Three of these proteins (SYCE1, SYCE3, and SIX6OS1) form a subcomplex of defined stoichiometry (Dunne and Davies, 2019a, b; Lu et al., 2014; Sanchez-Saez et al., 2020) and are required for initial nucleation of the SC (Bolcun-Filas et al., 2009; Dunce et al., 2018; Dunne and Davies, 2019b; Gomez et al., 2016; Schramm et al., 2011). The remaining two proteins (SYCE2 and TEX12) are not required for SC nucleation but are needed for full-length assembly of the SC along paired homologs (Bolcun-Filas et al., 2007; Davies et al., 2012; Hamer et al., 2006; Hamer et al., 2008). In keeping with this role, SYCE2 and TEX12 form a hetero-octameric complex that undergoes large-scale self-assembly in vitro into filament-like structures (Davies et al., 2012). While these findings represent significant progress in understanding the architecture and assembly dynamics of the SC, we still lack a comprehensive picture of how the central element assembles and interacts with TF proteins. In addition to dedicated CE proteins, the small ubiquitin-like modifier protein SUMO plays a key role in SC assembly, especially in the budding yeast *S. cerevisiae*. SUMO and ubiquitin are important regulators of meiotic prophase in many organisms, acting in a feedback pathway driven by meiosis-specific SUMO and ubiquitin E3 ligases (Ahuja et al., 2017; Nguyen et al., 2018; Pyatnitskaya et al., 2019; Rao et al., 2017a; Watts and Hoffmann, 2011; Zhang et al., 2018a). SUMO appears to also play a structural role in SC assembly in *S. cerevisiae*. One of the most highly SUMOylated proteins in S. cerevisiae meiosis is the CE protein Ecm11,

which is modified with polymeric SUMO chains (Bhagwat et al., 2021). SUMO chains (both free and Ecm11-conjugated) are required for the proper assembly and stability of Zip1-containing TFs, and Zip1 in turn promotes and stabilizes Ecm11 poly-SUMOylation (Voelkel-Meiman et al., 2013). The chromosome axis core protein Red1 is also highly SUMOylated in meiotic prophase (Eichinger and Jentsch, 2010), as is Zip1 itself (Bhagwat et al., 2021). While the architectural roles of SUMO and SUMO chains in the *S. cerevisiae* SC are not yet well-understood, they likely include stabilization of protein-protein interactions (through SUMO-interacting motifs or SIMs) (Eichinger and Jentsch, 2010), alteration of protein conformational states, and positive or negative effects on protein stability. The complex combination of signaling and architectural roles for SUMO, and for ubiquitin, in meiotic prophase represent an important area for future study.

2.5.2 The SC as a dynamic three-dimensional structure

Our structural understanding of the SC first developed from electron microscopy imaging of this structure from a variety of organisms beginning in the 1950s (reviewed in (Zickler and Kleckner, 1999)). While these studies revealed the canonical SC architecture, the use of fixed samples precluded detailed analysis of SC dynamics, and the preparation and staining methods for electron microscopy also limited the resolution of the resulting images. More recently, a combination of live-cell microscopy, super-resolution light microscopy of fixed samples, and cryo-electron tomography has dramatically improved our understanding of SC architecture and importantly, dynamics. The most stable part of the SC is the LEs, which are derived from the chromosome axes of paired homologs. As described above, these structures are likely assembled from the cooperative action of DNA-organizing cohesin complexes bound to filaments

of axis core proteins. Super-resolution microscopy analysis of the chromosome axis/LE in the *M. musculus* SC has revealed a 30-50 nm wide core made up of the C-terminal coiled-coil domains of SYCP2 and SYCP3 (Xu et al., 2019). The SYCP2 N-terminus, which contains its ARM/PH domain and its HORMAD-binding closure motif, extends away from this core. Both HORMADs and cohesin complexes also localize around the axis core, consistent with a model in which cohesin complexes interact with the N-terminal region of axis core proteins (Xu et al., 2019). LEs in *C. elegans* show similar dimensions, with HORMAD proteins colocalizing with cohesin complexes in two 30 nm wide LEs that are separated by 100 nm across the SC (Köhler et al., 2017). *C. elegans* lacks axis core proteins, and in this organism the LE does not form a cohesive structure until the SC assembles (see Section 2.6). Along the *C. elegans* LE, REC-8 containing cohesin complexes (which mediate sister cohesion) and COH-3/COH-4 cohesin complexes (which mediate axis assembly and likely extrude/constrain chromatin loops) are interspersed in a regular pattern alongside defined assemblies of HORMADs (Woglar et al., 2020). Finally, while the LE in most organisms appears as a single core that presumably binds and organizes a pair of sister chromosomes, in *D. melanogaster* the LE (defined by the meiotic cohesin subunit C(2)M) appears as a pair of cores separated by 50 nm, with one core presumably organizing each sister chromosome (Cahoon et al., 2017). In other organisms a single LE is sometimes observed to split into two “sub-LEs” (del Mazo and Gil-Alberdi, 1986; Zwettler et al., 2020), which may represent the subsets of axis proteins and cohesin complexes organizing the two sisters. Splitting of the LE into separate sub-LEs may contribute to the suppression of sister chromosome-mediated recombination at DSB sites, by physically separating these two strands from one another. Between the paired axes/LEs assemble two arrays of TF proteins, oriented with their C-termini embedded in the LEs and their N-termini associated with the CE at

the SC midline. Super-resolution light microscopy and high-resolution cryo-electron microscopy has revealed that TFs and the CE form a loosely defined three-dimensional network (Figure 2-5f) (Cahoon et al., 2017; Spindler et al., 2019; Zwettler et al., 2020), likely scaffolded by self-association of TF proteins' N-terminal coiled coil regions, and stabilized by 3D networks of CE proteins (Dunce et al., 2018). An important recent advance has been the finding that despite their highly ordered structure, TF proteins are actually highly dynamic within the SC. In *S. cerevisiae*, the TF protein Zip1 is continually deposited and exchanged even after the structure is fully assembled (Voelkel-Meiman et al., 2012). In C. elegans, a series of studies has revealed the SC to share physical properties with phase-separated macromolecular condensates, resulting in its description as a "liquid crystal" (Hurlock et al., 2020; Rog and Dernburg, 2015; Rog et al., 2017; Zhang et al., 2020). Moreover, SCs in multiple organisms can be reversibly disassembled by aliphatic alcohols that disrupt low-affinity hydrophobic interactions typical of phase-separated condensates (Voelkel-Meiman et al., 2012). A model of the SC as a liquid-like compartment whose assembly is templated by the LEs of paired homologous chromosomes is consistent with the observation that, in many organisms, TF and CE proteins can also form large, highly ordered aggregates termed "polycomplexes" in cells where SC assembly is compromised (Humphryes et al., 2013). The structures of polycomplexes are reminiscent of a multilayered SC when examined by electron microscopy, and can be dissolved by aliphatic alcohols, consistent with a model in which this structure self-assembles through cooperative, low-affinity hydrophobic interactions between TF and CE proteins (Rog et al., 2017). A liquid-crystal model of the SC can reconcile the highly reproducible architecture of this assembly as observed by electron microscopy with newer observations that its underlying subunits are highly dynamic. A dynamic liquid-crystal SC could accommodate continual chromosome axis/LE compaction during meiotic prophase driven

by cohesin-mediated loop extrusion, and explain phenomena like “synaptic adjustment” in which synapsed chromosomes shift and compact relative to one another during prophase (Henzel et al., 2011; Zickler and Kleckner, 1999). A model of the SC as a phase-separated condensate also provides a compelling framework for the SC’s roles in regulating meiotic recombination, through the specific recruitment or exclusion of particular proteins to recombination sites embedded within the SC “phase”. In support of this model, a family of regulatory SUMO/ubiquitin E3 ligases (ZHP-1, ZHP-2, ZHP-3, and ZHP-4) can partition into the dynamic SC in *C. elegans* (Voelkel-Meiman et al., 2012; Zhang et al., 2018a). In *S. cerevisiae*, the Hop1 regulator Pch2 localizes to both synapsed chromosomes and polycomplexes, possibly through a similar partitioning mechanism (Herruzo et al., 2019; San-Segundo and Roeder, 1999). Regardless of the terms used to describe the assembly mechanisms and behavior of the SC, it seems clear that the apparent structural stability of the SC as viewed by light and electron microscopy belies the highly dynamic nature of this structure. Key areas for future work include dissecting the interactions between TF proteins and proteins of the LEs and CE, determining the molecular basis for SC fluidity through cooperative, low-affinity interactions (Hurlock et al., 2020; Zhang et al., 2020), and determining how SC fluidity changes during meiotic prophase in response to post-translational modifications and other events (Gao and Colaiacovo, 2018). Whether and how specific recombination factors and regulators are recruited or excluded from the SC as meiotic prophase progresses, and whether the liquid-crystal nature of the SC is involved in this regulation, is another important outstanding question.

2.5.3. Functional coupling of recombination and synaptonemal complex assembly

In all organisms that assemble the SC in meiotic prophase, this structure nucleates at defined points along each pair of homologs as they become physically engaged, then extends along the entire length of the chromosomes. In some organisms, such as *C. elegans* and *D. melanogaster*, SC assembly occurs independently of Spo11-mediated DNA cleavage and recombination (see Section 2.6). More often, the SC nucleates at developing crossover sites (Albini and Jones, 1984; Fung et al., 2004; Oliver-Bonet et al., 2007; Zickler et al., 1992). Spo11-mediated DNA breaks vastly outnumber crossovers, and while most breaks are repaired using the homologous chromosome as a template, only a minority of sites ultimately become interhomolog crossovers. In most organisms, crossover sites show "interference" – that is, these sites are more evenly spaced and further apart along chromosomes than expected by random chance – suggesting that developing crossovers are able to signal along chromosomes to suppress the resolution of nearby recombination sites as crossovers. The physical basis of crossover interference and its relationship to chromosome architecture is not well understood and is not further discussed here, but is comprehensively reviewed elsewhere (Otto and Payseur, 2019; Zickler and Kleckner, 2015, 2016). As meiotic prophase progresses from leptotene to zygotene and pachytene, recombination sites designated to become crossovers are distinguished by binding of specific crossover-promoting factors including the Msh4:Msh5 complex (Borner et al., 2004; Novak et al., 2001) and a complex termed the synapsis initiation complex (SIC) or the ZZS complex (after its *S. cerevisiae* subunits Zip2, Zip4, and Spo16) (Pyatnitskaya et al., 2019). Msh4 and Msh5 are related to MutS family mismatch repair proteins, and are thought to recognize and stabilize a key recombination intermediate termed a double Holliday Junction, then recruit

the Mlh1:Mlh3 nuclease to resolve this intermediate into a crossover (Santucci-Darmanin et al., 2000; Snowden et al., 2004; Snowden et al., 2008). The ZZS subunits Zip2 (SHOC1 in mammals and plants) and Spo16 (SPO16 in mammals, PTD in plants) form a heterodimeric complex that specifically binds branched DNA structures in vitro (Arora and Corbett, 2019; De Muyt et al., 2018; Guiraldelli et al., 2018; Macaisne et al., 2011), while Zip4 (TEX11 in mammals, ZIP4 in plants) likely acts as a protein-protein interaction hub (Adelman and Petrini, 2008; Chelysheva et al., 2007; Perry et al., 2005; Shen et al., 2012; Tsubouchi et al., 2006). ZZS mutants in *S. cerevisiae*, plants, and mice fail to form crossovers, suggesting that one key role for the ZZS complex is to bind and stabilize a recombination intermediate to promote crossover formation (Chua and Roeder, 1998; Guiraldelli et al., 2018; Macaisne et al., 2008; Macaisne et al., 2011; Malavasic and Elder, 1990; Shinohara et al., 2008; Tsubouchi et al., 2006; Wijeratne et al., 2006; Zhang et al., 2019; Zhang et al., 2018b). A crucial second role for the ZZS complex is to functionally link crossover formation to SC assembly. In *S. cerevisiae*, ZZS proteins localize at the ends of elongating stretches of SC (Tsubouchi et al., 2006). ZZS mutants in both *S. cerevisiae* and mice fail to form full-length SC along chromosomes (Chua and Roeder, 1998; Guiraldelli et al., 2018; Shinohara et al., 2008; Tsubouchi et al., 2006; Zhang et al., 2018b). The *S. cerevisiae* ZZS complex interacts with both Msh4:Msh5 and the axis proteins Hop1, Red1, and Pch2, suggesting that the ZZS complex coordinates crossover formation with axis remodeling to promote SC assembly (De Muyt et al., 2018). In organisms where SC assembly is linked to crossover formation through the ZZS complex, formation of the SC on a given homolog pair can be interpreted as a chromosome-autonomous signal for successful crossover formation. As such, SC assembly is a crossroads for a number of signaling pathways regulating recombination and meiotic progression. One major pathway links SC assembly to the removal of most meiotic

HORMADs from the chromosome axis/LE through the recruitment of Pch2/TRIP13 (Borner et al., 2008; Capilla-Perez et al., 2021; Joshi et al., 2009; Lambing et al., 2015; Roig et al., 2010; Wojtasz et al., 2009). Removal of meiotic HORMADs from synapsed chromosome regions dramatically reduces new DNA breaks in these regions (Wojtasz et al., 2009), and also releases the HORMAD-dependent barrier to inter-sister recombination, allowing remaining breaks to be quickly repaired via the sister chromosome (Subramanian et al., 2016). In *S. cerevisiae*, loss of Hop1 from chromosome axes also reduces the levels of active Mek1 kinase, eventually relieving the Mek1-dependent block on expression of the key transcription factor Ndt80 (Chen et al., 2018; Prugar et al., 2017). Ndt80 expression enables cells to progress past pachytene into diplotene and the meiotic divisions. Finally, just as SC assembly serves as a signal for successful crossover formation, failure to assemble the SC is a strong signal that chromosomes have failed to identify and recombine with their homolog. Throughout eukaryotes, failure to assemble the SC triggers checkpoint mechanisms that delay meiotic progression and, in some cases, can trigger apoptosis as a means of culling defective gametes (Subramanian and Hochwagen, 2014). Thus, the SC is a central player in the quality control of meiosis, regulating the levels of DSB and crossover formation, and serving as a central signaling hub for meiotic progression and quality control pathways.

2.6 Why are C. elegans and D. melanogaster different?

The nematode *Caenorhabditis elegans* is a prominent model system for the study of meiosis because of its powerful genetics and its two large gonads, which provide a map of meiotic prophase progression that can be readily visualized by light microscopy in the live organism. While the broad strokes of *C. elegans* meiosis parallel other organisms like yeast, plants, and

mammals, many details are distinct. First, *C. elegans* lacks meiotic chromosome axis core proteins, and the best evidence to date suggests that at least one member of the expanded HORMAD protein family associates directly with meiotic cohesin complexes (Kim et al., 2014; Köhler et al., 2017; Severson et al., 2009). The four *C. elegans* meiotic HORMADs (HIM-3, HTP-1, HTP-2, and HTP-3) also use head-to-tail HORMA domain-closure motif interactions to assemble a distinctive hierarchical complex at the chromosome axis (Kim et al., 2014). Next, homolog synapsis occurs prior to meiotic DSB formation, and is mediated by a family of zinc finger proteins that associate with "pairing centers" near one end of each chromosome (Phillips and Dernburg, 2006; Phillips et al., 2009; Phillips et al., 2005). Early synapsis may explain the lack of axis core proteins in *C. elegans*: the SC itself appears to aid chromosome compaction and organization into a linear loop array in early prophase. Spo11-mediated DSB formation occurs in the context of synapsed homologs, and a single DSB on each chromosome is designated to become the crossover. This "perfect" crossover interference arises because of the relatively short length of *C. elegans* chromosomes (15-21 Mb) combined with strong crossover interference (Libuda et al., 2013). Formation of a single crossover per chromosome pair is critical, as *C. elegans* chromosomes are holocentric: they lack defined centromeres and instead assemble the spindle microtubule-binding kinetochore machinery along the length of each chromosome (Maddox et al., 2004). In order to achieve homolog segregation in meiosis I followed by sister chromosome segregation in meiosis II, *C. elegans* first defines "long" and "short" arms on either side of the single crossover. The hierarchical meiotic HORMAD complex, along with other proteins including the Aurora B kinase AIR-2, then directs the differential remodeling of these two arms, resulting in the assembly of a modified kinetochore-like structure on the long arms, and phosphorylation of cohesin complexes along the short arms (Martinez-Perez et al., 2008;

Nabeshima et al., 2005). Thus, the long arms of *C. elegans* chromosomes become functionally equivalent to centromeres in other organisms (Dumont et al., 2010). Separase-mediated cleavage of cohesin complexes on the short arms in meiosis I enables homolog segregation, while cohesin complexes on the long arm maintain sister-chromosome cohesion until meiosis II. The fruit fly *Drosophila melanogaster*, in which modern genetics was founded over a century ago (Morgan, 1911; Muller, 1916; Sturtevant, 1913), also displays significant differences in meiotic chromosome architecture and the sequence of meiotic prophase events when compared to other model organisms. In male *Drosophila*, chromosomes do not undergo crossing over and do not assemble the synaptonemal complex; in females, the smallest chromosome (chromosome IV) also does not form crossovers (reviewed in (Hughes et al., 2018)). Like *C. elegans* but distinct from most other organisms, homolog synapsis in *Drosophila* does not depend on Spo11-mediated DSB formation (McKim and Hayashi-Hagihara, 1998). Also like *C. elegans*, *Drosophila* lack chromosome axis core proteins and also lack recognizable homologs of meiotic HORMADs, indicating a distinctive mechanism for control of meiotic DSB formation (Tromer et al., 2021). Despite (or perhaps because of) its uniqueness, *Drosophila* continues to be a powerful and informative model system for understanding the complexities of meiosis, including the assembly and architecture of the synaptonemal complex, and the genetics and molecular mechanisms of meiotic crossover formation.

2.7 Conclusion

Meiotic prophase places unique demands on the eukaryotic genome, which must balance continued transcriptional activity with the introduction and accurate repair of dozens, sometimes hundreds, of DNA breaks. Successful reproduction depends on at least one of these

breaks per homolog pair developing into an interhomolog crossover, which will enable accurate homolog segregation and ploidy reduction in the meiosis I division. To address the unique demands of meiosis, eukaryotes have evolved a specialized DNA repair pathway along with a set of interlocking signaling pathways ensuring fidelity at every step. Two chromosome-scale protein assemblies, the chromosome axis and synaptonemal complex, play central roles in meiotic chromosome organization, recombination, and eventual segregation. The chromosome axis coalesces as axis core protein fibers capture loop-extruding cohesin complexes and form bundles, resulting in a linear array of chromatin loops. Axis-associated HORMAD proteins recruit DSB factors including the conserved RMM and Spo11 core complexes, then control the repair of the resulting DNA breaks to promote interhomolog crossover formation. A key recent development has been the identification of multiple pathways – including the fungal Hop1 PHD/WHD module and vertebrate ANKRD31– that boost the level of axis proteins, and recombination, on specific chromosomes or chromosomal regions that would otherwise present a high risk for failure to recombine and properly segregate (Boekhout et al., 2019; Papanikos et al., 2019; Ur et al., 2021). As the synaptonemal complex nucleates at developing crossover sites and extends along each pair of homologs, further recombination is progressively shut down along synapsed chromosomes through chromosome-autonomous and global feedback pathways, many of which are conserved across eukaryotes. As cells progress through the meiosis I and II divisions, interhomolog crossovers and the two-step removal of sister cohesion – enabled by the meiosis-specific cohesin subunit Rec8 – drive homolog segregation in meiosis I and sister chromosome segregation in meiosis II, resulting in the formation of haploid gametes. The significant recent advances in understanding meiotic chromosome architecture and dynamics have nonetheless left longstanding questions unanswered, while also introducing new questions. Many of these

questions center on cohesin complexes: for example, we lack a clear understanding of the subunit architecture and division of labor (sister cohesion versus loop extrusion and axis assembly) of the specialized meiotic cohesin complexes, especially in organisms that express meiosis-specific variants of kleisin, HAWK, and SMC ATPase subunits. Further, we lack a molecular understanding of how axis core proteins (or HORMADs, in some organisms) capture and control loop-extruding cohesin complexes to form the chromosome axis. Cohesin capture could be mediated through the axis core proteins' N-terminal ARM/PH domains, or alternatively could involve a mechanism similar to cohesin capture by the insulator protein CTCF (Li et al., 2020). The synaptonemal complex presents further questions. While the overall architecture of the SC, particularly the oligomeric structure of TF proteins, is becoming better understood, we still lack an understanding of the protein-protein interactions that hold this structure together. We do not know how TF protein N-termini interact with proteins of the CE, nor how TF protein C-termini interact with the chromosome axis/LE. These interactions may be difficult to identify or dissect using traditional techniques, due to the likelihood that the SC is a liquid-like structure held together by cooperative, low-affinity interactions typical of macromolecular condensates. At the same time, recognition of the SC as a liquid-like assembly – specifically, a liquid crystal that retains a defined architecture while individual subunits remain highly dynamic – is an exciting conceptual advance. Much more work will be required to understand whether, and how, the liquid-like nature of the SC mediates specific recruitment or exclusion of recombination or regulatory factors to promote crossover formation and facilitate the interlocking feedback pathways governing meiotic progression. It is an exciting time to study chromosome architecture and dynamics, especially in meiosis. New tools like live-cell and super-resolution light microscopy, cryo-electron tomography, and high-throughput sequencing methods are already revealing mei-

otic chromosomes at an unprecedented level of detail. At the same time, our ability to purify and characterize key protein complexes in vitro is reaching an inflection point where reconstitution of critical reactions like chromosome axis assembly or DSB formation no longer seems out of reach. Finally, while research in meiosis has traditionally been siloed into the study of particular model organisms – fungi, plants, insects, nematodes, and mammals – advances in sequence analysis and other areas are revealing the fundamental conservation of meiotic machinery, recombination mechanisms, and feedback pathways across all eukaryotes. Within this shared framework, distinctive features of meiosis in particular systems represent an opportunity to appreciate how evolution has adapted to the unique challenges posed by each organism's genome makeup and reproductive mechanisms.

2.8 Acknowledgements

We thank members of the Corbett laboratory for helpful discussions and feedback.

Chapter 2, in full, is a reprint of material as it appears in: **Ur, SN**, Corbett, KD. Architecture and Dynamics of Meiotic Chromosomes. Annual Review of Genetics (2021). The dissertation author was first author of this paper.

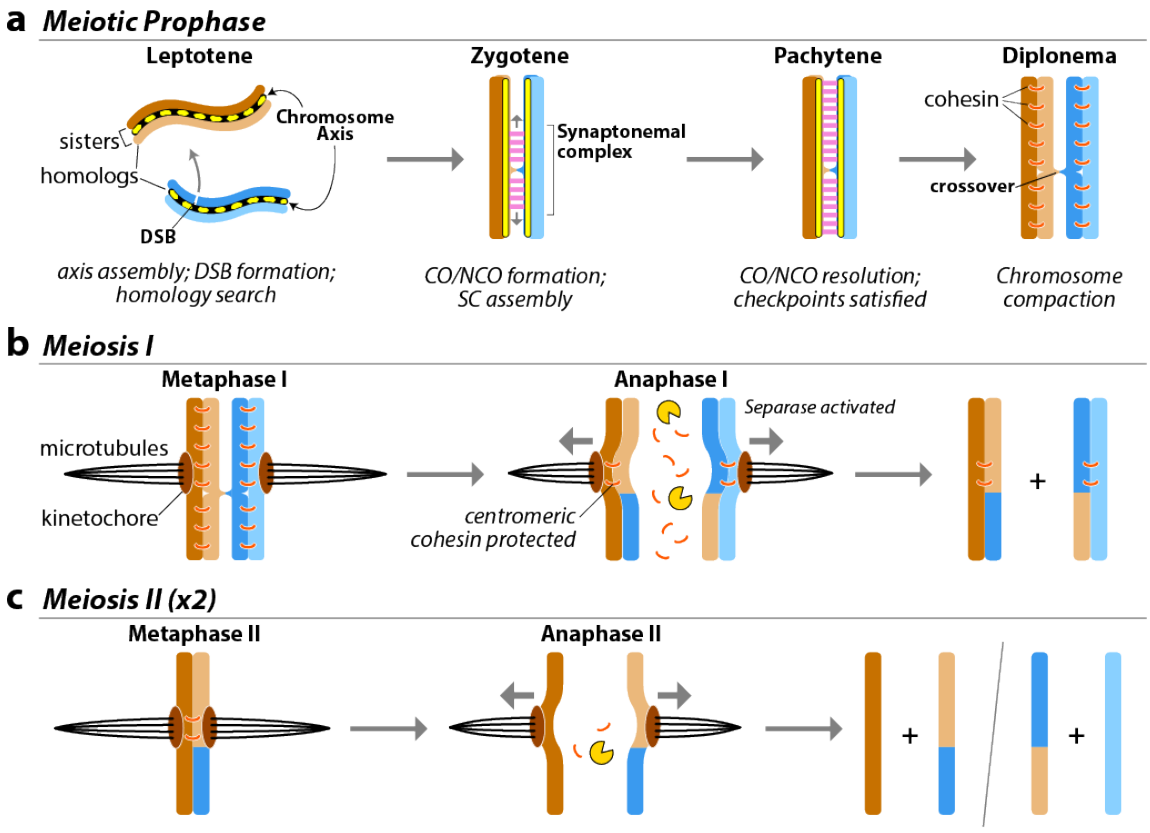

Figure 2.1: **Major events of meiosis** (a) In meiotic prophase, chromosomes undergo a defined series of morphological changes to generate interhomolog crossovers, In leptotene, chromosomes assemble the chromosome axis (yellow) and undergo the formation of DNA double-strand breaks (DSBs), which initiate homologous recombination. In zygotene, designated crossover sites initiate assembly of the synaptonemal complex (pink) between paired homologs. In pachytene, synaptonemal complex assembly is complete, shutting off feedback pathways that allow progression into diplotene and the meiotic divisions. (b) In meiosis I, sister kinetochores are fused or co-oriented to enable bi-orientation of homologs on the spindle (black). Cleavage of cohesin complexes on chromosome arms by separase (yellow) enables homolog segregation. (c) In meiosis II, sister kinetochores are bi-oriented on the spindle and segregate when the remaining centromeric cohesin complexes are cleaved by separase.

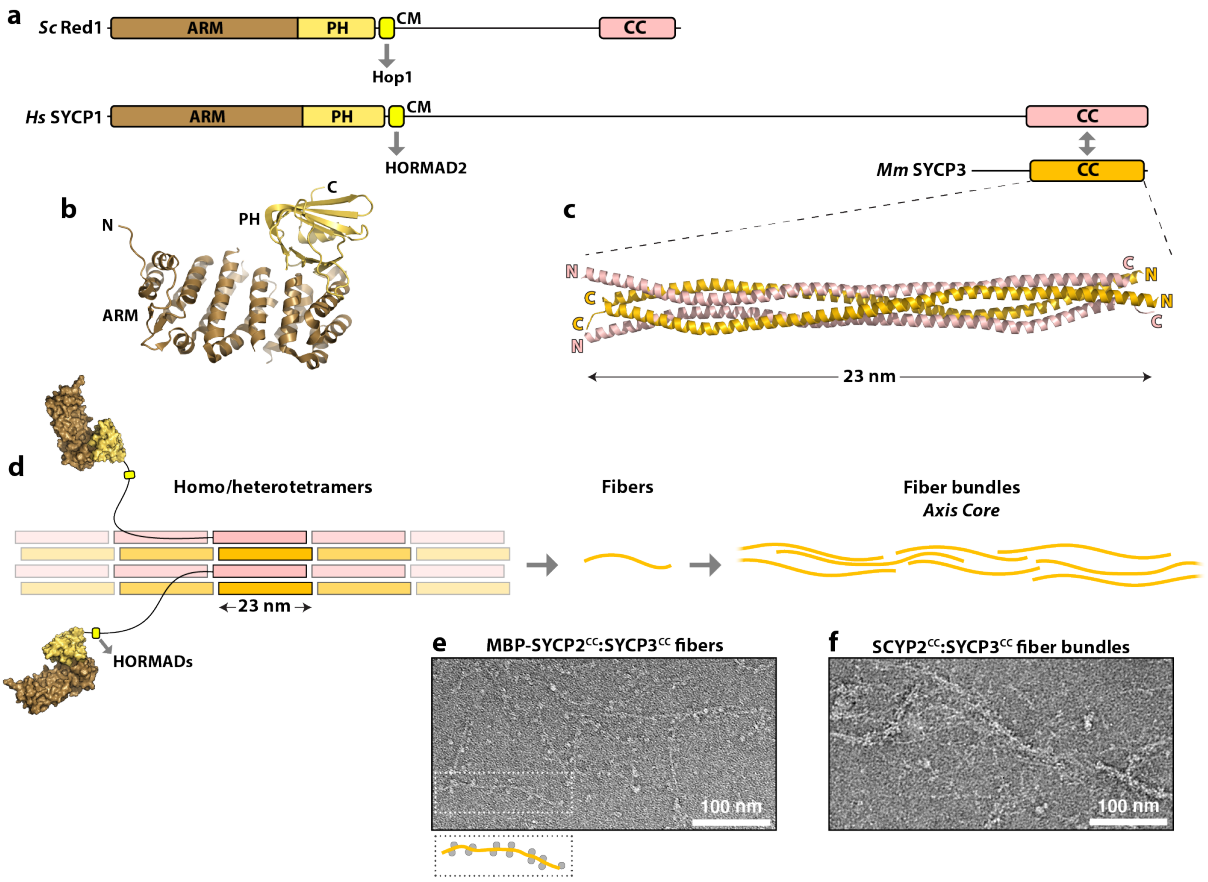

Figure 2.2: **Chromosome axis core protein structure and self-assembly** (a) Schematic of domain architecture in S. cerevisiae Red1 (top) and *M. musculus* SYCP2 and SYCP3 (bottom). Red1 and SYCP2 encode an N-terminal ARM/PH domain (panel b), followed by a closure motif that binds meiotic HORMADs (West et al., 2019; West et al., 2018; Woltering et al., 2000). These domains are followed by an extended disordered region and a C-terminal coiled-coil domain. In *S. cerevisiae* Red1, this domain forms a homotetramer (West et al., 2019). M. musculus SYCP3 encodes a coiled-coil domain that assembles into homotetramers and 2:2 heterotetramers with the SYCP2 C-terminal coiled-coil (Syrjanen et al., 2014; West et al., 2019). (b) Structure of the *M. musculus* SYCP2 N-terminal ARM/PH domain (PDB ID 5IWZ; (Feng et al., 2017)). (c) Structure of the *H. sapiens* SYCP3 coiled-coil homotetramer (PDB ID 4CPC; (Syrjanen et al., 2014)), colored pink/orange to represent a model for a 2:2 heterotetramer of SYCP2 and SYCP3 (West et al., 2019). (d) Model for chromosome axis assembly. SYCP2:SYCP3 heterotetramers (and potentially SYCP3 homotetramers) assemble end-to-end to generate fibers, which self-associate to form bundles that make up the chromosome axis core. (e) Negative-stain electron microscopy (EM) image of fibers assembled from MBP-tagged *M. musculus* SCYP2 coiled-coil domain (SYCP2CC) and untagged SYCP3 coiled-coil domain (SYCP3CC). Inset: pairs of globular densities spaced 23 nm apart along the fiber correspond to the repeating unit of the fiber. Reprinted from (West et al., 2019). (f) Negative-stain EM image of SYCP2CC:SYCP3CC fiber bundles. Reprinted from (West et al., 2019).

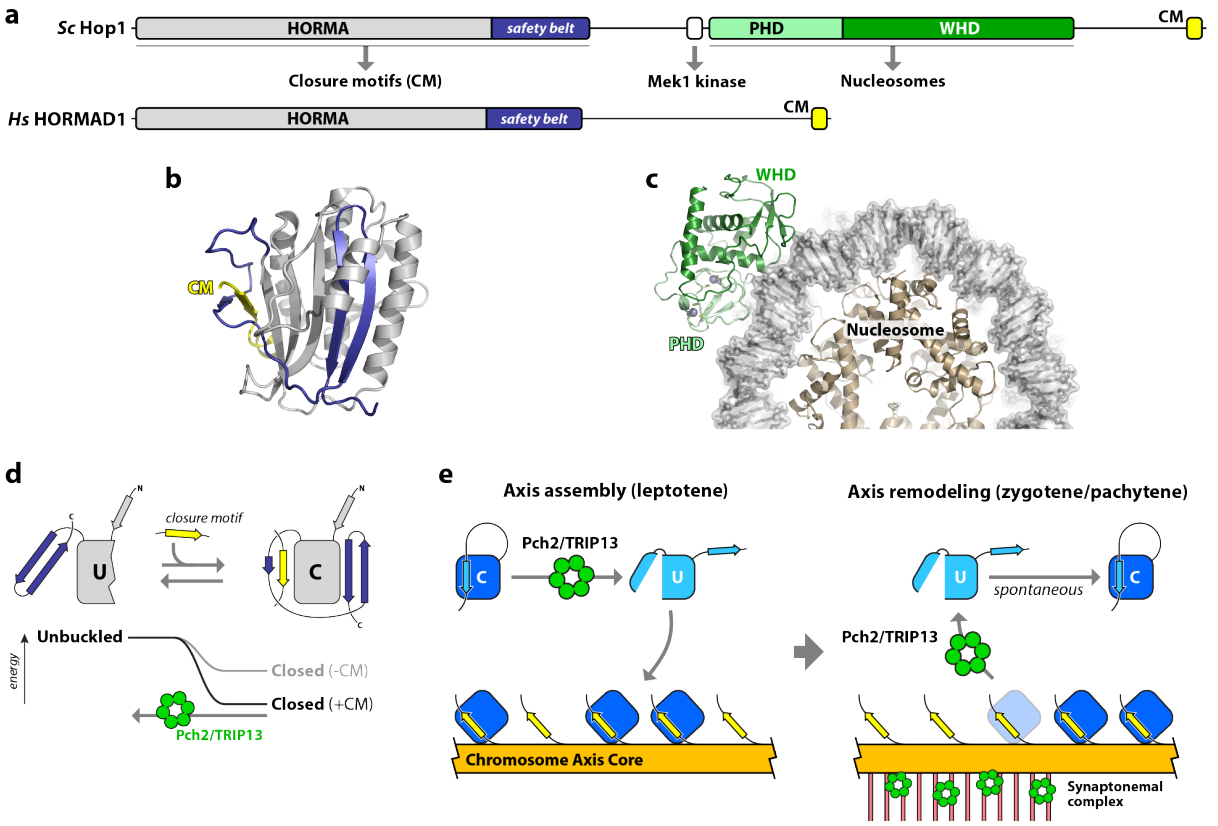

Figure 2.3: **Meiotic HORMAD structure and regulation** (a) Schematic of domain architecture of *S. cerevisiae* Hop1 (top) and *H. sapiens* HORMAD1 (bottom). Both proteins encode an N-terminal HORMA domain (gray/blue) and a C-terminal closure motifs (yellow) (Kim et al., 2014; West et al., 2018). *S. cerevisiae* Hop1 T318 forms a docking site for the Mek1 kinase when phosphorylated (Carballo et al., 2008; Xie et al., 2018). Fungal and plant meiotic HORMADs encode a central DNA-binding domain comprised of a PHD finger domain (PHD) and diverged winged-helix turn helix domain (WHD) (Ur et al., 2021). (b) Structure of *C. elegans* HIM-3 (gray, with C-terminal safety belt blue) bound to a closure motif from HTP-3 (yellow) (PDB ID 4TZJ; (Kim et al., 2014)). (c) Structure of the *S. cerevisiae* Hop1 PHD/WHD module (green) bound to a nucleosome. The composite DNA-binding interface uses surfaces on both the PHD and WHD domains, and specifically recognizes strongly bent nucleosomal DNA (Ur et al., 2021). (d) Conformational dynamics of meiotic HORMADs and regulation by Pch2/TRIP13. The HORMA domain can adopt two conformations, a high-energy "unbuckled" state (U) with the C-terminal safety belt disengaged from the HORMA domain core, and a lower-energy "closed" (C) state with the safety belt bound to a closure motif (yellow). Pch2/TRIP13 partially unfolds the HORMA domain N-terminus to destabilize the closed state and trigger closure motif dissociation (Ye et al., 2017; Ye et al., 2015). (e) Model for HORMAD association with the chromosome axis. In early meiotic prophase (leptotene), soluble meiotic HORMADs in an autoinhibited "self-closed" state are remodeled by soluble Pch2/TRIP13 to the unbuckled state, enabling their association with closure motifs on axis core proteins or axis-associated cohesin complexes (yellow). In zygotene/pachytene, the assembling synaptonemal complex (pink) recruits Pch2/TRIP13 to chromosomes, where it remodels HORMA-axis complexes to remove HORMADs from the axis. Spontaneous self-closure of removed HORMADs prevents reassociation with the chromosome axis.

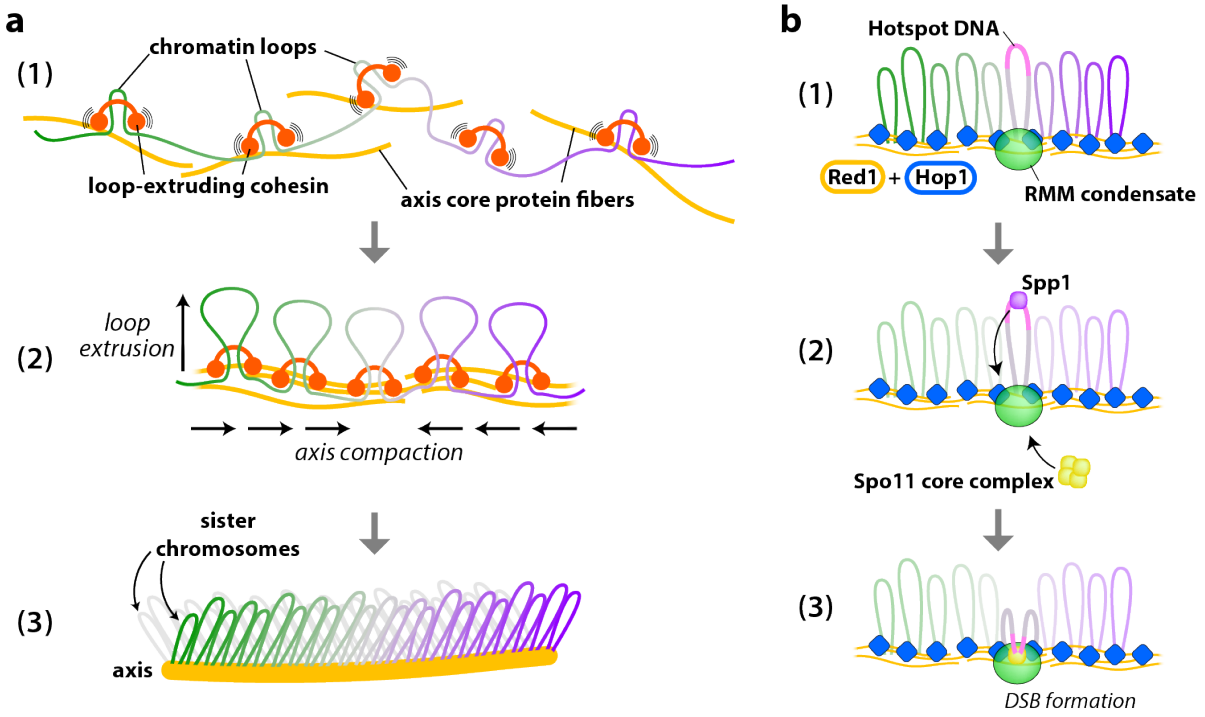

Figure 2.4: **Model for chromosome axis assembly and DSB formation** (a) Model for meiotic chromosome organization through cooperative action of cohesin and axis core proteins. (1) Active loop-extruding cohesin complexes (orange) are captured by axis core protein fibers (yellow) through an unknown mechanism. (2) Loop extrusion by cohesin complexes and bundling of axis core protein fibers result in the formation and continual compaction of the chromosome axis. (3) The completed chromosome axis organizes parallel arrays of sister chromosomes (gray and green-purple). (b) Model for axis-mediated DSB formation in *S. cerevisiae*. (1) Axis-associated Hop1 (blue) recruits the RMM proteins Rec114, Mei4, and Mer2 to form a phase separated condensate (green) on the axis (Claeys Bouuaert, 2021; Rousova, 2020; Tsai et al., 2020). (2) Spp1 (purple) recognizes epigenetic marks at hotspots and recruits these loci to RMM condensates (Acquaviva et al., 2013; Sommermeyer et al., 2013). (3) RMM condensates further recruit the Spo11 core complex (yellow) to generate a DSB (Claeys Bouuaert, 2021).

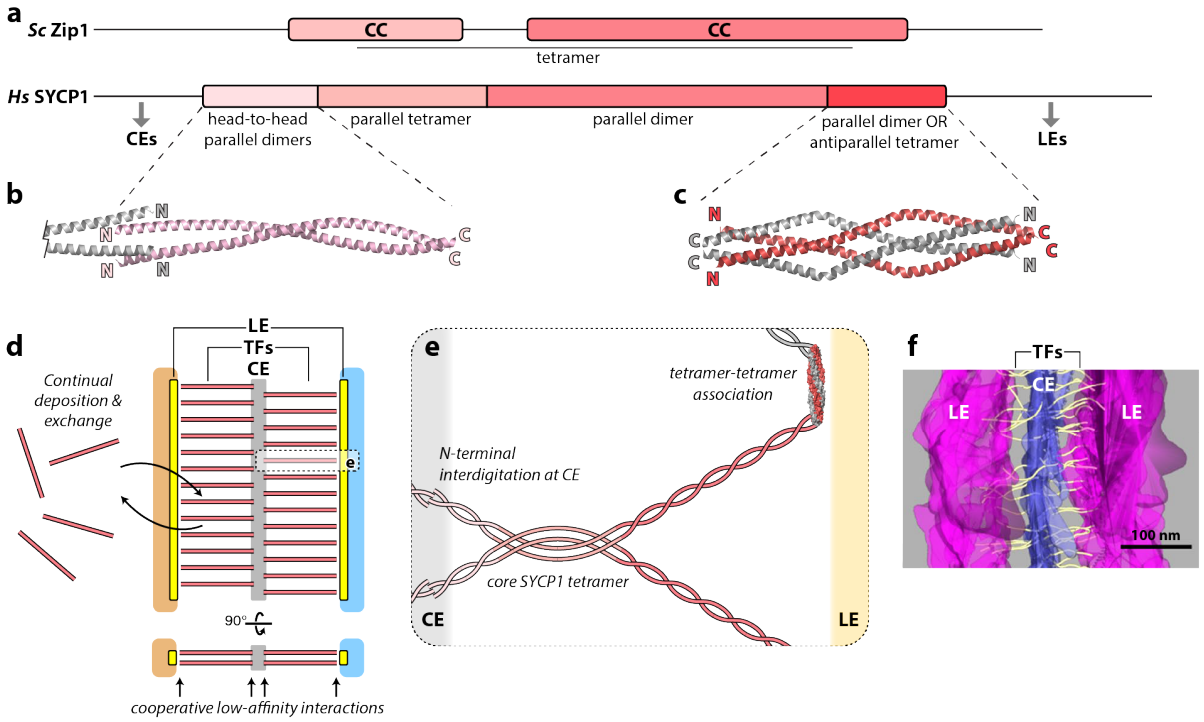

Figure 2.5: **Self-assembly of the synaptonemal complex transverse filaments** (a) Schematic of SC TF proteins from *S. cerevisiae* (Zip1, top) and *H. sapiens* (SYCP1, bottom). Predicted coiled coil regions for both are shown in pink. A fragment of *S. cerevisiae* Zip1 encompassing residues 243-700 (of 875) forms homotetramers in solution (Dong and Roeder, 2000). The four shaded regions of *H. sapiens* SYCP1 form coiled-coil oligomers as shown in vitro (Dunce et al., 2018). (b) Structure of a head-to-head pair of parallel coiled-coil dimers of the *H. sapiens* SYCP1 N-terminal coiled coil region (PDB ID 6F62; (Dunce et al., 2018)). (c) Structure of an antiparallel coil-coil tetramer of the *H. sapiens* SYCP1 C-terminal coiled coil region (PDB ID 6F63; (Dunce et al., 2018)). (d) Model for dynamic assembly of the SC, with TF N-termini embedded in the CE (gray) and C-termini interacting with the LEs (yellow). TF proteins are continually deposited and exchanged into the SC even after assembly. The proposed "liquid crystal" nature of the SC may be mediates by cooperative, low-affinity interactions between TF proteins and with both CE and LE proteins. (e) Closeup schematic of a single *H. sapiens* SYCP1 TF, with the protein's N-terminal coiled-coil region mediating self-interactions at the CE by interdigitation, the core SYCP1 tetramer assembled through the tetrameric coiled-coil segment, and a pair of dimeric coiled-coils extending to the LE. The C-terminal region of the SYCP1 coiled-coil may mediate interactions with other SYCP1 tetramers through the formation of antiparallel coiled-coil tetramers (Dunce et al., 2018). Not shown are the disordered N- and C-termini of SYCP1 that likely mediate interactions with CE and LE proteins, respectively. (f) Annotated density of a *M. musculus* SC from a cryo-electron tomography experiment, with LEs colored magenta, the CE blue, and the 3D network of TFs yellow. Scale bar = 100 nm. Reprinted from (Spindler et al., 2019).

Figure 2.6: **Architecture of cohesin complexes** (a) Loop extrusion by cohesin (adapted from (Fudenberg et al., 2016)). (1) A loop-extruding complex (orange) binds chromosomal DNA (green-gray-purple gradient); (2) Processive motor activity mediates nucleation and expansion of a chromatin loop; (3) loop extrusion halts when the complex encounters a boundary in the form of DNA-bound CTCF (blue). (b-c) Schematic of the active loop-extruding form of cohesin from *S. cerevisiae* (b) and *H. sapiens* (c), based on a recent cryo-EM structure of the DNA-bound *H. sapiens* cohesin complex (Shi et al., 2020). Meiosis-specific subunits are noted with dashed outlines (see Table S1 for cohesin subunits in other model organisms). The conserved CTCF binding site on the HAWK-kleisin complex (Li et al., 2020) is denoted with a dashed outline on the SA1/2 subunit (green). (d) Top: Schematic of the organization of interphase chromosomes into TADs (topologically associating domains) by cohesin complexes (orange) and CTCF (red). Bottom: Schematic of chromatin contact patterns revealed by Hi-C in regions organized into TADs (Dixon et al., 2012; Rao et al., 2014). High contact levels are indicated by deeper shades of red. (e) Top: Schematic of the organization of meiotic prophase chromosomes into linear loop arrays by the chromosome axis (yellow). Bottom: Contact patterns of meiotic prophase chromosomes revealed by Hi-C in *S. cerevisiae* (left) and *M. musculus* (right). In *S. cerevisiae*, reproducible cohesin binding sites function as chromatin loop bases, resulting in a semi-regular pattern of focal interactions (Schalbetter et al., 2019). In *M. musculus*, loops are longer than in *S. cerevisiae* and are largely randomly positioned, resulting in a more diffuse contact pattern (Patel et al., 2019).

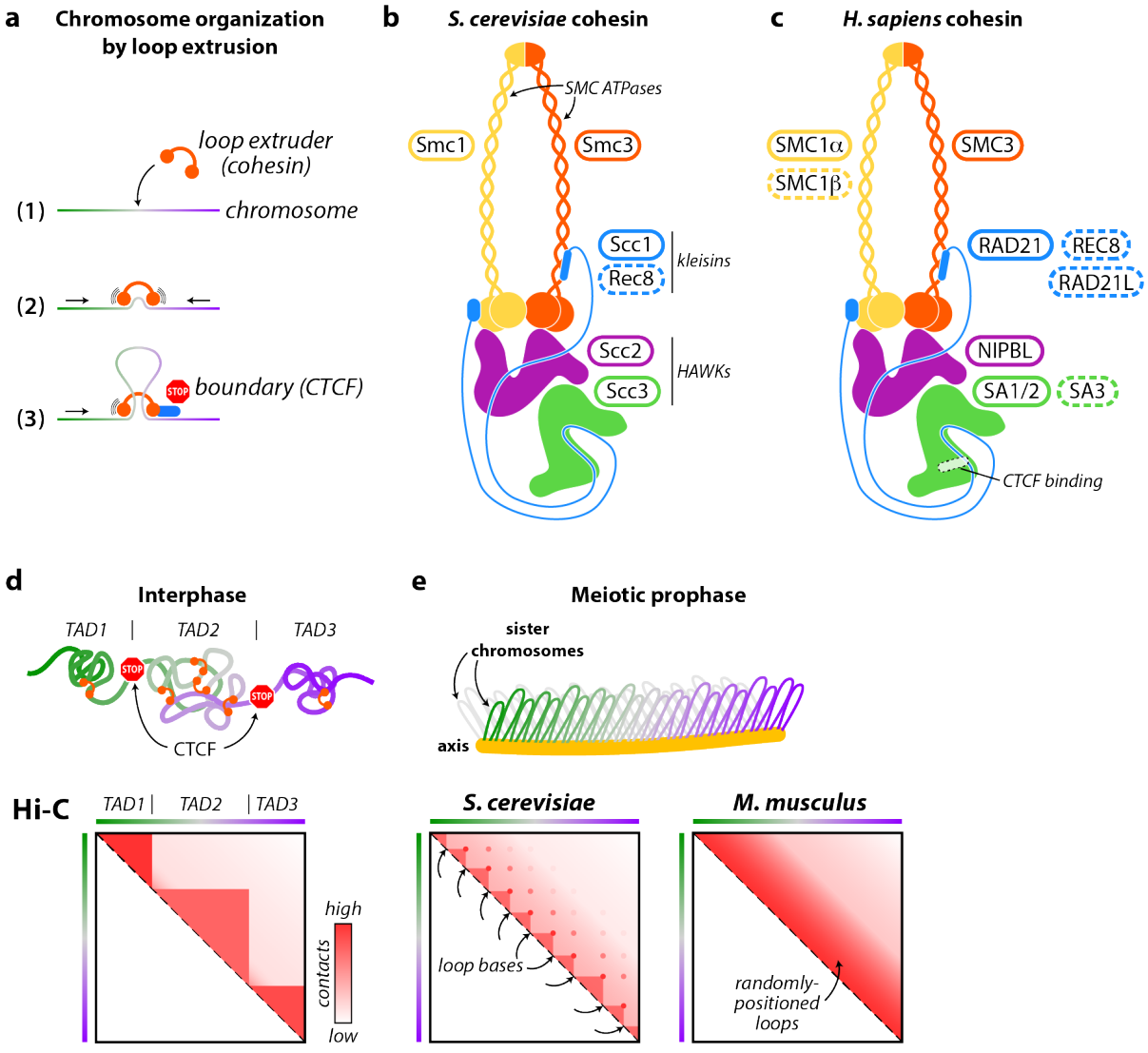
a
Chromosome organization by loop extrusion
loop extruder (cohesin)
(1)
chromosome
(2)
(3)
STOP
boundary (CTCF)
b
S. cerevisiae cohesin
SMC ATPases
Smc1
Smc3
Scc1
Rec8
kleisins
Scc2
Scc3
HAWKs
c
H. sapiens cohesin
SMC1α
SMC1β
SMC3
RAD21
REC8
RAD21L
NIPBL
SA1/2
SA3
CTCF binding
d
Interphase
TAD1
TAD2
TAD3
STOP
CTCF
e
Meiotic prophase
sister chromosomes
axis
Hi-C
TAD1
TAD2
TAD3
high
contacts
low
S. cerevisiae
loop bases
M. musculus
randomly-positioned loops

Table 2.1: **Major Meiotic Chromosome Associated Proteins**

Cohesin complex	*Saccharomyces cerevisiae*	*Schizosaccharomyces pombe*	*Mus musculus*	*Homo sapiens*	*Drosophila melanogaster*[2]	*Caenorhabditis elegans*	*Arabidopsis thaliana*
Somatic							
SMC ATPase	Smc1 (P32908)	Psm1 (O94383)	SMC1A (Q9CU62)	SMC1A (Q14683)	SMC1 (FBgn0040283)	HIM-1/SMC-1 (O01789)	SMC1 (Q6Q1P4)
SMC ATPase	Smc3 (P47037)	Psm3 (O42649)	SMC3 (Q9CW03)	SMC3 (Q9UQE7)	SMC3 (FBgn0015615)	SMC-3 (B2FDA8)	SMC3 (Q56YN8)
Kleisin	Mcd1/Scc1 (Q12158)	Rad21 (P30776)	RAD21 (Q61550)	RAD21 (O60216)	vtd (FBgn0260987)	SCC-1 (Q19325)	SYN2 (Q9FQ20), SYN3 (Q9FQ19), SYN4 (Q8W1Y0)
HAWK	Irr1/Scc3 (P47037)	Psc3 (O13816)	SA-1/STAG1 (Q9D3E6), SA-2/STAG2 (O35638)	SA-1/STAG1 (Q8WVM7), SA-2/STAG2 (Q8N3U4)	SA/Stromalin (FBgn0020616)	SCC-3 (Q19555)	SCC3 (O82265)
"loader" HAWK (req. for loop extrusion)	Scc2 (Q04002)	Mis4 (Q09725)	NIPBL (Q6KCD5)	NIPBL (Q6KC79)	Nipped-B (FBgn0026401)	PQN-85 (Q95XZ5)	SCC2 (A5HEI1)
"loader" accessory	Scc4 (P40090)	Ssl3 (O94459)	MAU2 (Q9D2X5)	MAU2 (Q9Y6X3)	Mau2 (FBgn0038300)	MAU-2 (O17581)	SCC4 (Q9FGN7)
Meiosis-specific							
SMC ATPase	-	-	SMC1B (Q920F6)	SMC1B (Q8NDV3)	ORD (FBgn0003009)[4]	-	
Kleisin (sister cohesion)	Rec8 (Q12188)	Rec8 (P36626)	REC8 (Q8C5S7)	REC8 (O95072)	SOLO (FBgn0283440)	REC-8 (Q9XUB3) COH-3 (Q19232), COH-4	SYN1 (Q9S7T7)
Kleisin (axis assembly)	-	-	RAD21L (A2AU37)	RAD21L Q9H4I0	C(2)M (FBgn0028525)	(Q95XJ4)[3]	-
HAWK	-	Rec11 (Q92380)	SA-3/STAG3 (O70576)	SA-3/STAG3 (Q9UJ98)	SUNN (FBgn0052088)		
Chromosome axis							
Axis core (long)	Red1 (P14291)	Rec10 (Q09823)	SYCP2 (Q9CUU3), SYCP2L (A0A0M3U1B0)[1]	SYCP2 (Q9BX26), SYCP2L (Q5T4T6)[1]	-	-	ASY3 (Q0WR66)
Axis core (short)	-	Rec27 (Q9USR4)	SYCP3 (P70281)	SYCP3 (Q8IZU3)	-	-	ASY4/At2g33793 (F4IFY5)
other axis-associated		Rec25 (Q9C115), Mug20 (Q9HGN4)					
Meiotic HORMAD(s)	Hop1 (P20050)	Hop1 (Q9P7P2)	HORMAD1 (Q9D5T7)	HORMAD1 (Q86X24)	-	HIM-3 (G5EBG0) HTP-1 (Q20305), HTP-2	ASY1 (F4HRV8)
			HORMAD2 (Q5SQP1)	HORMAD2 (Q8N7B1)		(Q95XC8)[3] HTP-3 (O01820)	ASY2 (F4JTJ9)
Pch2/TRIP13	Pch2 (P38126)	-	TRIP13 (Q3UA06)	TRIP13 (Q15645)	Pch2 (FBgn0051453)	PCH-2 (Q09535)	PCH2 (Q8H1F9)
Synaptonemal Complex							
Transverse filament	Zip1 (P31111)	-	SYCP1 (Q62209)	SYCP1 (Q15431)	C(3)G (FBgn0000246)	SYP-1 (Q9N5K3) SYP-5 (Q9N3E8), SYP-6 (O44741)[3]	ZYP1a (Q9LME2), ZYP1b(P61430)
Central element	Ecm11 (Q04110)	-	SYCE1 (Q9D495)	SYCE1 (Q8N0S2)	Corona/CONA (FBgn0038612)	SYP-2 (O76388)	
	Gmc2 (Q06201)	-	SYCE2 (Q505B8)	SYCE2 (Q6PIF2)	Corolla (FBgn0267967)	SYP-4 (Q9N5K3)	
			SYCE3 (B5KM66)	SYCE3 (A1L190)			
			TEX12 (Q9CR81)	TEX12 (Q9BXU0)			
			SIX6OS1 (Q9CTN5)	SIX6OS1 (Q8N1H7)			
other (lateral)						SYP-3 (O62238)	

[1]Human SYCP2L localizes to SCs and centromeres in oocytes (PMID 26362258). Sequence analysis reveals a common domain structure with SYCP2 (DOI 10.1101/2021.02.06.430040)

[2]Flybase (flybase.org) identifiers reported for Drosophila melanogaster proteins

[3]Functionally redundant paralogs

[4]Assignment of *D. melanogaster* ORD as a likely SMC ATPase is based on structure prediction using the HHPRED server (https://toolkit.tuebingen.mpg.de/tools/hhpred)

Chapter 3

A Dual Mechanism for Meiotic Chromosome Axis Assembly.

3.1 Introduction

Meiosis, a hallmark of eukaryotic life required for sexual reproduction, is a two-staged cell division that gives rise to haploid gametes containing half the parental chromosome number. This ploidy reduction is made possible by homologous recombination in meiotic prophase I, a process of specific recognition and physical linkage of the homologs that enable their specific segregation. Meiosis II then acts to segregate the sister chromosomes for a final haploid product. After DNA replication, during which sister chromosomes are held together in a pair via cohesin complexes, meiotic recombination begins as a series of highly coordinated and ordered events. The foundation for homologous recombination is created by the deposition of the chromosome axis, a proteinaceous structure that organizes chromosomes into a linear array of loops (van Heemst and Heyting, 2000; Zickler and Kleckner, 1999). The axis consists

of three components; ring-like cohesin complexes containing a meiosis-specific kleisin subunit (Rec8 in the budding yeast *Saccharomyces cerevisiae*), axis core proteins (Red1) and a meiotic HORMAD protein (Hop1). Rec8-containing cohesin complexes act to extrude chromatin loops, contributing to the looped axis structure (Davidson et al., 2019)(Fudenberg et al., 2016)(Kim et al., 2019). Cohesin complexes are likely captured and consolidated by Red1, which assembles into coiled-coil fibers to form a long filamentous structure (West et al., 2019). Red1 also directly recruits the HORMAD protein Hop1. Axis localized Hop1/HORMADs act as master regulators of meiotic prophase I, first coordinating formation of double strand DNA breaks (DSBs) by Spo11 and associated proteins, then directing the repair of DSBs towards a crossover fate through inter-homolog repair. In late meiotic prophase, HORMADs are largely removed from the axis upon assembly of the synaptonemal complex, which links the chromosome axes of paired homologs and aids the resolution of recombination. The remaining axis components become integrated into the synaptonemal complex as this structure's so-called "lateral elements". Because of the importance of inter-homolog crossover formation to successful ploidy reduction and gamete formation, eukaryotes have evolved a range of mechanisms to ensure that each homolog pair receives at least one crossover. In *S. cerevisiae*, these mechanisms include boosting the levels of initial double-strand breaks on the smallest chromosomes, which otherwise may not receive a break. The mechanisms underlying this "small chromosome effect" are mostly unknown, though recent work has shown that chromosome axis and double-strand break protein levels are boosted on these chromosomes (Murakami et al., 2020). We recently found that in *S. cerevisiae* Hop1 mediates localization of the axis protein Red1 to chromosomes when the cohesin subunit Rec8 is deleted (Heldrich 2020). Hop1-dependent axis localizes to specific chromosome regions we term "islands" that are defined by high protein-coding density and

high nucleosome occupancy (Heldrich 2020). These islands are also enriched on the smallest chromosomes, suggesting that Rec8-independent axis-protein localization may underlie the enrichment of axis and DSB proteins on these chromosomes (Heldrich 2020). The *S. cerevisiae* meiotic HORMAD Hop1 has three well-characterized domains: an N-terminal HORMA domain (Aravind and Koonin, 1998), an "SQ/TQ cluster domain" (SCD) that is phosphorylated as part of a DSB-dependent signaling cascade, and a C-terminal "closure motif". The N-terminal HORMA domain binds closure motif sequences including in its own C-terminus and in the axis core protein Red1 (Kim et al., 2014; West et al., 2019; Woltering et al., 2000). In addition to these well-known domains, *S. cerevisiae* Hop1 also possesses a conserved central domain that has been suggested to encode a DNA-binding zinc finger fold, based on the presence of several conserved cysteine residues (Hollingsworth 1993). Subsequent studies with this isolated domain showed weak DNA binding activity . Nonetheless, the structure and biological roles of this domain remain mostly unknown. Here, we show that the Hop1 central region encodes a zinc-binding PHD finger domain tightly associated with a variant winged-helix family DNA binding domain. We find that this two-domain assembly tightly and specifically binds nucleosomes by recognizing the highly bent DNA at the nucleosome perimeter. Deletion of this "Chromatin Binding Region" (CBR), or targeted disruption of its nucleosome binding activity, compromises Rec8-independent axis assembly and results in a complete failure to produce viable gametes. Strikingly, most HORMAD proteins across eukaryotes encode a Hop1-like CBR or a similar domain with distinct architecture, suggesting that direct chromatin binding by meiotic HORMADs is a near-universal property of meiosis. We propose that HORMAD CBRs play multiple roles in meiosis, including tuning double-strand break levels across the genome to boost recombination on vulnerable chromosomes or chromosome regions.

3.2 Results

Meiotic HORMADs possess a highly variable central domain involved in direct chromatin binding

Meiotic HORMADs universally encode an N-terminal HORMA domain that binds short "closure motif" peptides in axis core proteins, and potentially other binding partners, to mediate their localization to the chromosome axis (West et al., 2018; Woltering et al., 2000). Unique among HORMA domain proteins, meiotic HORMADs also encode closure motifs at their own C-termini, which in *C. elegans* are involved in assembly of a hierarchical HORMAD complex but more commonly play an auto-inhibitory role to control the timing and extent of axis localization (Kim et al., 2014). In addition to the HORMA domain and closure motif, meiotic HORMADs encode a highly variable central region whose functions are not well-understood. *S. cerevisiae* Hop1 has been reported to encode a DNA-binding zinc finger domain within this region (Hollingsworth and Johnson, 1993), though its roles in chromosome axis assembly and meiotic recombination have not been investigated. To identify conserved domains in meiotic HORMADs, we used hidden Markov modeling methods. We identified meiotic HORMADs in a set of 110 diverse eukaryotes, then aligned these proteins and generated profile hidden Markov models (HMMs), then compared these to a database of conserved domains and structures (Figure 3-1a). We could identify meiotic HORMADs in 81 out of 110 genomes, and observed that those genomes lacking meiotic HORMADs also usually lack homologs of the chromosome axis core proteins (Red1, SYCP2/SYCP3) (Tromer et al., 2021). The meiotic HORMADs we could identify almost always encode both an N-terminal HORMA domain and a C-terminal closure motif, but show a strikingly variable architecture within their central domain. The most common feature

is a 60-70 residue domain predicted to adopt a winged helix-turn-helix (wHTH) fold, which is found in many DNA binding proteins. This domain is found across eukaryotic supergroups, and appears as either a single domain or a tandem repeat of two such domains (Figure 3-1a-b, Figure 3-3a). Specifically in Saccharomycetaceae – the fungal group that contains *S. cerevisiae* – we detected a conserved C-terminal extension to the wHTH domain, which we term HTH-C) (Figure 3-1c, Figure 3-3 b). In a large set of meiotic HORMADs from fungi and metazoa, a single wHTH domain is situated alongside a predicted PHD (Plant HomeoDomain) finger domain. The PHD domain encodes a set of seven conserved cysteine residues and one conserved histidine, which together coordinate two structural zinc ions. PHD domains are found in many chromatin reader proteins and chromatin-remodeling complexes, and typically bind modified or unmodified lysine residues in histone tails (Sanchez and Zhou, 2011). The PHD domain in meiotic HORMADs possesses a set of conserved hydrophobic and negatively-charged residues surrounding the putative lysine-binding pocket, supporting a role for these domains in binding histone tails (Figure 3-2). Curiously, these residues are highly diverged in the Saccharomycetaceae fungi, suggesting that *S. cerevisiae* Hop1 and its close relatives may have lost the ability to bind histone tails despite retaining the PHD domain (Figure 3-2a-c). Based on the conserved domains within the meiotic HORMAD central region, we propose that the last common ancestor (LCA) of eukaryotes encoded a meiotic HORMAD protein with one or two wHTH domains. In Opisthokonta, which includes fungi and metazoa, this architecture was modified to include a PHD finger domain situated N-terminal to a single wHTH domain, which was further elaborated to include the HTH-C domain in some fungi. Many groups, notably including mammals, have since lost these domains, and their meiotic HORMADs apparently encode only an N-terminal HORMA domain and a disordered C-terminal domain with a closure motif. Strikingly, however, the majority of

meiotic HORMADs across eukaryotes encode a central region with putative DNA or histone-tail binding activity. Based on the predicted functions of these domains, we term the central region of meiotic HORMADs the Chromatin-Binding Region or CBR.

Structure of the budding-yeast Hop1 CBR

To better understand the architecture of the meiotic HORMAD CBR, we purified and determined a 1.5 Å-resolution crystal structure of the central region of Hop1 from the budding yeast *Vanderwaltozyma polyspora* (residues 317-535; 34% identical to *S. cerevisiae* Hop1 in this region). This structure revealed a PHD finger domain spanning residues 319-374, which coordinates two zinc ions through its eight conserved cysteine and histidine residues (Figure 3-1d, Figure 3-2a-b). Despite the conservation of the zinc coordinating sites, we see a total degradation of the 4 key residues thought to bind modified or unmodified histone tails in the Saccharomycetaceae (Figure 3-2b,c). However, once we broaden the alignments, we see that other fungi have seemingly maintained conservation of key residues in the hydrophobic pocket (Figure 3-2a) and likely may still function to bind histone tails. The PHD domain is tightly associated with a variant wHTH domain (residues 374-439 in *V. polyspora*) (Figure 3-4a). The HTH-C domain that we identified in Saccharomycetaceae folds around the PHD and wHTH domains, with three β-strands forming a divergent wing in the wHTH domain, and a long C-terminal α-helix that folds against both domains to stabilize their rigid association (Figure 3-4b).

The Hop1 CBR module specifically binds nucleosomes

The presence of a PHD domain and a wHTH domain in the Hop1 CBR strongly suggests that this domain binds chromatin, potentially recognizing nucleosomes through a bipartite

DNA + histone tail recognition mechanism. To test this idea, we tested binding of both the *V. polyspora* and *S. cerevisiae* Hop1 CBRs to DNA and to mononucleosomes. We first attempted a streptavidin pulldown of the Hop1 CBR with biotinylated unmodified mononucleosomes, and saw a strong 1:1 association in the elution (Figure 3-5a). We next used cryo-electron microscopy (cryo-EM) to determine a high-resolution structure of the *S. cerevisiae* Hop1 CBR bound to a mononucleosome. We incubated purified mononucleosomes with a 20-fold molar excess of the Hop1 CBR and lightly crosslinked the sample using glutaraldehyde, then purified the complex by size exclusion chromatography (Figure 3-5b). We collected a cryo-EM dataset comprising 902,072 particles initially extracted from 1,314 micrographs. After 2D classification, we selected 353,418 particles for 3D reconstruction with multiple classes. The predominant class (160,538 particles) showed only a nucleosome, comprising an octamer of histone proteins (two copies each of histones H2A, H2B, H3, and H4) wrapped with 147 bp of DNA. A second class (96,535 particles) showed a nucleosome with clear density for a Hop1 CBR (Figure 3-6a-e). After particle re-extraction and 3D refinement, we obtained a 2.84 Å-resolution structure of the nucleosome alone (Figure 3-6f), and a 3.06 Å-resolution structure of the Hop1 CBR-bound nucleosome (Figure 3-6g, Figure 3-7a-b). A third minor class showed weak density for two Hop1 CBRs bound to symmetry-related positions on the two-fold symmetric nucleosome, but this class contained too few particles for a high-resolution reconstruction. The structure shows that the Hop1 CBR binds the strongly-bent nucleosomal DNA in a specific location at SHL3 (DNA bases 25-33 from the dyad axis). Here the CBR interacts with the major and minor groove of one DNA gyre through three DNA-binding loop regions, with K340 in the PHD domain interacting with the opposite DNA gyre to further stabilize the binding. Given the lack of histone interaction, we measured binding affinity of the Hop1 CBR for nucleosomes and for an isolated 40-base pair DNA fragment,

and observed a strong preference for binding intact nucleosomes (*Kd*=760 nM) over dsDNA (*Kd*=2.4 μM) (Figure 3-7d). We speculate that this difference in binding preference is based on the unique bent conformation of the nucleosomal DNA around the histone core. Interestingly, there is no electron density present for any histone tails in our structure (Figure 3-7a-c), indicating that the Hop1 CBR does not interact with either the folded histone-protein core regions or tails. The tail situated closest to the Hop1 PHD domain is the H2B N terminal tail. Although not present in the EM density, this tail appears to be ideally located to emerge between the two DNA gyres adjacent to the PHD domain. Despite the lack of electron density for the H2B tail, we reasoned that this tail may nonetheless be dictating the binding position of the Hop1 CBR on the nucleosome. To test this idea, we tested binding of the Hop1 CBR to reconstituted nucleosomes lacking the H2B tail, and observed no difference in binding affinity compared to nucleosomes assembled with full-length H2B. Moreover, we assembled complexes and collected an additional Cryo-EM dataset on the Hop1 CBR bound to nucleosomes lacking the H2B tail, and observed that the Hop1 CBR binds in the same position as observed in our high-resolution structure. Thus, at least in Saccharomycetaceae fungi, the Hop1 CBR interacts solely with the bent DNA of a nucleosome despite the presence of a PHD domain.

Identification of key residues and DNA structure necessary for binding

Based on our structure, we identified three loops in the Hop1 CBR that mediate DNA binding. Loop 1 is positioned in the PHD domain, with the side-chains of N362 and H365 interacting with the minor groove of base pair step SHL -2.5 (as measured from the nucleosome dyad axis). Loop 2 is in the wHTH domain, with R402, K403, K404, and K405 inserting into the minor groove of base pair step SHL -3 (Figure 3-7c). Through a structural comparison with

a nucleosome only structure from the same dataset, we see that Loop2 widens the gap in the minor groove of the DNA by 1 Angstrom at its binding location (Figure 3-8a-b).. Curiously, despite sharing a common fold with canonical DNA-binding wHTH domains, the Hop1 wHTH domain binds DNA on a distinct surface compared with these domains. Finally, Loop3 is in the HTH-C domain, with K452 and R458 binding base pair step SHL -3.5. To test the role of these three loops in nucleosome binding by the Hop1 CBR, we generated alanine mutants of each loop, plus constructs with two or all three loops mutated. We used electrophoretic mobility-shift assays (EMSAs) to test the affinity of each Hop1 CBR mutant for mononucleosomes. All single-loop and double-loop mutants reduced the Hop1 CBR's binding affinity for the nucleosome (Figure 3-7e-h). The most dramatic effects were observed with the Loop 2 alanine mutant and the Loop 1-2-3 mutant, reducing the affinity to 680μM and 180μM, respectively. These data allow us to conclude that Loop 2 is likely the most critical element in the Hop1 CBR for nucleosome binding. Curiously, Loop 2 is not conserved outside Saccharomycetaceae fungi (Figure 3-1c), lending further credence to the idea that these organisms' HORMAD CBR has evolved a chromatin binding mechanism distinct from other HORMADs encoding a PHD-wHTH domain pair.

The Hop1 CBR is required for proper meiosis

To assess the importance of the Hop1 CBR for meiosis, we generated a mutant *S. cerevisiae* strain with the Hop1 CBR (residues XXX-XXX) deleted, but maintaining the protein's other functionally-important domains. We observed a spore viability of 0% for the *hop1*Δ*CBR* strain, on par with that of a *hop1*Δ strain, suggesting a severe defect in one or more Hop1 functions. In the *hop1*Δ*CBR* strain, Hop1 was expressed and phosphorylated with near-wildtype levels and

timing (Figure 3-9b), and localized to chromosomes as observed by immunostaining spread meiotic chromosomes (Figure 3-9c). Using quantitative mass spectrometry of chromatin-enriched S. cerevisiae extracts, we showed that most important meiotic chromosome-localized proteins were able to localize to chromatin (Figure 3-9d). Finally, measurement of DNA double-strand breaks along one chromosome using Southern blots revealed only a slight reduction in DSB levels, alongside a minor shift in the pattern of DSBs indicating a shift in hotspot usage (not shown).Thus, most known functions of Hop1, including chromatin localization, phosphorylation, and DSB production, are unaffected by deletion of the Hop1 CBR. We speculate that the *hop1*Δ*CBR* strain may be severely defective for interhomolog crossover formation, potentially explaining the low spore viability.

The Hop1 CBR module is responsible for Rec8-independent axis localization

Our prior data (Heldrich 2020) revealed that Hop1 is responsible for Rec8-independent recruitment of the chromosome axis protein Red1 to “islands” along meiotic chromosomes, defined by high coding density and high nucleosomal occupancy. To determine the role of the Hop1 CBR in this activity, we performed ChIP-Seq for Hop1 and Red1 in *rec8*Δ, *hop1*Δ*CBR*, and double-mutant strains. The *hop1*Δ*CBR* strain showed a near-wild-type distribution of Hop1 and Red1 along chromosomes. In the *rec8*Δ strain, we observed the characteristic islands of Rec8-independent axis assembly. The double mutant strains showed near-zero occupancy of both Hop1 (Figure 3-9e) and Red1(Figure3-9f) on chromosomes, confirming that the Hop1 CBR is directly responsible for Rec8-independent chromosome axis assembly.

3.3 Discussion

Here we have determined the structure of the conserved non-vertebrate Hop1 central domain to be a CBR. We determined the structure of the CBR bound to a nucleosome and showed that this interaction is with the bent DNA around the nucleosome. We show how the CBR interacts with the DNA by an insertion of the protein's critical DNA binding loop 2 into the minor groove and a stabilization of K340 binding to the opposite DNA gyre. We see no evidence of interaction with the histone proteins at either their core or tail, suggesting that histone tail modifications play no role in the Saccharomycetaceae's CBR preference for nucleosomal binding and further its chromatin localization. However, due to the broad conservation of this domain (Figure 3-10a), we hypothesize that the HORMAD protein CBR of non-Saccharomycetaceae fungi and other Opisthokonts may have an ability to associate with histone tails. This data explains the previously published finding that Rec8-independent islands of axis-protein binding occur in nucleosome-enriched areas of the genome. Our prior work showed that in wild-type *S. cerevisiae* cells, the pattern of axis-protein deposition on chromosomes is a composite of focal Rec8-dependent peaks and broader Hop1-dependent islands, indicating that Hop1 is a critical factor for determining wild-type chromosome axis structure (Heldrich 2020). We previously showed that Hop1-dependent islands have higher levels of DSB formation and higher levels of the crossover factor Zip3 than the genome as a whole (Heldrich 2020). Our preliminary unpublished data also reveals altered crossover dynamics, and suggests a reduction of crossovers in the absence of the CBR (not shown). This suggests that the regulation of meiotic recombination may differ across the genome, based on whether the axis in that region has been assembled in a Rec8- or Hop1-dependent manner (Figure 3-10b). We further hypothesize that in regions of high nucleosome density, the chromosome axis can be deposited at a higher density leading to

enriched dynamics of recombination factors. Meiotic HORMADs directly interact with the RMM complex (Rec114, Mei4, MER2), which is a precursor to Spo11 recruitment and therefore the formation of DSBs (Kumar et al., 2018; Li et al., 2006). Work from other labs has shown that a higher density of the RMM recombination-promoting complex can alter their dynamics to form phase separated species (Claeys Bouuaert, 2021). It is possible that this higher density of nucleosomes leads to a higher seeding of chromosome axis and therefore Hop1 density, leading to a higher density of recombination factors, allowing them to form preferential sites for crossovers. Our data clearly demonstrate a critical role for the *S. cerevisiae* Hop1 CBR in both assembly of the chromosome axis and in regulation of DSBs to become interhomolog crossovers. Based on the broad distribution of a putative CBR in meiotic HORMADs across eukaryotic supergroups (Figure 3-10a), we propose that these proteins' CBRs play similar roles in chromosome axis assembly and meiotic recombination across eukaryotes. One key role for these HORMAD CBRs may be to bias the distribution of chromosome axis components, DSBs, and recombination to regions of the genome which, like the three smallest chromosomes of S. cerevisiae, may be at risk of chromosome mis-segregation without this bias. Species that have lost the HORMAD CBR may have evolved alternative mechanisms for biasing DSB and recombination distribution in the genome, such as the vertebrate specific ANKRD31 protein that promotes axis formation at the X and Y chromosome PAR and other regions to promote accurate homolog segregation(Acquaviva et al., 2020; Papanikos et al., 2019).

3.4 Materials and Methods

Protein Expression and Purification

Ligation-independent cloning was used to clone *S. cerevisae* Hop1$^{322-537}$ and *V polyspora* Hop1$^{319-529}$. To express TEV protease-cleavable, His6-tagged or His6-MBP tagged constructs, Hop1 fragments were cloned into 29666 (His6) and 29706 (His6-MBP)respectively. DNA binding mutants were generated by mutagenic PCR using the MBP tagged construct. For protein expression, plasmids encoding Hop1 fragments were transformed into *E. coli* LOBSTR cells, and grown in 2XYT media supplemented with ZnCl2, carbencillin, and chloroemphenical. Cells were grown at 37°C to an OD600 of 0.6, shifted to 20°C and protein expression induced with 0.25 mM IPTG, and grown 16 hours. For protein purification, cells were harvested by centrifugation, suspended in resuspension buffer (20 mM Tris–HCl pH 7.5, 300 mM NaCl, 20 mM imidazole, 2uM BME and 10% glycerol) and lysed by sonication. Lysate was clarified by centrifugation (16 000 rpm 30 min), then supernatant was loaded onto a Ni2+ affinity column (HisTrap HP, GE Life Sciences) pre-equilibrated with resuspension buffer. The column was washed with resuspension buffer, and eluted with a buffer containing 250 mM imidazole and 100 mM NaCl. The elution was loaded onto an anion-exchange column (Hitrap Q HP, GE Life Sciences) and the desired protein was collected in the flow through. The flow through was then concentrated to 500μL by ultrafiltration (Amicon Ultra-15, EMD Millipore), then passed over a size exclusion column (HiLoad Superdex 200 PG, GE Life Sciences) in a buffer containing 20 mM Tris–HCl pH 7.5, 300 mM NaCl, 10% glycerol and 1 mM DTT. For crystallization experiments, the N-terminal His6-tag on *V polyspora* Hop1$^{317-535}$ was cleaved over night with TEV protease, passed over a second Nickel column, concentrated and ran over a size exclusion column. Purified proteins

were concentrated by ultrafiltration and stored at 4°C for crystallization, or aliquoted and frozen at 80°C for biochemical assays. All mutant proteins were purified as wild-type.

Nucleosome Core Particle Reconstitution

Unfolded xenopus histones were bought in powder form from the Histone source and assembled by refolding together. Briefly, histones were resuspended in Unfolding Buffer (6M Guanidinium HCL, 20mM Tris pH 7.5, 5mM DTT) to a concentration of 2mg/mL and mixed together in a molar ratio of 1:1:0.9:0.9 for H2B:H2A:H4:H3 and diluted to a final concentration of 1mg/mL. The solution was placed in a dialysis cassette (Slide-A-Lyzer 3.5kDa cutoff) and buffer exchanged 3 times (4h, 12h, 4h) in Refolding Buffer (2M NaCl, 10mM Tris pH 7.6, 1mM EDTA, 1mM DTT). Lastly, the octamer was run on a S200 Size exclusion column in Refolding Buffer to separate from any unassembled dimer. The Widom 601 sequence was amplified using a PCR reaction and purified by loading and elution onto an anion exchange column (HiTrap Q HP, GE Life Sciences). DNA and the histone core particles were then folded together by overnight dialysis from 1.4M TEK (1.4M KCl, 10mM Tris pH 7.5, 0.1mM EDTA, 1mM DTT), to 10mM TEK (10mM KCl, 10mM Tris pH 7.5, 0.1mM EDTA, 1mM DTT). Folded nucleosomes were purified on a size exclusion column (Superose 6) to ensure quality and purity.

X-ray Crystallography

V. polyspora Hop1 was buffer exchanged into Crystalization Buffer (20mM Tris pH 7.5, 50mM NaCl, 1mM DTT) concentrated to 20mg/ml and screening trays were set with a wide array of predefined crystal screens, using a MOSQUITO tray setter. Initial crystals were strong enough to pick from the screening tray with the condition 0.1M MES pH 6.5 and 30% (v/v) PEG

400. A dual dataset was collected using the ALS 12.3.1 beamline to generate a native and an additional set using the Zn wavelength to phase off of. For structure determination the following programs were used; XDS for indexing and integration, AIMLESS and TRUNCATE for scaling and structure-factor calculation. hkl2map/SHELX for site identification, Phenix Autosol pipeline for phasing and automatic model building, model rebuilt in COOT, and refined in phenix.refine.

Cryo-electron Microscopy Sample Preparation

Nucleosomes were incubated with a 20 fold excess of *Sc* Hop1 CBR in crosslinking buffer (20mM HEPES 7.5, 50mM NaCl), for 30mins on ice, brought to room temperature for 5 mins, then crosslinked with a final concentration of 0.02% glutaraldehyde for 30 mins. The crosslinking reaction was the quenched using 1 volume of 1M glycine, concentrated and run over a Superose 6 column, then concentrated again to 3μM for cryo-grid setting.

Cryo-EM Data Collection and Refinement

A full dataset of 1,314 micrographs were collected using a FEI Titan Krios G3 at magnification 130,000x, using a K2 Summit direct electron detector, at a defocus range of -0.5 to -2μm. CryoSparc was used as a pipeline to process data and extract 902,072 particles total. From that particle set, 353,418 were refined and after iterative sorting and re-extraction, the Hop1 CBR with Nucleosome structure was generated from 96.535 particles. The Nucleosome alone structure was generated from 160,538 particles. To build the model, used PDB ID 3LZ0 as a template for the nucleosome core particle, and a threaded model of *Sc* Hop1$^{322-524}$ generated by PHYRE server using structure of *Vp* Hop1$^{319-529}$ as a template. model rebuilt in COOT, real-space refined in phenix.refine. The nucleosome has overall two-fold rotational (C2) symmetry,

but the Widom 601 nucleosome positioning sequence is not symmetric. Since our structures are unable to unambiguously assign the identity of each nucleotide base in our maps, we independently built and refined models with both orientations and examined the model-map correlation across the entire DNA sequence. For both Hop1-bound and unbound nucleosome structures, one DNA orientation clearly showed a higher model-map correlation than the other, especially in the positions that differ in purine versus pyrimidine identity between the two orientations (not shown).

EMSA Gel Shifts

EMSA reactions were prepared in Binding Buffer (20 mM Tris–HCl pH 7.5, 2uM BMe, 25mM NaCl, 10% glycerol) by keeping the Nucleosome concentration constant at 50 nM and varying the protein concentration. After 15 min incubation and addition of 5% (w/v) sucrose, free Nucleosome and DNA-protein complexes were resolved by electrophoresis on 6% TBE-acrylamide gels pre-equilibrated (pre-run for 60 min at 150 V) in 0.2X TBE running buffer. Gels were run for 90 min at 120V at 4°C. Gels were stained with SytoxGreen DNA stain and imaged using a Bio-Rad ChemiDoc system using filters to image SYBRGreen. Gel bands were quantified using ImageJ (https://imagej.net), and binding curves were calculated using GraphPad Prism (https://www.graphpad.com).

3.5 Acknowledgements

SU acknowledges support from the UCSD Molecular Biophysics Training Grant (NIH T32 GM008326) and the National Science Foundation Graduate Research Fellowship program. KDC is supported by NIH R01 GM104141. This work was partially conducted at the Advanced

Light Source (ALS), a national user facility operated by Lawrence Berkeley National Laboratory on behalf of the Department of Energy, Office of Basic Energy Sciences, through the Integrated Diffraction Analysis Technologies (IDAT) program, supported by DOE Office of Biological and Environmental Research. Additional support comes from the National Institute of Health project ALS-ENABLE (P30 GM124169) and a High-End Instrumentation Grant S10OD018483.

Chapter 3, is a reprint of material currently being prepared for submission for publication: **Ur, SU.***, Milano C*, Gu Y, Vale-Silva LA, Hochwagen A, Corbett K. A dual mechanism for meiotic chromosome axis assembly. *in preparation*. The dissertation author was the primary author.

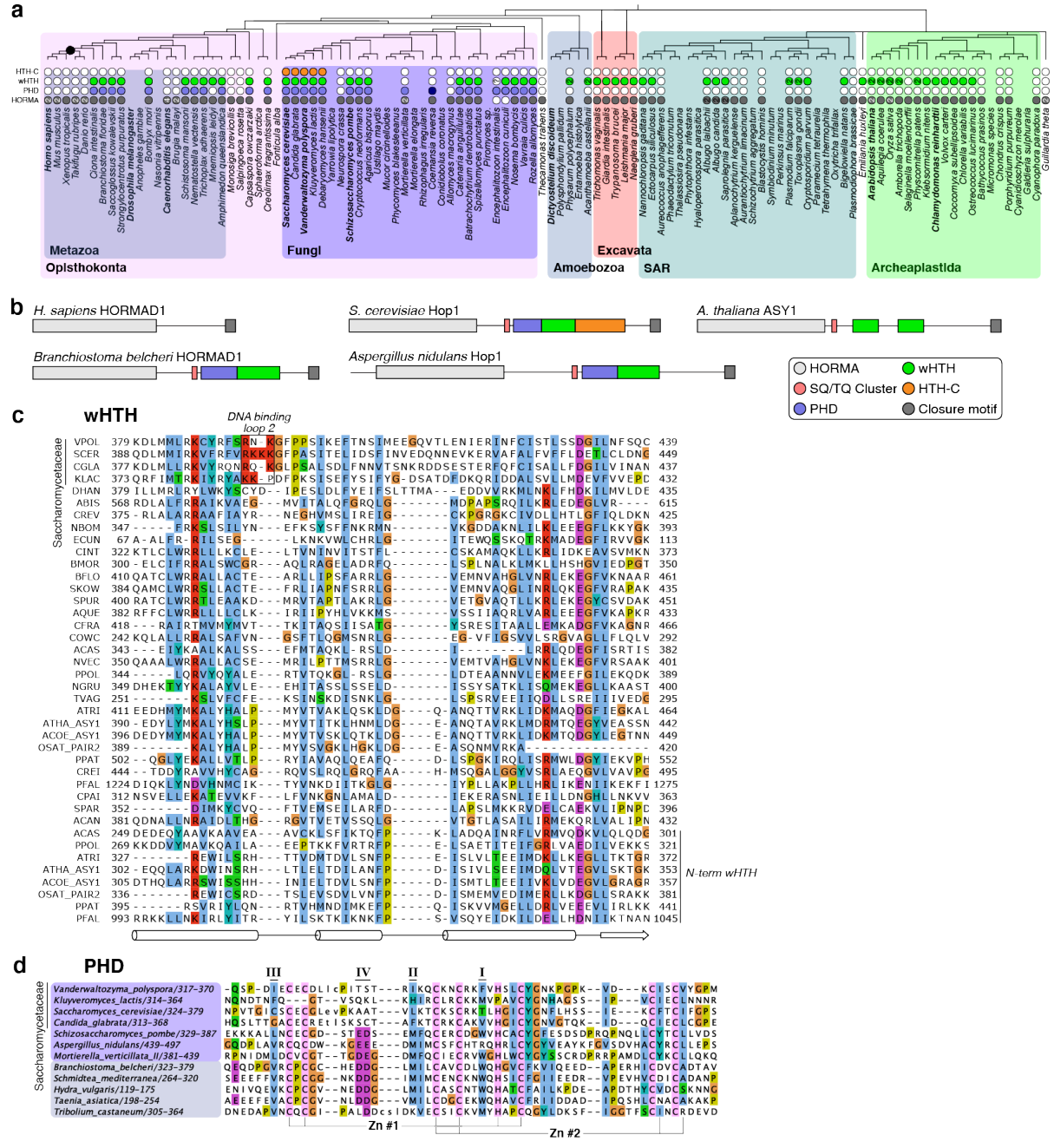

Figure 3.1: **Meiotic HORMADs encode a variable central chromatin-binding regiona.** Evolutionary tree of 110 diverse eukaryotes, with individual domains in meiotic HORMAD proteins (as detected by HMM searches) noted. **b.** Domain structures of meiotic HORMAD proteins from *H. sapiens* (Opisthokonta, Metazoa), Branchiostoma belcheri (Opisthokonta, Metazoa), *S. cerevisiae* (Opisthokonta, Fungi), *Aspergillus nidulans* (Opisthokonta, Fungi), and *Arabidopsis thaliana* (Archeaplastida). Domains are colored as in panel (a). **c.** Sequence alignment of the meiotic HORMAD wHTH domain, showing a subset of identified domains. See Figure 3-3 for full alignment. **d.** Sequence alignment of the meiotic HORMAD PHD domain, showing a subset of identified domains. See Figure 3-2a for full alignment, and Figure 3-2c for an expanded alignment of Saccharomycetaceae PHD domains.

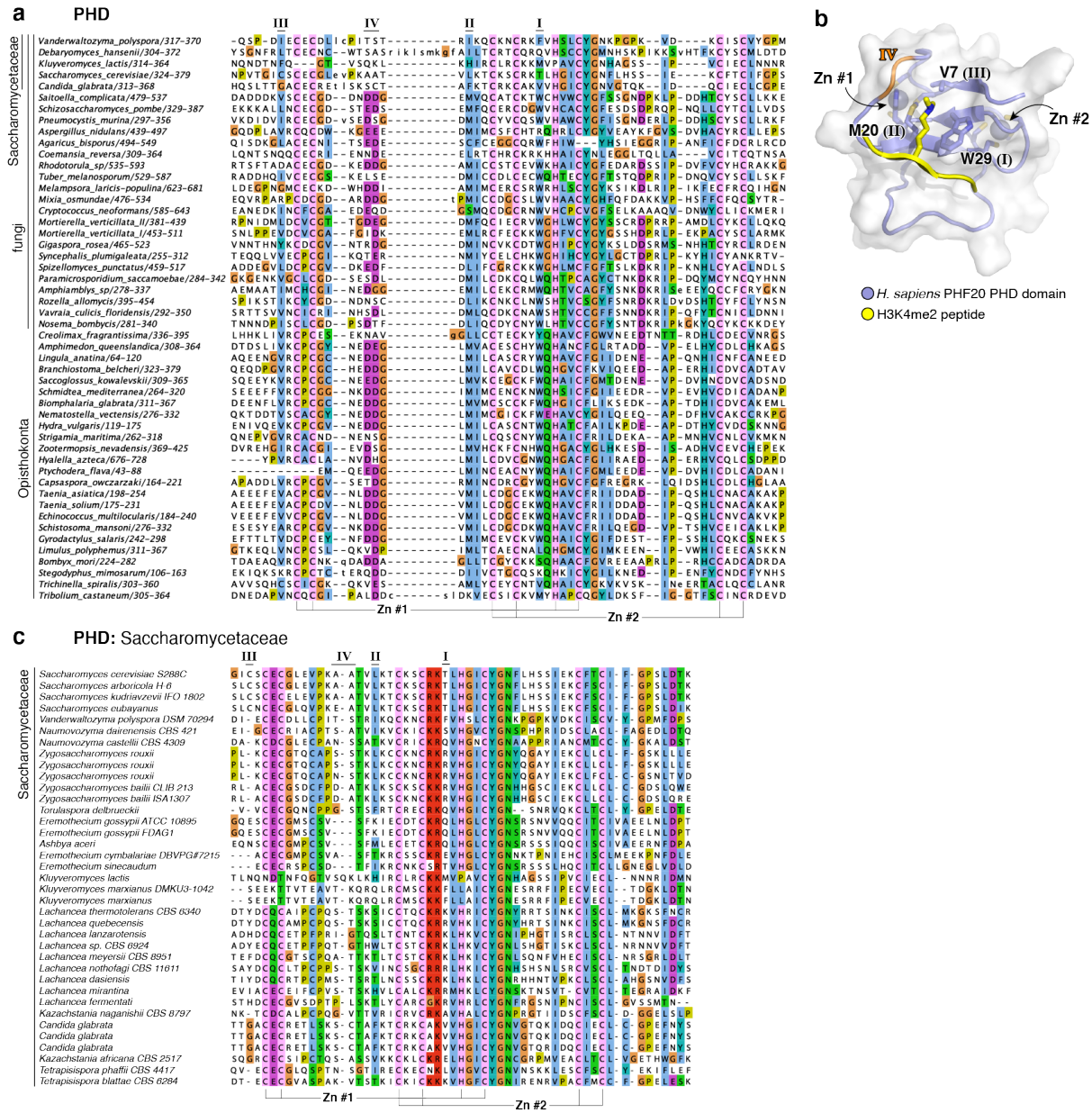

Figure 3.2: **Alignments of the CBR PHD domain a.** Larger Opisthokonta alignment of meiotic HORMAD PHD domains, showing conservation of key residues I, II, III, IV of the hydrophobic pocket in all but the Accharomycetaceae. **b.** Hydrophobic pocket of *H. sapiens* PHF20 PHD domain showing the 4 key residues involved in histone peptide binding. **c.** Saccharomycetaceae PHD alignments show a total degradation of key pocket residues I, II, III, IV.

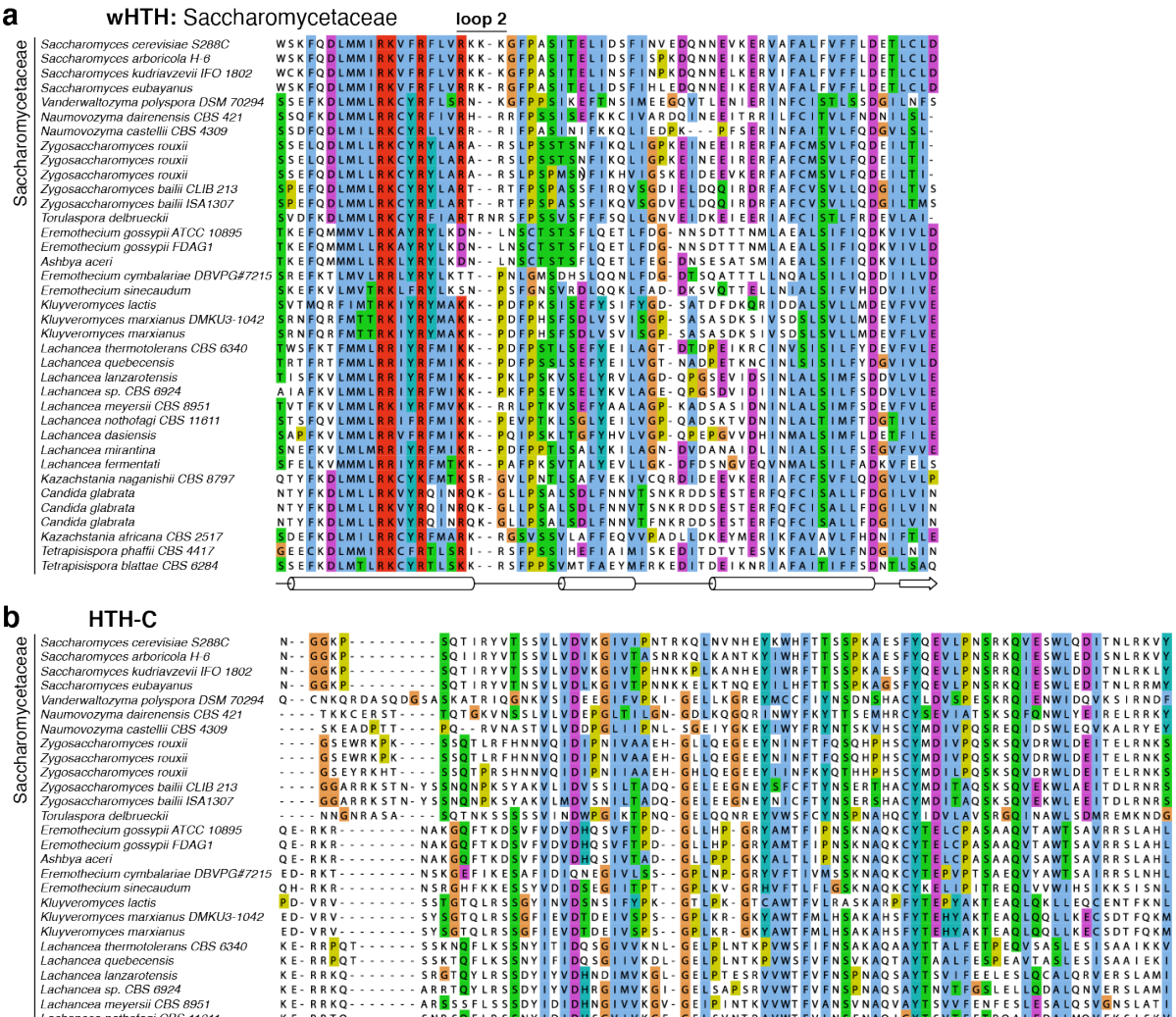

Figure 3.3: **Alignments of the CBR HTH domains a.** Saccharomycetaceae wHTH alignments show a conservation of predicted 3 alpha helices followed by a short beta sheet. **b.** Saccharomycetaceae HTH-C alignments show weaker conservation of a pair of beta sheets followed by a C terminal longer alpha helix.

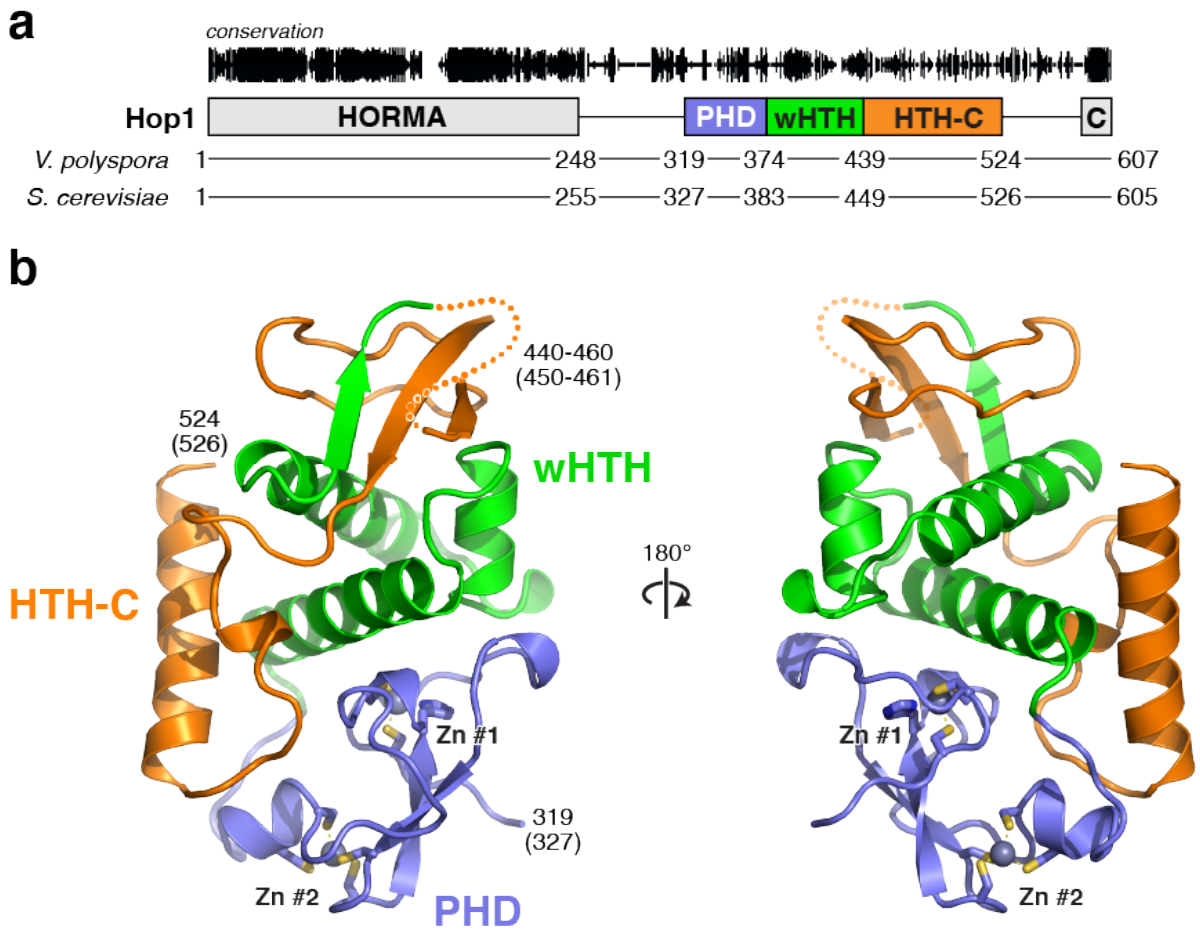

Figure 3.4: **Structure of the budding-yeast Hop1 CBR a.** Domain structure of budding-yeast Hop1, with domain boundaries for *S. cerevisiae* and *V. polyspora* Hop1 noted. **b.** Two views of the *V. polyspora* Hop1 CBR, with PHD domain colored blue, wHTH green, and HTH-C orange. Residue numbers are noted for *V. polyspora*, with equivalent residue numbers for S. cerevisiae.

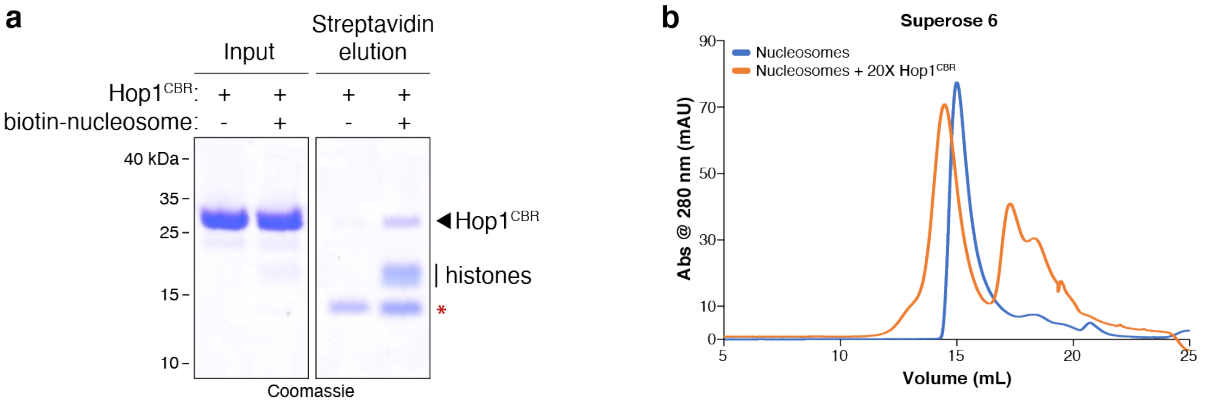

Figure 3.5: **Initial biochemical characterization of nucleosome binding to the Hop1 CBR** **a.** Streptavidin pull down with and without biotinylated nucleosomes with the Hop1 CBR. Hop1 CBR is pulled down with the nucleosome in a close to 1:1 ratio. **b.** Superose 6 columns of Nucleosomes alone (blue) or Nucleosome crosslinked with the Hop1^{CBR} (orange) show a 0.5mL shift in the crosslinked complex.

Figure 3.6: **Cryo-EM workflow a.** Sample micrograph of nucleosome with Hop1^{CBR}. Scale bar is 50nm. **b.** Representative 2D class averages of the 902,072 particles. **c.** Workflow of initial 3D models, to re-extracted and refined final 3D models. **d.** FSC Resolution of the nucleosome only structure shows a resolution of 2.84 Angstroms. **e.** FSC Resolution of the nucleosome with Hop1^{CBR} structure shows a resolution of 3.06 Angstroms. **f.** Local resolution map of the nucleosome only structure. **g.** Local resolution map of the Hop1^{CBR} with nucleosome structure.

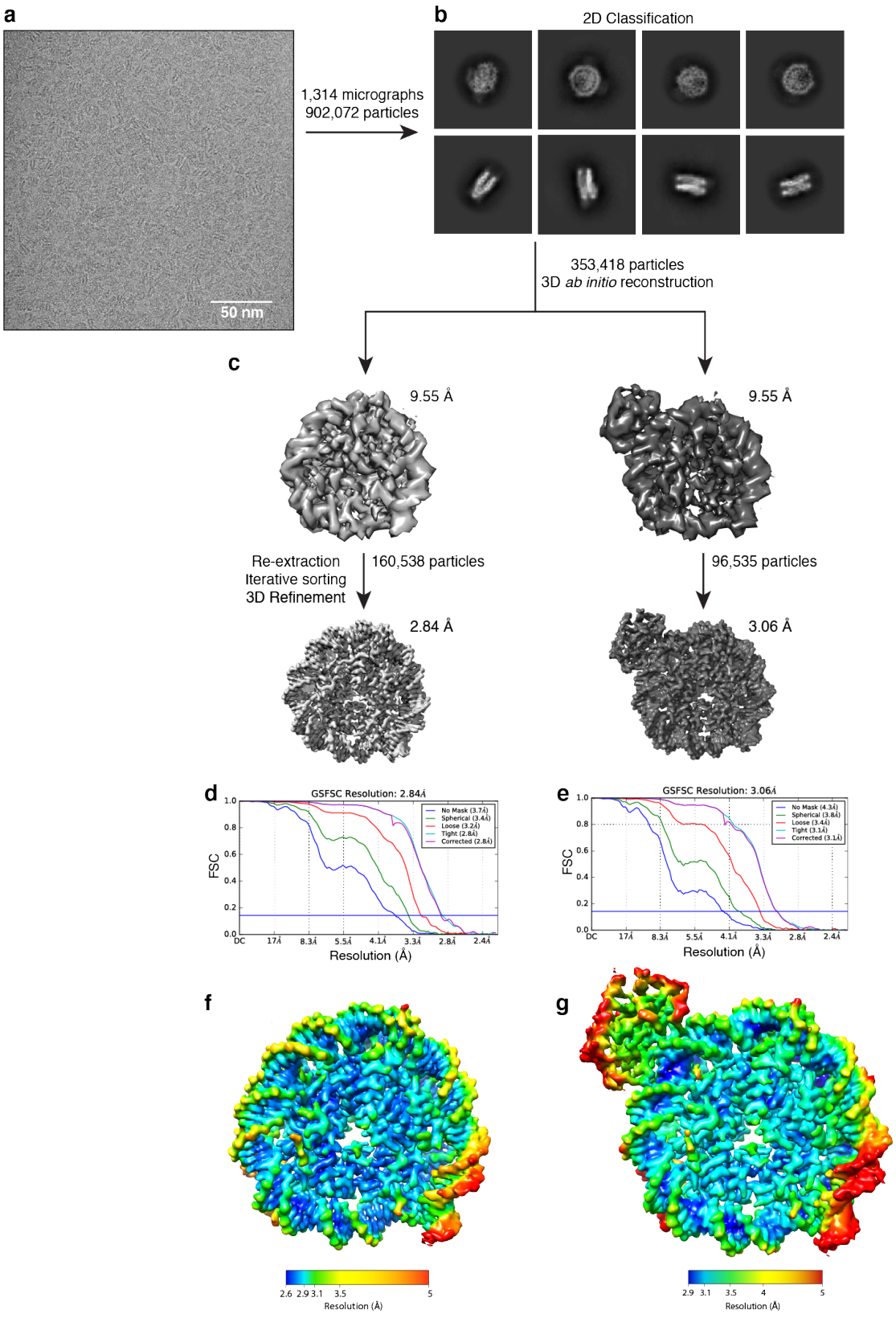
a
50 nm
1,314 micrographs
902,072 particles
b
2D Classification
353,418 particles
3D ab initio reconstruction
c
9.55 Å
9.55 Å
Re-extraction
Iterative sorting
3D Refinement
160,538 particles
96,535 particles
2.84 Å
3.06 Å
d
GSFSC Resolution: 2.84Å
FSC
Resolution (Å)
e
GSFSC Resolution: 3.06Å
FSC
Resolution (Å)
f
Resolution (Å)
g
Resolution (Å)

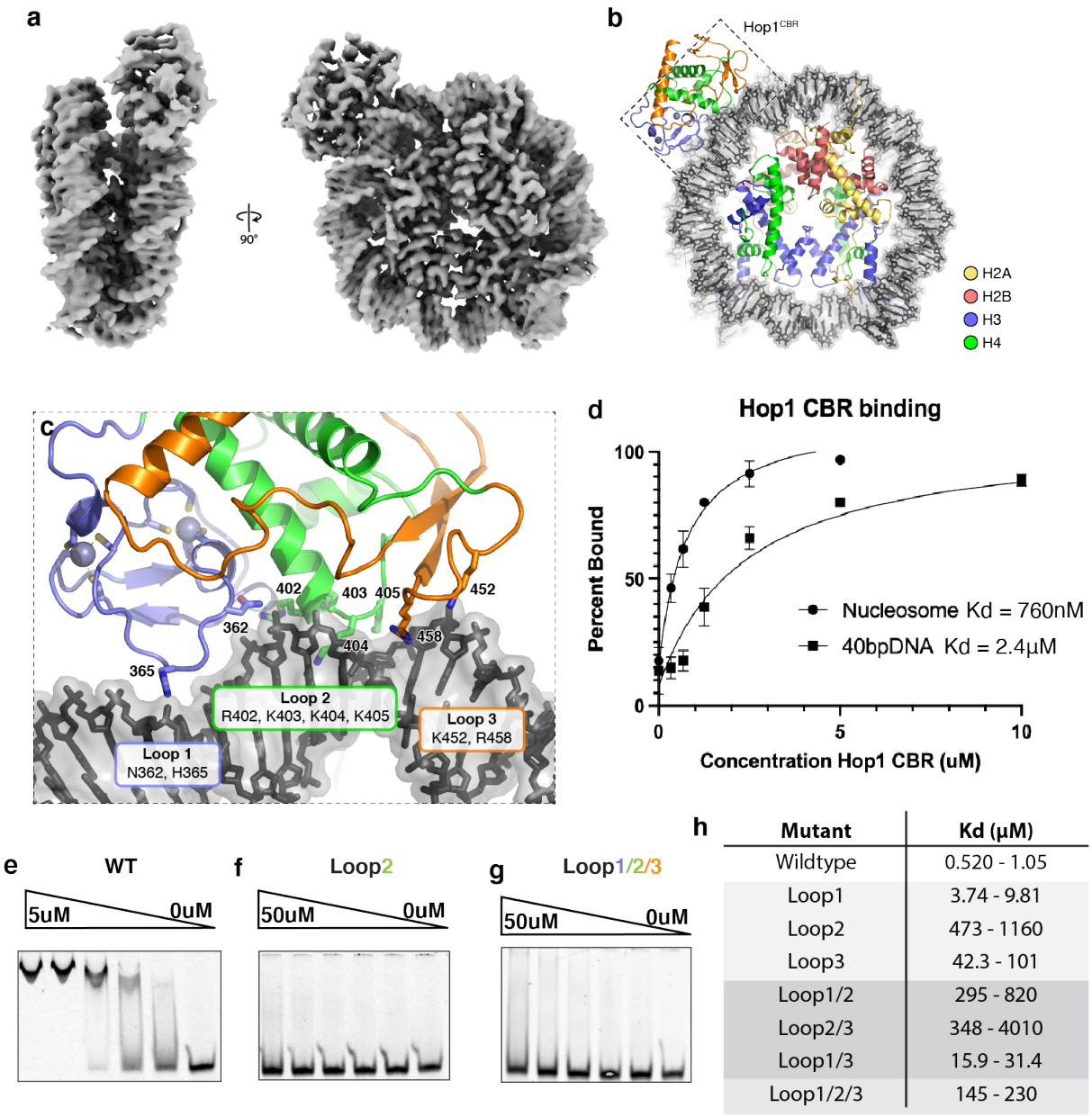

h

Mutant	Kd (µM)
Wildtype	0.520 - 1.05
Loop1	3.74 - 9.81
Loop2	473 - 1160
Loop3	42.3 - 101
Loop1/2	295 - 820
Loop2/3	348 - 4010
Loop1/3	15.9 - 31.4
Loop1/2/3	145 - 230

Figure 3.7: **Structure of the Hop1 CBR bound to a nucleosome a.** Two views of a 3.06 Å resolution cryo-EM map of the *S. cerevisiae* Hop1 CBR bound to a nucleosome. **b.** Hop1^{CBR} -nucleosome structure, with DNA colored gray, histones colored yellow (H2A)/red (H2B)/blue (H3)/green (H4), and the Hop1 CBR colored as in Figure 3-4. **c.** Closeup view of nucleosomal DNA binding by the Hop1 CBR, with DNA binding loops 1, 2, and 3 noted. **d.** Electrophoretic mobility shift assays (EMSAs) measuring nucleosome vs 40bp dsDNA binding by the wild-type Hop1 CBR, show a stronger affinity for the whole Nucleosome. **e.** WT Hop1 CBR EMSA gel shift with Nucleosome. **f.** The Hop1 CBR Loop2 alanine mutant completely disrupts CBR binding. **g.** The Hop1 CBR Loop1/2/3 alanine mutant completely disrupts CBR binding. **h.** Kd ranges of all CBR mutants tested by EMSA gel shifts

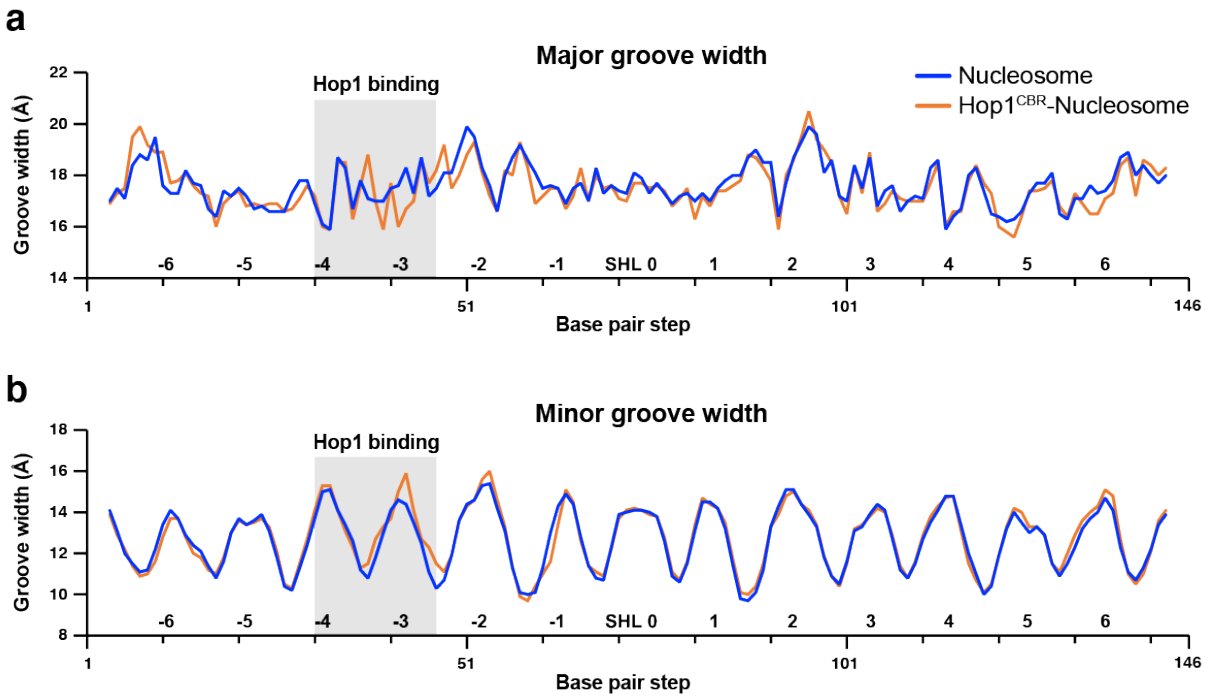

Figure 3.8: **DNA binding groove width changes with the Hop1 CBR a.** Major groove width analysis of the nucleosome with (orange) and without (blue) show major groove width decreases at SHL 3. **b.** Minor groove width analysis of the nucleosome with (orange) and without (blue) show the CBR inserts itself in and pries open the minor groove at SHL 3.

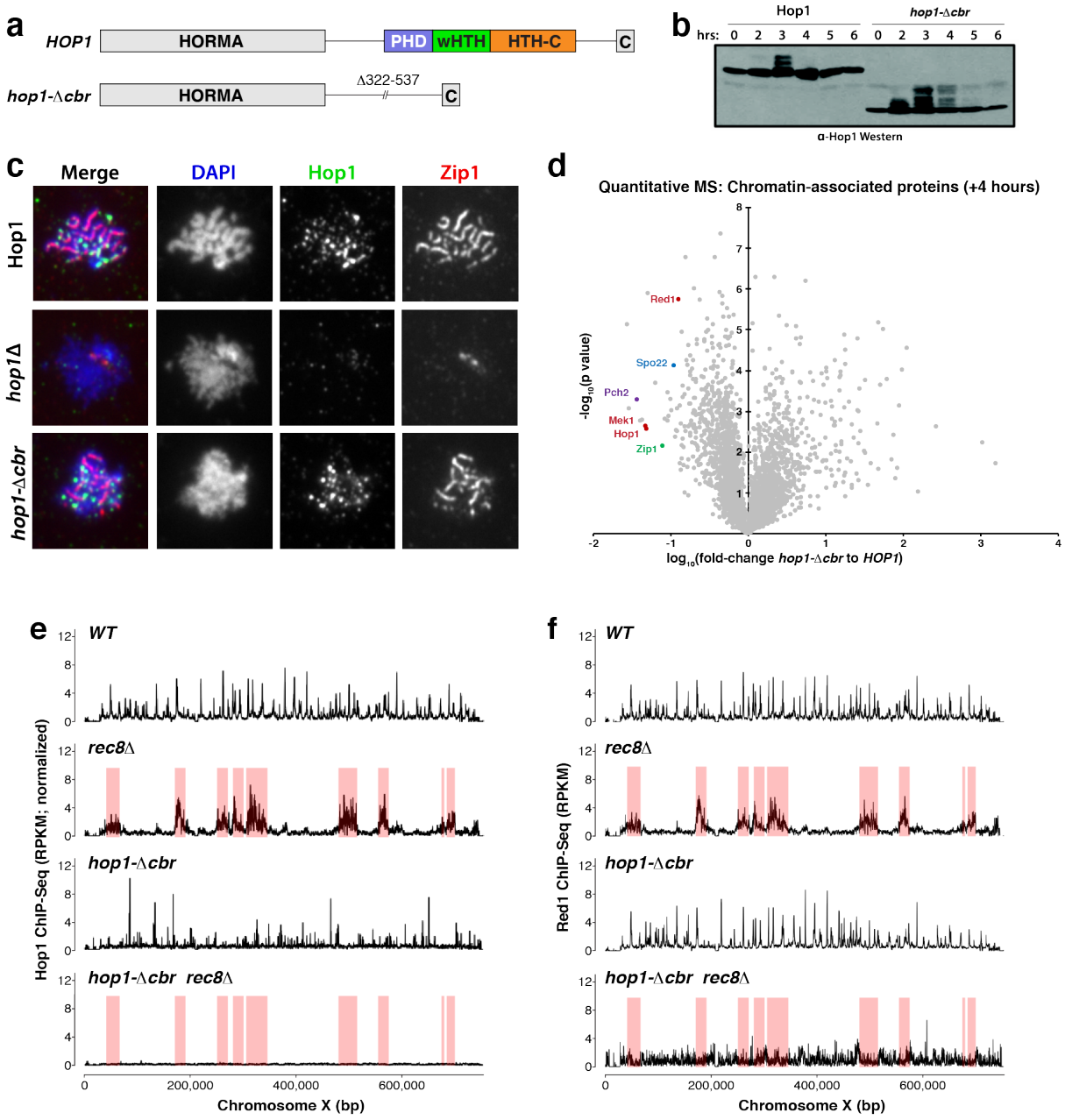

Figure 3.9: **The Hop1 CBR mediates Rec8-independent axis assembly a.** Domain structure of the full-length S. cerevisiae HOP1 gene (top), and the *hop1-Δcbr* allele with codons 322-537 deleted. **b.** Western blot for Hop1 show near wildtype expression and phosphorylation of hop1-cbr. **c.** Chromosome spreads of wildtype, *hop1-Δ*, and *hop1-Δcbr*, show near wildtype localization of Hop1 and Zip1 in the *hop1-Δcbr* mutant. **d.** Quantitative mass spec analysis of chromatin enriched fractions of wildtype vs the *hop1-Δcbr* show approximately a 2 fold reduction in common meiotic proteins. **e.** Chromosome X Hop1 ChIP-Seq signal (spike-in normalized) for wild-type, *rec8Δ*, *hop1-Δcbr*, and *hop1-Δcbr/rec8Δ* cells. Red shading indicates previously-identified Rec8-independent Hop1 "islands" **f.** Chromosome X Red1 ChIP-Seq signal (spike-in normalized) for wild-type, *rec8Δ*, *hop1-Δcbr*, and *hop1-Δcbr/rec8Δ* cells.

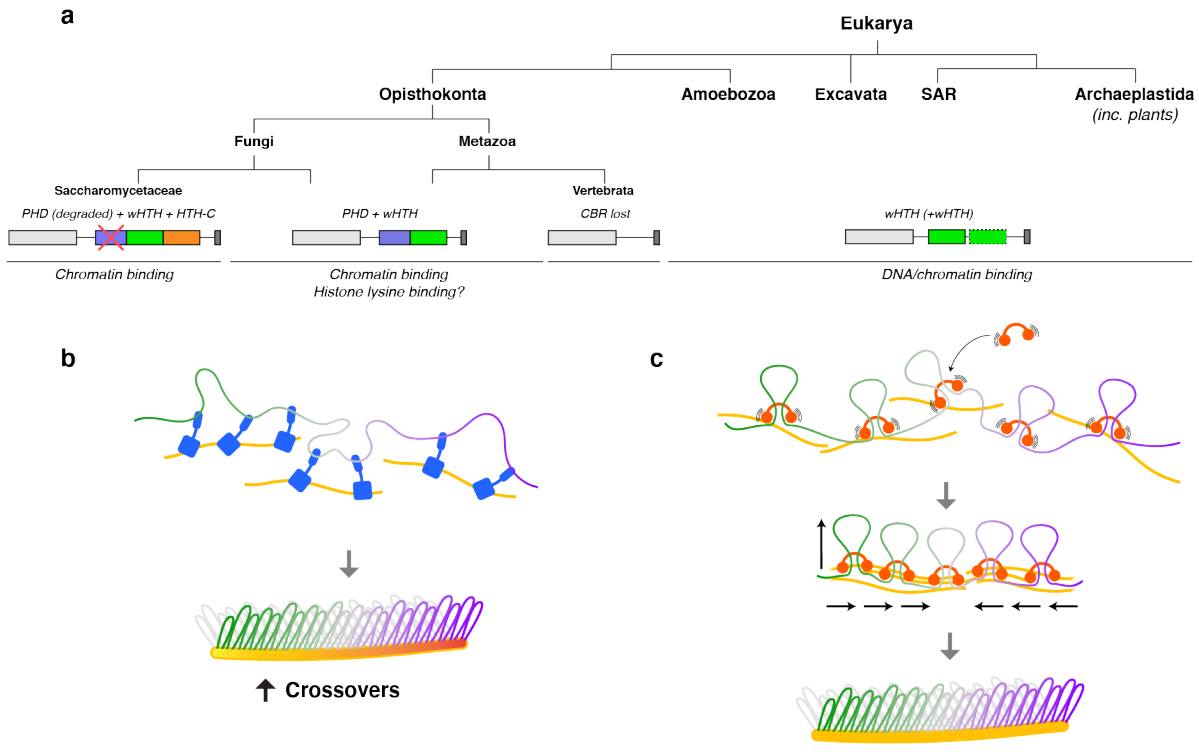

Figure 3.10: **Model for dual axis assembly mechanisms. a.** Schematic of conservation of various DNA binding domains present in meiotic HORMADs **b.** Schematic of our novel mechanism for chromosome axis assembly. The Hop1 CBR directly binds to chromatin, in the absence of Rec8, and creates a chromosome axis structure that promotes crossovers. **c.** Schematic of Rec8 dependent chromosome axis assembly. Rec8 extrudes DNA loops while also connecting to a filamentous Red1, to create the loop axis structure.

Chapter 4

Biochemical Characterization of *S. cerevisiae* Msh4:Msh5

4.1 Introduction

Accurate segregation of homologous chromosomes in the meiosis I division depends on specific recognition, physical association, and eventual formation of DNA crossovers between each pair of homologs in meiotic prophase. The homologous recombination pathway that generates crossovers in meiosis is initiated by Spo11, a conserved nuclease that generates double-strand DNA breaks (DSBs)(Keeney, 2001). Spo11 acts in the context of the chromosome axis, a protein scaffold that assembles in early meiosis I and organizes chromosomes into linear arrays of chromatin loops, recruits recombination machinery (Goodyer et al., 2008; Woltering et al., 2000), promotes DSB repair through the homolog (Humphryes and Hochwagen, 2014), and provides a platform for synaptonemal complex assembly (Shin et al., 2010). The S. cerevisiae chromosome axis consists of cohesin complexes containing a meiosis-specific kleisin subunit,

Rec8 (Klein et al., 1999), and the meiosis-specific proteins Red1 (Smith and Roeder, 1997) and Hop1 (Hollingsworth et al., 1990). Cohesin rings cinch sister chromosomes together, while Red1 localizes to cohesion sites and serves as a linker to bring Hop1 to the chromosome axis. Hop1 then acts as a master regulator of meiosis by recruiting double strand break machinery, then encouraging repair off the homolog as opposed to the sister. After crossovers are initiated, Hop1 is then stripped off of the meiotic chromosome axis by Pch2 in coordination with formation of the inter-homolog synaptonemal complex.

The number of DSBs formed in early meiotic prophase dramatically outnumber eventual crossovers, with the bulk of DSBs being repaired as so-called noncrossovers (Allers and Lichten, 2001). The mechanisms behind the decision of which DSBs are processed to become crossovers and which become noncrossovers remains unclear. It is known that crossover number and overall distribution are tightly regulated, ensuring that each homolog pair has a minimum of one crossover (referred to as “crossover assurance”), and that neighboring crossovers are more evenly spaced than a random distribution would suggest (referred to as “crossover interference”) (Bishop and Zickler, 2004).

Proteins of the so-called ZMM group play crucial roles in both inter-homolog recombination and in functionally linking recombination to downstream events like synaptonemal complex assembly. In budding yeast, this functionally diverse set of proteins includes signaling proteins (Zip3), DNA-binding recombination mediators (Zip2, Zip4, Spo16, Mer3, Msh4, and Msh5), and subunits of the synaptonemal complex itself (Zip1). Mutation in any of the ZMM proteins leads to a deficiency in meiotic crossovers (Borner et al., 2004). The E3 ligase Zip3 is thought to mediate crossover homeostasis to ensure proper crossover number and location, affecting phenomena like crossover interference and crossover assurance (refs). Zip3 is also required for initial re-

cruitment of Zip1 into foci at recombination sites (refs). Zip1 is the main “transverse filament” protein of the synaptonemal complex itself. It is suggested by some data that Zip1’s further assembly along chromosomes requires a complex including Zip2, Zip4, and Spo16, which are found at the “leading edge” of assembling Zip1 structures (refs). Mer3 is a 5’-3’ DNA helicase with poorly-defined roles in crossover formation.

The final members of the ZMM group are Msh4 and Msh5, which form a complex homologous to the mismatch-recognizing Msh2-Msh6 complex involved in the DNA mismatch repair pathway. This complex plays a key, but poorly understood, role in meiotic crossover formation, likely by recognizing and stabilizing a crossover-specific recombination intermediate and then mediating the assembly of a “recombination nodule” (Shinohara et al., 2008). The Msh4 and Msh5 names arise because of their homology to bacterial MutS (MutS Homologs), and most members of this family in both bacteria and eukaryotes directly recognize DNA mismatches to initiate DNA mismatch repair. In eukaryotes, the seven MSH proteins form several different heterodimers, each with distinct functions. After mitotic DNA replication, the MSH2-MSH6 and MSH2-MSH3 complexes function in the repair of mismatches. Recognition of a mismatched nucleotide provokes an ADP-to-ATP exchange, resulting in the formation of a stable hydrolysis-independent sliding clamp (Gradia et al., 1997). This clamp is capable of diffusion for at least 1 kb along the DNA adjacent to the mismatch. In both eukaryotes and prokaryotes, ATP-bound MutS/MSH complexes recruit downstream factors to cleave and repair the mismatched DNA. Crystal structures of *T. aquatiqus* and *E. coli* MutS have revealed that the proteins consist of five subdomains that together clasp the DNA; Domain I has been shown to bind the mismatch directly, as seen in Figure 4.1a (Acharya et al., 2003).

Msh4 and Msh5 form a dimer via their C-terminal domains (Kolas and Cohen, 2004), and

immunostaining data suggests that Msh4 and Msh5 form foci and colocalize in zygotene when homologs begin to synapse until late pachytene, when sister chromatids separate from each other.(Lenzi et al., 2005) *In vitro* work has shown that the human MSH4-MSH5 heterodimer binds to Holliday junction DNA, and this binding causes an ADP-to-ATP exchange followed by a conformational change in the MSH4-MSH5 complex, resulting in a sliding clamp action (Snowden et al., 2004). In the absence of the ordered DNA binding domains, a large cavity may be created in the center of the Msh4-Msh5 heterodimer. This cavity is presumably large enough for a Holliday Junction (Figure 4.1b) and may indicate how the Msh4-Msh5 complex interacts with its DNA substrates.

Msh4 and Msh5 in different species have been individually shown to interact with components of the double strand break repair pathway, such as the recombinases Rad51 and Dmc1, Mlh1 and the recombination SW1/SNF helicase RAD54(Neyton et al., 2004; Santucci-Darmanin et al., 2000; Snowden et al., 2008). Taken together, these results suggest a model where the Msh4-Msh5 complex binds and stabilizes an early recombination intermediate, potentially either the D-loop product of initial strand invasion or alternatively a Holliday Junction, and promote the assembly of crossover-specific and likely ZMM machinery. *In toto*, this machinery probably constitutes the “recombination nodules” previously observed by low-resolution electron microscopy on meiotic chromosomes.

4.2 Results and Discussion

Purification of the Msh4-Msh5 complex

Prior studies have reconstituted the *Homo sapiens* MSH4-MSH5 complex and showed that the complex binds Holliday Junction DNA and forms a sliding clamp on DNA Snowden, 2004 252. As our lab is focused on reconstituting larger recombination-mediating protein networks from the budding yeast *Saccharomyces cerevisiae*, I developed and optimized a protocol to purify *S. cerevisiae* Msh4-Msh5 in *Tni* insect cells using a baculovirus expression system. Either Msh4 or Msh5 was fused to a His6-Maltose Binding Protein tag to enhance solubility and enable purification, and the tagged subunit was coexpressed with its untagged partner to generate the 1:1 Msh4-Msh5 complex. The His6-MBP tag was placed on either protein of the heterodimer to ensure the bulky tag did not interfere with substrate binding. As both variations of tag had the same binding affinity for Holliday Junction DNA, I determined that either protein could be tagged without a decrease in functionality of the heterodimer. In addition to full length Msh4-Msh5, I also expressed and purified N-terminally truncated proteins missing short N-terminal disordered regions. I tested Msh4 truncations missing the first 25, 62 or 93 residues, and Msh5 truncations lacking the first 18, 23 or 48 residues. All Msh4-Msh5 complexes co-purified in a 1:1 stoichiometric ratio, consistent with other heterodimeric MutS-family complexes (Figure 4.2b). I have found that the complexes need MBP for solubility, and have been unable to successfully cleave the MBP tag off and maintain a high yield of protein.

DNA binding of the Msh4-Msh5 complex

In an effort to mimic all potential DNA intermediates, I designed a suite of DNA oligonucleotides that I could anneal in different combinations to generate all possible recombination intermediates from simple 5' or 3' overhangs to full Holliday junctions (Figure 4.3a-b). Previous studies have shown that human Msh4-Msh5 binds with nanomolar affinity to a Holliday junction and a pre-Holliday junction (a step just prior to a completed Holliday Junction in the recombination pathway) (Snowden et al., 2004). However, as Msh4-Msh5 localize and form foci before Holliday Junctions are formed, it is necessary to test the minimum DNA substrate required for Msh4-Msh5 binding. I performed electrophoretic mobility shift assays (EMSAs) with TBE-PAGE gels and fluorescently-labeled DNA oligos incubated with the *S. cerevisiae* MBP-Msh4-Msh5 complex. I observed strong binding to the Holliday junction (Kd = 0.63μM) and pre-Holliday junction (Kd = 1.37μM) intermediates, and slightly lower affinity binding to the Y branch and Y branch+ intermediates (Figure 4.3c-e). Little to no Msh4-Msh5 binding was observed with the less-complex DNA intermediates such as 3' and 5' overhangs, double-stranded DNA, and single stranded DNA. From this data, I determined that *S. cerevisiae* Msh4-Msh5 prefers to bind branched DNAs like Holliday junctions, consistent with prior work on *H. sapiens* MSH4-MSH5.

Identification of key residues for DNA binding

Msh family homologs feature a mismatch DNA binding domain at their N-terminus. However, in Msh4 and Msh5 homologs, these ordered domains are replaced with shorter disordered regions of varying length amongst homologs, that have low conservation (Figure 4.4a-b). To test the roles of these N-terminal regions in DNA binding by Msh4-Msh5, I generated three progressive truncations on each protein, purified the resulting complexes, and test DNA binding. I

truncated Msh4 at residue 26, 63, and 94, with 94 being the beginning of the structured connector domain of Msh4. Interestingly, truncating the first 26 residues of Msh4 had no effect on the binding of Msh4-Msh5 to Holliday Junctions (Kd = 0.44μM), while the truncations at residues 63(Kd = 2.85μM), and 94(Kd = 6.3μM), had a severe effect on binding affinity (Figure 4.4d). We can therefore conclude that Msh4 residues 26-94 are necessary for Holliday Junction binding. I could identify two moderately-conserved charged residues in this region: K52 and R83. It will be important for future work to determine whether mutating these residues has a similar effect on Holliday junction binding. For Msh5, I generated truncations starting at residues 19, 24, and 49, with 49 being the beginning of the structured connector domain of Msh5. Truncating Msh5 at residues 19(Kd = 0.43μM), or 24(Kd = 0.71μM), had no effect on Holliday junction binding, but truncating the protein at residue 49 nearly eliminated all Holliday junction binding (Figure 4.4e). I can therefore conclude that Msh5 residues 24-49 are necessary for Holliday Junction binding and recognition. Despite knowing the range of residues required for binding, based on alignments of fungal relatives there are no clearly identifiable conserved residues on the Msh5 N terminal tail that could be coordinating binding. Thus, a major goal for future structural work will be to determine the roles of both the Msh4 and Msh5 N-termini in Holliday junction binding.

Toward a cryo-EM structure of Msh4-Msh5

A major goal of this project was to determine a high-resolution structure of the Msh4-Msh5 complex, either in the presence or absence of Holliday junction DNA. Toward this goal, I was able to optimize the preparation of stable Msh4-Msh5-Holliday Junction complexes for analysis by either x-ray crystallography or cryo-electron microscopy (cryo-EM). I performed initial crystallization screens with both DNA-bound and unbound Msh4-Msh5, but did not identify

conditions for crystallization of either complex. I next turned to cryo-EM, which is more suited to high-resolution structural analysis of large (over 200 kDa) macromolecular complexes that may show structural disorder that inhibits crystallization. As a step towards a single particle cryo-EM structure, I prepared negative-stain samples of purified Msh4-Msh5 complexes. From an initial dataset of images, I manually picked single particles and generated 2D class averages using Relion2 software. As seen in Figure 4.5, initial negative-stain images(Figure 4.5a) show a good quality of sample for single particles (Figure 4.5b), and the 2D class averages (Figure 4.5c) mimic various shapes which fit the predicted structure based on the Msh2-Msh6 structure. In order to obtain a high resolution dataset, I next prepared samples for plunge-freezing and analysis by cryo-EM. These efforts were stymied by consistently high levels of apparent protein aggregation upon application to cryo-EM grids and freezing (Figure 4.5d). After attempting several different freezing conditions, and preparing samples both in the presence and absence of Holliday Junction DNA, I was unable to achieve homogenous samples amenable to high-resolution structure determination.

Discussion

The scope of this project was to define on a molecular level how the *S. cerevisiae* Msh4-Msh5 complex shuttles DNA intermediates towards a crossover fate. Msh4-Msh5 has been well studied *in vivo* but specific structural details are lacking. Although I was unable to achieve the ultimate goal of a high resolution structure of the Msh4-Msh5 complex bound to a relevant DNA substrate, I was able to further define its biochemical role. I was able to establish a protocol to create a high quality and reproducible protein complex of Msh4-Msh5. I verified that the *S. cerevisiae* Msh4-Msh5 complex functions similarly to its *H. Sapiens* homolog by preferably

binding the complex DNA intermediate of a Holiday junction. I also identified regions within the short disordered N-terminal tails of both Msh4 and Msh5 that are critical for this interaction. This work is another small step towards further understating the Msh4-Msh5 complex's role in meiotic recombination.

4.3 Materials and Methods

Protein Expression and Purification

S.c. Msh4 and Msh5 were cloned into the Macrolab's baculovirus dual expression vector. Standard protocols (Bac to Bac, Fisher Scientific) were followed to generate baculovirus and express it. Briefly, baculovirus was generated by transfecting a vector containing various versions of both Msh4 and Msh5 into the SF9 cells, and amplified with three passages of virus. P3 virus was used to infect *Tni* cells at 2x 10ô/ml, which were grown for 48 hours then harvested, centrifuged and resuspended in Buffer A (25mM Hepes pH 7.8, The Msh4-Msh5 complex was purified by using a dounce homogenizer to lyse the insect cells in the presence of protease inhibitors (aprotinin, leupeptin, pepstatin, PMSF), pelleting cellular debris by centrifugation (30min at 17,000rpm). Cell lysate was then flowed over a gravity Ni2+-affinity column and complex was eluted off with Nickel Elution Buffer (25mM Hepes pH7.8, 200mL NaCl, 5mM MgCl2, 250mM Imidazole pH 8.0, 10% glycerol). Nickel elution containing the complex was then incubated overnight with amylose-affinity resin preequilibrated in Amylose Column Buffer (ACB, 20mM Hepes pH 7.8, 200mM NaCl, 1mM EDTA, 10% glycerol, 1mM DTT). The next day, protein was eluted off with ACB with 10mM Maltose, concentrated and passed over a Superose 6 size-exclusion column in Gel Filtration buffer (25mM Hepes pH 7.8, 1mM DTT, 200mM NaCl,

10%glycerol, 5mM MgCl2) , yielding highly purified protein complex. Samples for EM were incubated with ADP for 30 minutes on ice, then run on an Superose 6 column after incubation with a Gel Filtration buffer containing ADP and no glycerol (25mM Hepes pH 7.8, 1mM DTT, 200mM NaCl, .1mM ADP, 5mM MgCl2).

Gel Shifts

DNA binding substrates were created based off of relevant recombination intermediates, with arms of 20bp length, or a full length of 40bp of DNA 5'-labeled with 6-carboxyfluorescein (5'-6-FAM). DNA oligos were annealed in Oligo Annealing Buffer (10 mM Tris–HCl pH 8.0, 50 mM NaCl, 1 mM MgCl2, 1 mM EDTA) by combining the oligos to a final concentration of 10μM and heating to 95°C and dropping one degree every two minutes down to 20°.EMSA reactions were prepared in Binding Buffer (25 mM Hepes pH 7.8, 1mM DTT, 100mM NaCl, 5% glycerol, 5mM MgCl2) by keeping the DNA substrate concentration constant at 5nM and varying the protein concentration. After 15 min incubation and addition of 5% (w/v) sucrose, free DNA and DNA-protein complexes were resolved by electrophoresis on 6% TBE-acrylamide gels pre-equilibrated (pre-run for 40 min at 150 V) in 0.2X TBE running buffer. Gels were run for 30-60 mins, based on DNA substrate size, at 150V at 4℃. Fluorescent DNA substrates in their bound and unbound states were imaged using a Bio-Rad ChemiDoc system using filters to image Alexa488. Gel bands were quantified using ImageJ (https://imagej.net), and binding curves were calculated using GraphPad Prism (https://www.graphpad.com).

Election Microscopy Methods

Samples for negative stain and cryo-EM were prepared as noted in the above section. For negative stain, samples were diluted from 0.1μM – 1μM and 5ul of sample was applied to a glow discharged Electron Microscopy Sciences 400 square mesh copper grids for 60 seconds. Grids were then gently washed in 2% Uranyl Acetate, 5 washes total, dried and imaged on a FEI Tecnai G2 Sphera Microscope. Images were acquired at 55,000x magnitude, and recorded with a Gatan 2k x 2K CCD camera. 75 micrographs were processed and particles were picked using a standard Relion 2.0 workflow to generate class averages based on negative stain data. Samples for cryo-EM were taken directly from the Superose 6 column and taken for processing on the Vitrobot. Briefly, samples were prepared at 100nM, 500nM, and 2.5μM either with or without 0.01% NP40 for cryo-fixation. Quantifoil CU200 grids were cleaned and glow discharged for plunge freezing in liquid ethane prior to sample application. Grids were loaded into the Vitrobot, and 3μl of sample was applied to the grid with a blot time of 3.5s. Images were collected using the Talos Arctica TEM and a Gatan K2 Summit direct electron detector. No dataset was collected due to the poor quality of sample.

4.4 Acknowledgements

The authors would like to thank the UCSD Cryo EM facility staff for their training efforts for this project. This work was supported in part by the UCSD Health Sciences Research Grant. S.U. has been supported by the National Science Foundation Graduate Research Fellowship and the UCSD Molecular Biophysics Training Grant.

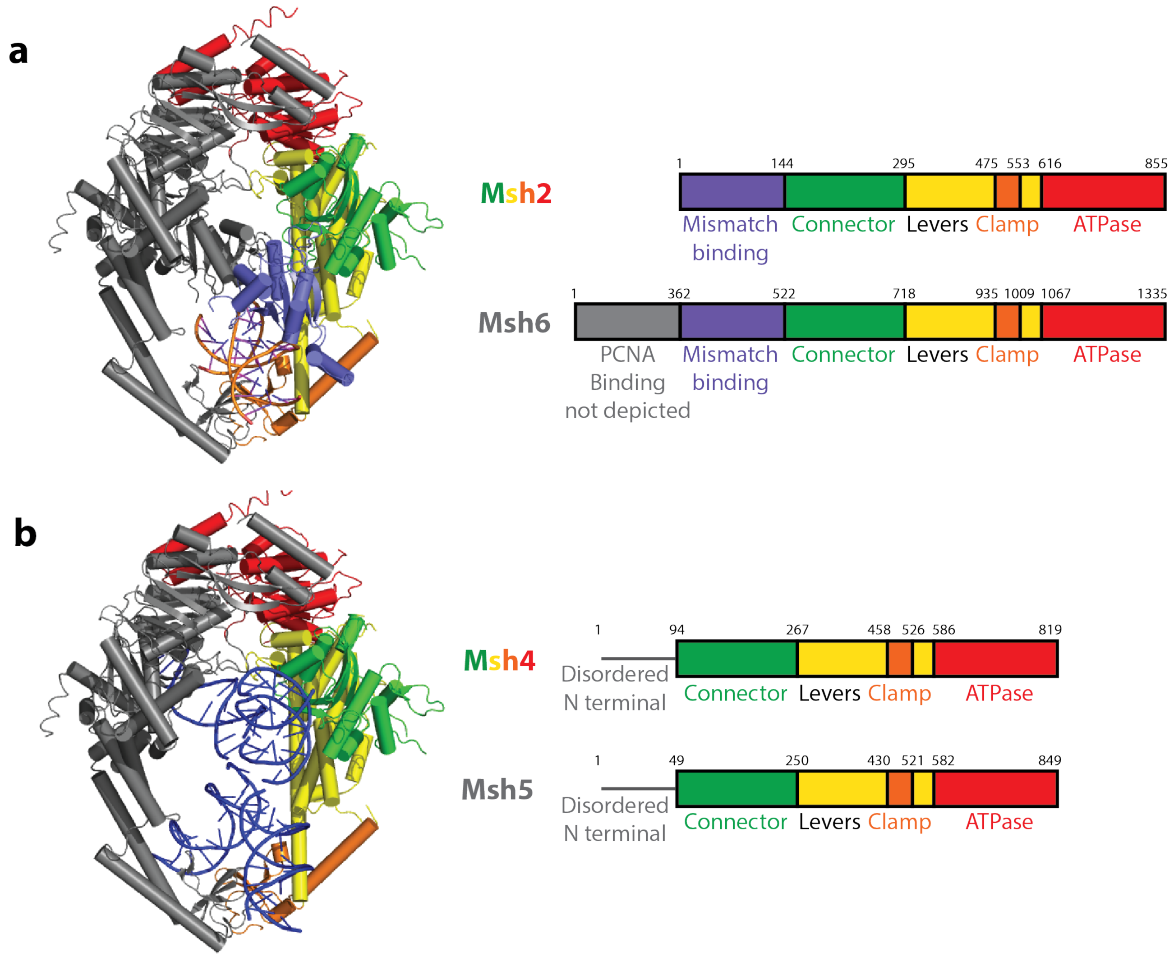

Figure 4.1: **Msh Family Domains and Modeled Structure a.** Crystal structure of Msh2-Msh6 (PDB 2O8B) bound to a DNA mismatch, Msh2 colored by domain, Msh6 colored grey. Domains of both are to the right. Domain residue boundary numbers are generated from the *H. sapiens* Msh2-Msh6 **b.** Our predicted structure of Msh4 colored by domain and Msh5 colored grey, bound to a Holliday Junction. Domain residue boundaries are predicted from the threaded model.

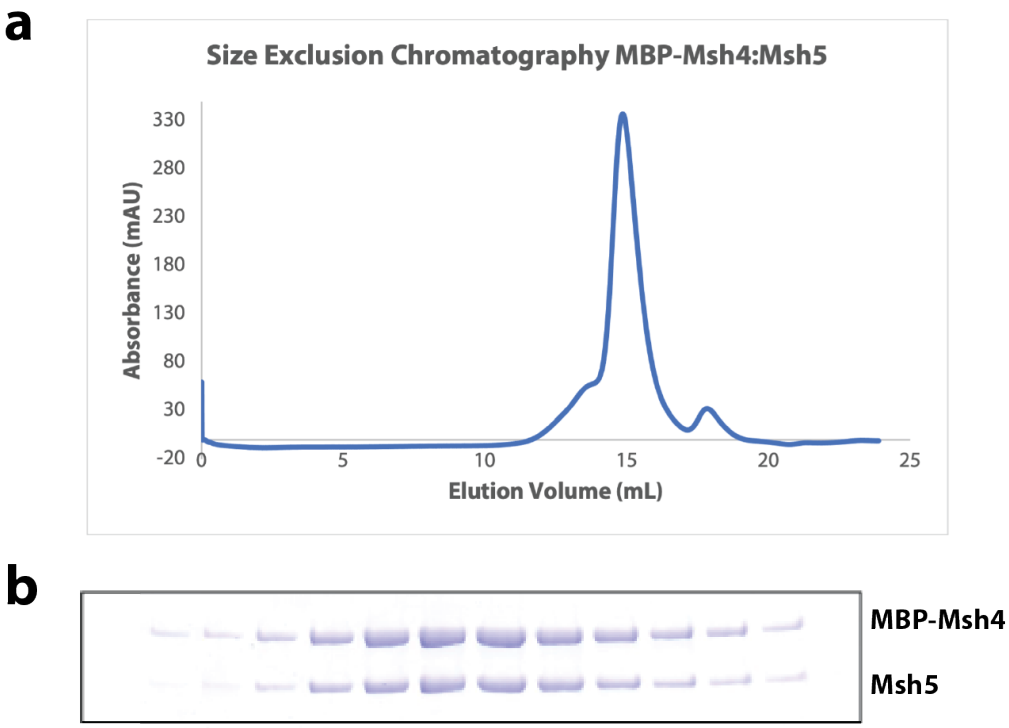

Figure 4.2: **Purification of S. cerevisiae Msh4 and Msh5 from insect cells.** Disordered N-terminals were either truncated to improve in vitro behavior or left full length for DNA binding studies. A dual-expression construct was generated for the creation of Baculovirus in Sf9 cells, then used to infect Tni cells for protein expression. **a.**: Size exclusion column of MBP-Msh4 and Msh5 in complex, bound to ADP. **b.**: Coomassie stained SDS-PAGE gel of samples from elution volumes 14.5-17mL. Expected MBP-Msh4 and Msh5 bands are at 132 and 97kDa respectively.

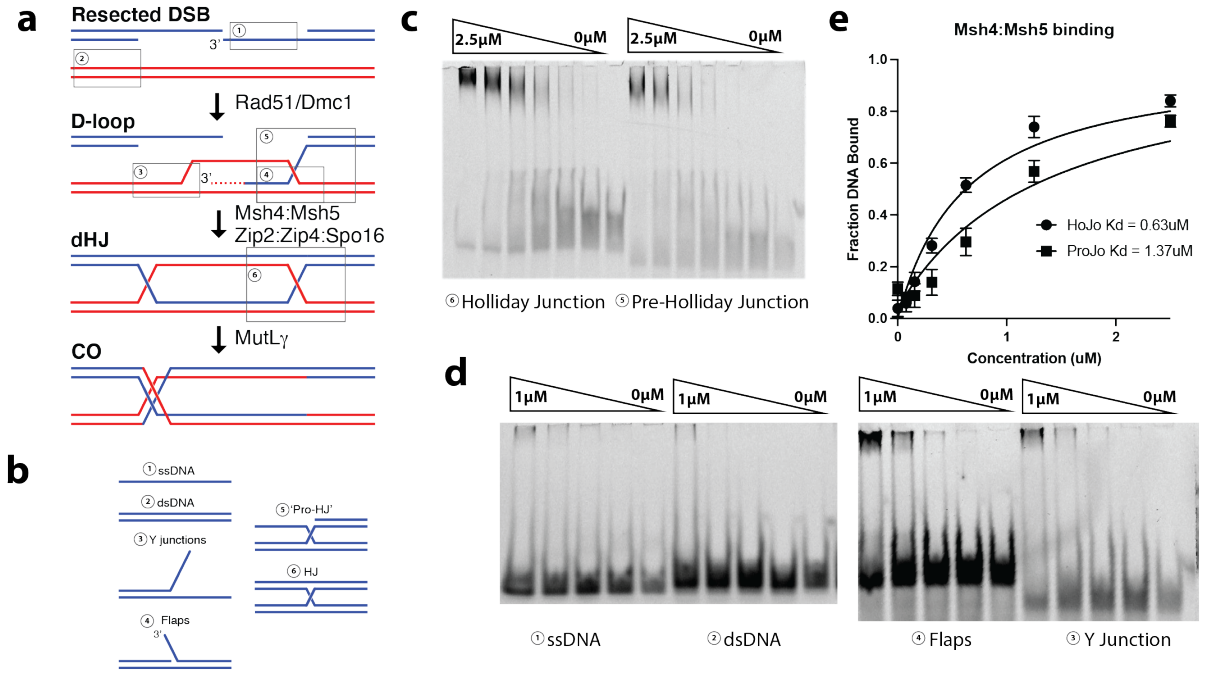

Figure 4.3: **Schematic of DNA binding experiments, based on meiotic crossover intermediates. a.**: Type I Crossover formation pathway, with crucial meiotic crossover-promoting proteins noted. Intermediates feature in Figure 4-3b are boxed and numbered. **b.** Proposed DNA substrates for binding with Msh4-Msh5. Substrates correspond to numbering in Figure 4-3a. **c.** Representative EMSA binding gels of Msh4-Msh5 full length bound to Holliday junction(6) and Pre-Holliday junction (5). Concentrations start at 2.5μM and decrease by half each well. **d.** Representative EMSA binding gels of Msh4-Msh5 full length bound to ssDNA (1), dsDNA (2), Flaps (4) and Y Junction (3). Concentrations start at 1μM and decrease by half each well. /textbfe.: Quantification of Full length Sc Msh4-Msh5 binding to a Holliday junction or pre-Holliday junction. Show the Holliday junction binds with 0.63μM affinity while the pre-Holliday junction only binds with 1.37 μM affinity.

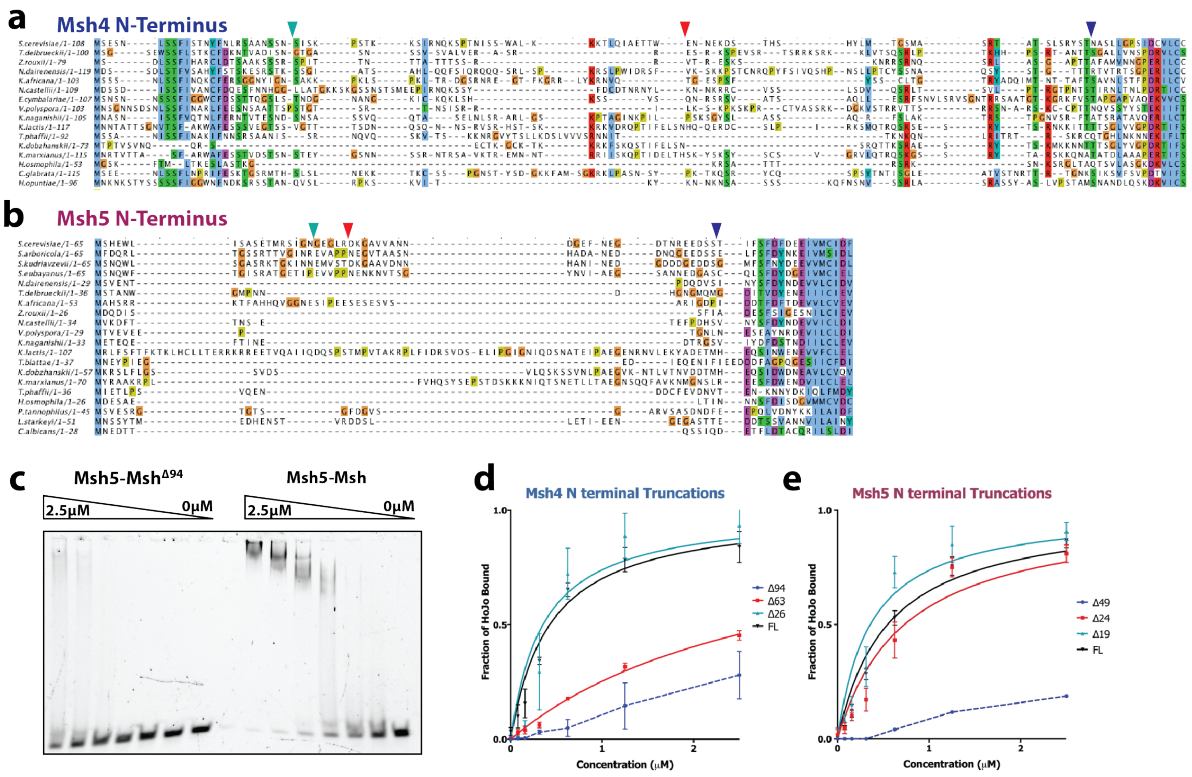

Figure 4.4: **The role of the disordered N-termini of Msh4 and Msh5. a.** A protein alignment of fungal Msh4 N-termini shows limited conservation of the disordered tail. Truncations were made at the residues indicated with arrows. **b.** Alignments of fungal Msh5 show even less conservation of the largely negatively charged tails. Again, truncations were made at the residues indicated with arrows. **c.** Representative EMSA binding gel of Msh5-Msh4$^{\Delta 94}$ and Msh4-Msh5 full length binding to Holliday junction. **d.** Msh4 N terminal truncations show no effect until residue 63, at which point binding affinity is dramatically decreased. **e.** Msh5 N terminal truncations show no effect until residue 49, indicating an important region for Holliday junction binding between residues 24 and 49 of Msh5.

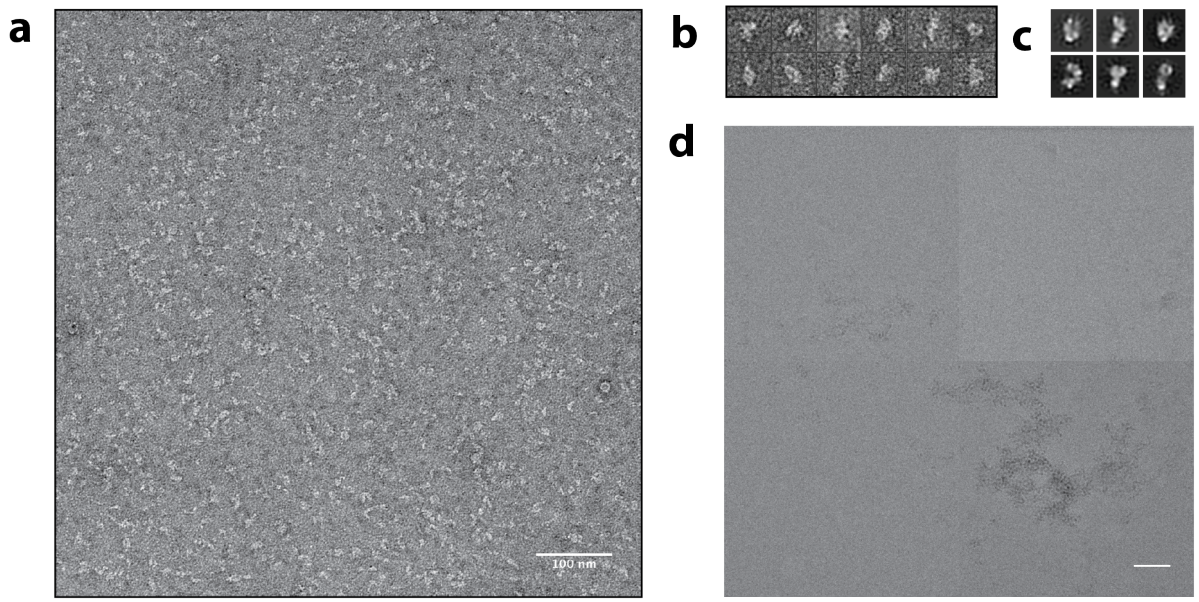

Figure 4.5: **Initial Negative Stain and Cryo-EM Micrographs with Negative Stain Generated 2D Class Averages. a.** Sample negative stain images taken with a 200kV FEI Tecnai Sphera at 55,000x magnification. Scale bar is 100μM. **b.** Sample particles were extracted using Relion from 75 micrographs. **c.** Extracted particles were then used to calculate 2D class averages, which demonstrate the excepted clamp structure and sides views based on the Msh2-Msh6 known structure. **d.** Sample cryo-EM image taken with the Talos Arctica TEM, shows a large amount of sample aggregation on the grid.

Chapter 5

Creation of a Time Resolved Network of Meiotic Chromosome Associated Proteins

5.1 Introduction

Meiosis, a hallmark of sexual reproduction, reduces the ploidy of a cell by undergoing two rounds of chromosome segregation and cell division after a single round of chromosome replication. In the first meiotic division, termed meiosis I, each pair of homologous chromosomes must identify one another and become physically linked in order to enable their accurate segregation from one another in the meiosis I division. Physical linkage of homologs occurs through meiotic recombination, a complex, highly ordered series of events involving double strand DNA breaks (DSBs), and the eventual resolution of a select few DSBs to mature inter-homolog crossovers.

A large number of protein complexes work together in a spatially and temporally ordered fashion to organize chromosomes and coordinate meiotic recombination. While extensive work has been done to study individual proteins or small protein complexes and their functions in meiosis, there have only been a few studies that examine meiosis as a whole. *S. cerevisiae* represent a highly desirable model organism for the study of meiosis, due to their genetic tunability, speed of growth, and their ability to undergo a highly synchronous meiosis. It's no surprise then, that large scale examinations of meiosis have all utilized *S. cerevisiae* (Brar et al., 2012; Cheng et al., 2018; Chu et al., 1998). Groundbreaking studies used microarray (Chu et al., 1998) and ribosome profiling (Brar et al., 2012) techniques to provide a framework of the yeast meiotic program from an mRNA and translational standpoint. These studies identified previously-unknown recombination factors, revealed transcriptional dynamics, and demonstrated the immense organellar remodeling that takes place during meiosis. In the most recent wide-scale meiosis study, the Brar group combined analysis of mRNA, ribosome profiling, and protein levels to create an understanding of transcriptional and translation regulatory mechanisms in meiosis. They were able to conclude that mRNA levels don't necessarily correlate with protein levels, and transcription factors (TFs) play highly diverse roles where single TFs can both activate and repress transcription of separate sets of genes (Cheng et al., 2018). Prior studies have largely focused on the whole of a cell during meiosis. However, there have been no studies done specifically on where these expressed proteins localize during meiosis. Meiotic recombination is a series of highly complex and coordinated assembly and disassembly events on the chromatin, especially during prophase of meiosis I. To address the lack of global knowledge on the assembly and disassembly of chromosomal complexes in meiotic prophase, we set out to create a protocol that provided chromatin localization information specifically during meiosis I of *S. cerevisiae*.

Specifically we set out to create a more specific tandem mass spectroscopy protocol to study how protein complexes associate and disassociate with meiotic chromatin to orchestrate meiotic recombination.

5.2 Results and Discussion

Method and Experimental Setup Summary

S. cerevisiae have an inherent advantage for this type of experiment due to their unique ability to undergo a synchronous meiosis when cultured with a sporulation media. In order to take advantage of this, I took samples every hour from 0-9 hours after addition of sporulation media. This 0-9 hour time point covers Prophase of Meiosis I, the phase when meiotic homologous recombination occurs, as pictured in Figure 5-1a. Using hourly timepoints we were able to parse out the timing of major events such as chromosome axis deposition, synaptonemal complex formation, and the localization or other key meiotic recombination players. Meiotic cells were lysed and separated out using a density gradient, the chromatin containing fractions were then striped of their protein with a Urea elution. Samples, were cut with trypsin, timepoints labeled with TMT tags, and pooled for quantitative comparison. For the deepest mass spectroscopy results possible, proteins were further separated into 40 fraction using a Basic Reverse Phased column, and pooled for a final 20 fractions to shoot. By using a novel strategy of using a chromatin enriched fraction, we were able to pickup key meiotic proteins in our sample that have been previously unseen in other whole cell lysate meiotic time courses.

Verification of Method through Cluster Analysis

In order to verify our method was capable of detecting meiosis-specific patterns amongst the 3,265 proteins detected, we analyzed them via clustering (Figure 5-2a). Cluster analysis compares patterns amoungst our 0-9h timepoints for each protein, and group proteins based on the similarity of their abundance pattern. Importantly, we saw known meiotic partners cluster together, such as chromosome axis components Hop1 and Rec8, which were immediately adjacent to each other, and Red1 which was associated close by (Figure 5-2b). We also saw the obligate heterodimeric partners Msh4 and Msh5 cluster directly adjacent to each other, as well as components of the synapsis initiation complex, Spo16 and Spo22 (Figure 5-2c). Interestingly, synaptonemal complex components were clustered slightly further away, given we saw Ecm11 appear to stay associated with the chromatin longer than Zip1(Figure5-2c). Importantly, by using chromatin enriched fractions and separating fraction with a BRP column, we were able to detect meiosis specific proteins that were missing from whole cell lysate meiotic proteomics experiments(Cheng et al., 2018). These proteins included but were not limited to, Spo16 (the smaller component of the synapsis initiation complex), Xrs2 (a member of the MRX recombination complex), and Rec107 (a member of the RMM recombination complex).

Verification of Method through known protein analysis

To further verify our method, I next examined well studied meiotic recombination proteins. Specifically, proteins were broken up into four different well-studied meiotic classes: (1) the chromosome axis; (2) the synaptonemal complex; (3) the synapsis initiation complex and other ZMMs; and (4) downstream recombination factors. Amongst the chromosome axis proteins (Hop1, Red1, and Rec8) Rec8 localized first, with Hop1 and Red1 localizing shortly af-

ter. This is as expected, given that Rec8 is the meiosis-specific kleisin subunit of the cohesin complex, which is deposited during pre-meiotic DNA replication and holds sister chromosomes throughout meiosis. Overall, we see Hop1 and Rec8 sharing their peak at 3 hours, and Red1 peaking at 4 hours (Figure 5-3a) showing that the chromosome axis all assembles in close to the same stage of meiosis, while also indicating a clear order of operations. The Hop1 trace is very consistent with known western blot data for the protein (Ur et al., 2021; Wan et al., 2004). Synaptonemal complex proteins (Zip1, Gmc2, and Ecm11) peak at 4-5 hours (Figure 5-3b), concurrent with the knowledge that the SC assembles after the chromosome axis. Various recombination factors and again show the characteristic peak of 4-6 hours (Figure5-3c-d), consistent with these proteins peaking during recombination of Meiosis I.

Application of Method to Knockout Strains

Lastly, we applied our new protocol to knockout strains to assay how individual proteins can affect the structures present on the chromatin. Four timepoints were used, 0h, 3h, 6h, and 9h to capture a range of processes throughout Prophase of Meiosis I. Wildtype was compared to data of a δhop1 (Figure 5-4a-d) and a δndt80 strain (Figure 5-4e-h). When Hop1 is deleted, there is still localization of Red1 at wildtype levels (Figure 5-4a), however, the synaptonemal complex protein Gmc2 and synapsis initiation protein Spo22 are both greatly reduced during the peak of recombination activity (3h-6h) compared to wildtype (Figure 5-4b-c). Next we looked at the deletion of ndt80, a transcription factor required for exit of Prophase 1 of meiosis. Concurrent with an arrest at this stage, we see synaptonemal complex, synapsis initiation, and recombination proteins all accumulating on the chromatin past when these structures should have been disassembled in the wildtype (Figure 5-4f-h). Again this data confirms earlier pub-

lished data showing that Ndt80 is required for complete recombination resulting in crossovers and disassembly of the SC(Allers and Lichten, 2001; Xu et al., 1995).

Discussion

Taken together, these data show that I have generated a quantitative protocol capable of tracking protein complexes on chromatin throughout Prophase I of meiosis. Our method was able to identify 3,265 proteins in our chromatin enriched fraction. Although some of those proteins were involved in more dense metabolic structures and not necessarily specific to meiotic chromatin, this method was sensitive enough to pick up lower abundance proteins Spo16, Xrs2, and Rec107, known to be important for meiotic recombination, but previously unseen in other meiotic proteomic studies. By closely examining clustered heatmaps, analysis of individual well-studied proteins, and through the deletion of previously characterized meiotic mutants I was able to robustly validate this method as a way to identify chromatin-associated proteins throughout the course of Prophase I. By applying this method to a variety of mutant and/or deletion strains, future work will help shed light on the interconnectivity of various meiotic components and broaden the global understanding of meiotic recombination mechanisms. Through our preliminary deletion experiments, in the absence of Hop1 we saw a pronounced decrease in the central element proteins Ecm11 and Gmc2 despite seeing no difference in the chromosome axis protein Red1. These data show that Hop1 is a key regulator of synaptonemal complex assembly, and hints that Red1 likely plays more of a structural role in meiosis. By taking a proteomics approach to analyzing novel meiotic mutants, we can enhance our understanding of the interplay and dependencies of structural components such as the chromosome axis and the synaptonemal complex, as well as less-abundant recombination factors. With this

method, I have generated a spatio-temporal atlas of meiotic chromosome-associated proteins, and outlined how various protein complexes assemble and disassemble from chromosomes to orchestrate meiotic recombination.

5.3 Materials and Methods

Cell Growth and Sample Harvesting

S288c wildtype, $\triangle$hop1 or $\triangle$ndt80 yeast cells were grown to saturation in YPD for 16 hours, diluted into BYTA and grown overnight for pre-sporulation. Cells were then washed and resuspended in Sporulation Media (0.3% KAc, 0.02% Raffinose) at an OD600 of 1.8. Timepoints were taken every hour from 0h-9h for wildtype cells or at 0, 3, 6, and 9 hour for deletion strains. Each hour, 10mL of cells were harvested, pelleted, and each pellet was washed.

Purification of Chromatin Enriched Fractions

Cell pellets from 10mL of sporulating culture at an OD600 of 1.6 (100μL) were resuspended in 1mL pre-warmed Reducing Buffer (50mM PIPES pH 9.4, 10mM DTT) and incubated at 30°C for 5 mins. Next, 1mL of pre-warmed Spheroplasting Solution (50mM Phosphate Buffer pH 7.5, 1M Sorbitol, 10mM DTT) was added and cells were spheroplasted with the addition of Lyticase and incubation for 30-60 minutes at 30°C. Spheroplasts were then spun at 2,500 rpm for 5 mins at 4°C. Pelleted spheroplasts were resuspended in 1mL of ice-chilled Washing Buffer (100mM KCl, 50mM HEPES pH 7.5, 1M Sorbitol) and spun at 2,500 rpm for 10 min at 4°C. The washed spheroplast pellet was then resuspended in EB Buffer (50mM HEPES pH 7.5, 100mM KCl, 5mM EDTA pH 8, PMSF, aprotinin, leupeptin, pepstatin). 10% Triton X-100 was added to

the resuspended spheroplasts to a final concentration of 0.5%, samples were then placed on a nutating rocker for 5 mins at 4°C, and allowed to sit on ice for 10 minutes after for maximum lysing. Next, lysate was gently layered a top a 30% Sucrose Solution (30% sucrose w/v, 50mM Tris-HCl pH 8, 100mM KCl) and spun at 13,000 rpm for 15 minutes at 4°C. From this density separation, the chromatin containing pellet was kept. Proteins were eluted off of the chromatin in a Chromatin Elution Buffer (8M Urea, 200mM Kcl, and 100mM Phosphate Buffer pH8) with DTT added fresh to a final concentration of 10mM.

Preparation of Samples for Mass Spectroscopy

Immediately after the addition of Chromatin Elution Buffer, samples were sonicated, incubated at 55°C for 15 mins, sonicated again, and incubated again at 55°C for 5 mins. Samples were centrifuged, supernatant harvested, and alkylated with 2-iodacetimide at 30mM, 3x the DTT concentration. Samples were then quantified via Bradford, and either frozen down or 200μg of protein was diluted with 25mM Phosphate Buffer pH8 to a Urea concentration of 1.5M and cut overnight at 37°C with 2 μg trypsin (Promega). The next day, samples were acidified with TFA at a final concentration of 0.5%. Digested samples were loaded onto and desalted using a C18 Sep-Pak cartridge (Waters) , and eluted off with a solution containing 80% acetonitrile and 0.1% acetic acid. Samples were dried down using a speed vac, resuspended in 25mM Phosphate Buffer pH8 and labeled overnight with Thermo Scientific TMT10plex labels (TMT10-127N, TMT10-128C, TMT10-129N, or TMT10-130C). Although the Thermo Fisher Scientific Orbitrap Fusion LUMOS Tribrid mass spectrometer is capable of reading 10 different tandem mass tags, the 4 with the largest differences amongst them were chosen to ensure accuracy and depth of peptide reads. Due to this, for the large 0-9 hour timepoint study, that meant having

one consistent sample across 3 different mass spectroscopy experiments for normalization. We chose to keep the 3 hour sample constant across experiments, as it is the beginning of peak expression of recombination master regulator Hop1. Samples pooled together were 0h, 1h, 2h, 3h for run 1, 3h, 4h, 5h, 6h for run 2, and 3h, 7h, 8h, 9h for run 3. By keeping 3h constant, we were able to normalize all time points to that sample for analysis, and maintain quantitative ratios. Equal amounts of each of the 4 tagged samples were pooled, run over another C18 column, lyophilized and this time resuspended in 10mM Ammonium Bicarbonate. To create the deepest possible read counts, pooled samples were then fractionated into 40 fractions using a Basic Reverse Phased column. Two fraction samples were then pooled with the furthest sample from them (ie 1 and 21, 2 and 22) to create 20 samples total for analysis on the Orbitrap Mass Spectrometer.

Analysis of Mass Spectroscopy

Datasets from the Thermo Fisher Scientific Orbitrap Fusion LUMOS Tribrid were compared against a database of all known s288c proteins and peptide counts were identified and quantified using the Trans-Proteomic Pipeline (TPP) software. Specifically, the COMET peptide search engine was used in the TPP software to identify peptides, results were then quantified using the TMT capabilities of the Libra software tool. In order to assure accuracy data were filtered as follows: only proteins with 3 or more peptides were included, the cutoff score for peptide identification probability was set to 0.9, and the spectral intensity cutoff was greater than 1000. As mentioned in the preparation for mass spec section, samples for the 0-9h study were normalized to the 3 hour timepoint. From here, cluster analysis was performed and heat maps generated by inputting the normalized spreadsheet into the Heatmaply package, built in R.

5.4 Acknowledgements

The authors would like to thank Ray Sunhandyata and Huilin Zhou for critical discussion of method creation and for invaluable effort and support with the mass spectroscopy sample preparation and machine. S.U. has been supported by the National Science Foundation Graduate Research Fellowship and the UCSD Molecular Biophysics Training Grant.

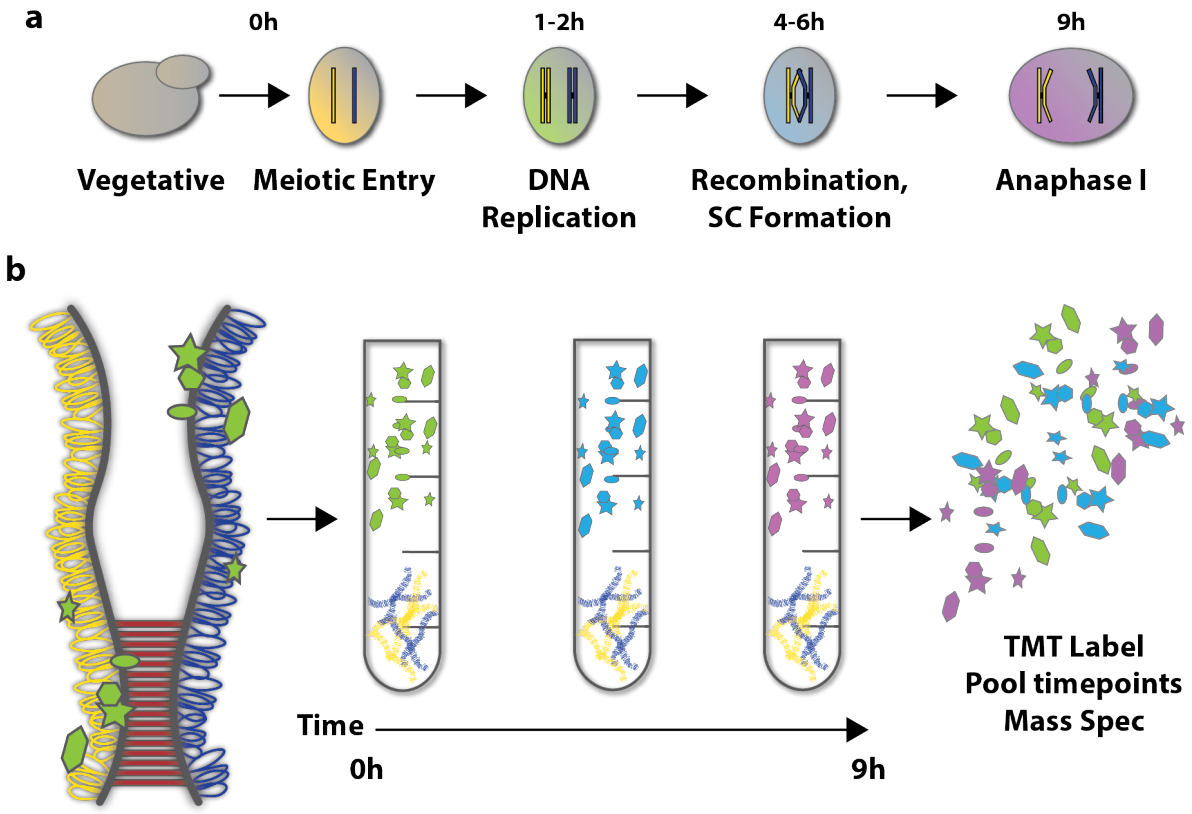

Figure 5.1: **Creation of a Novel Protocol to Assay Chromatin Associated Meiotic Proteins.** Cell lysates were created from cultures 0-9 hours after meiotic induction. From these lysates a chromatin enriched fraction was prepared through density centrifugation, and proteins eluted off using urea. Samples were then cut, labeled using TMT, pooled, fractionated on a basic reverse phase column, and analyzed using mass spec.

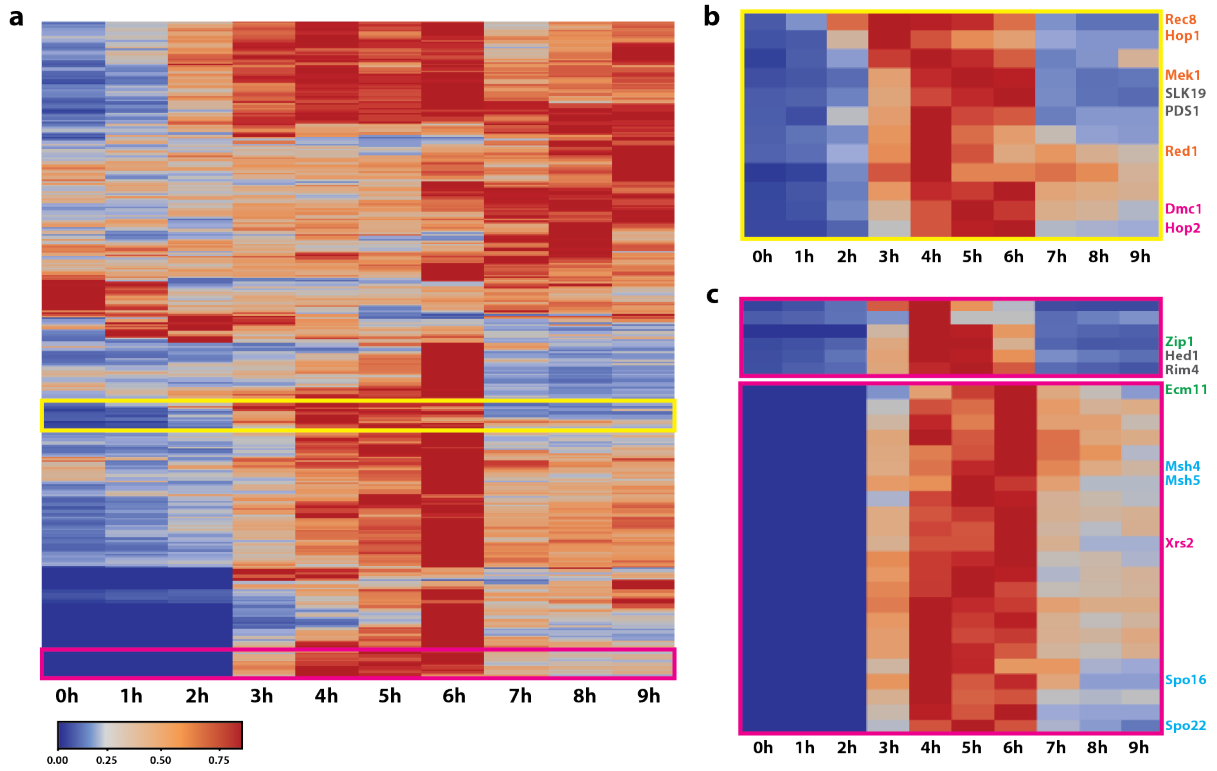

Figure 5.2: **Cluster Analysis of Temporal Localization Of Meiotic Recombination Components a.** Cluster analysis of timepoints 0-9 hours of chromosome enriched fractions of SK1 yeast cells undergoing meiosis. Boxed section are magnified in Figure5-2b-c. **b.**Magnified section that shows clustering of the components of the chromosome axis (bolded in orange) and early recombination factors (bolded in pink). This cluster also shows kinetochore binding protein SLK19 and secruin, PDS1. **c** Cluster analysis shows late recombination factors such as synapsis initiation complec (blue) and the synaptonemal complex proteins (green) group together along with some early recombination factors (grey).

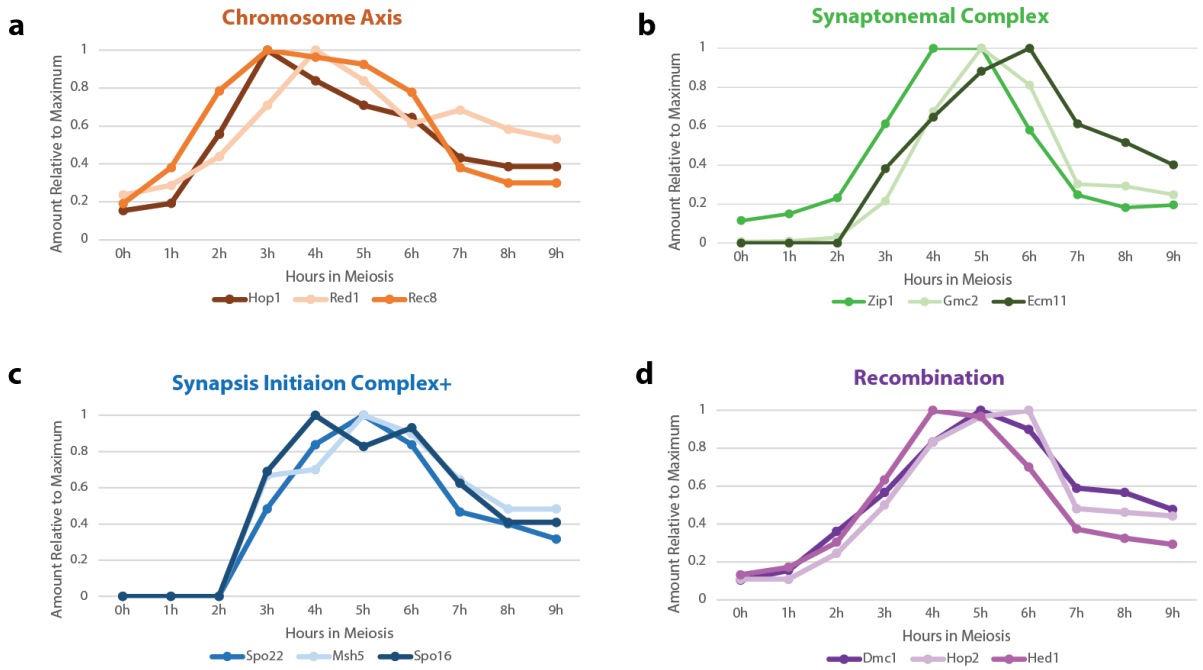

Figure 5.3: **Individual Analysis of Temporal Localization of Meiotic Recombination Components**. **a.** Chromosome axis components track together and assemble early in yeast meiosis. Featured proteins include the yeast meiotic HORMAD, Hop1, the chromosome axis core protein Red1, and the meiotic cohesion component Rec8. **b.** Synaptonemal complex (SC) components assemble onto chromatin 1-2 hours after the chromosome axis begins to localize. SC proteins featured here are the lateral element protein Zip1 and the central element proteins Ecm11 and Gmc2. **c.**Proteins involved in late recombination consist of Spo16 and Spo22, two components of the synapsis initiation complex, and their known ZMM counterpart Msh5. **d.** Proteins involved in early recombination include Dmc1, Hop2, and Hed1.

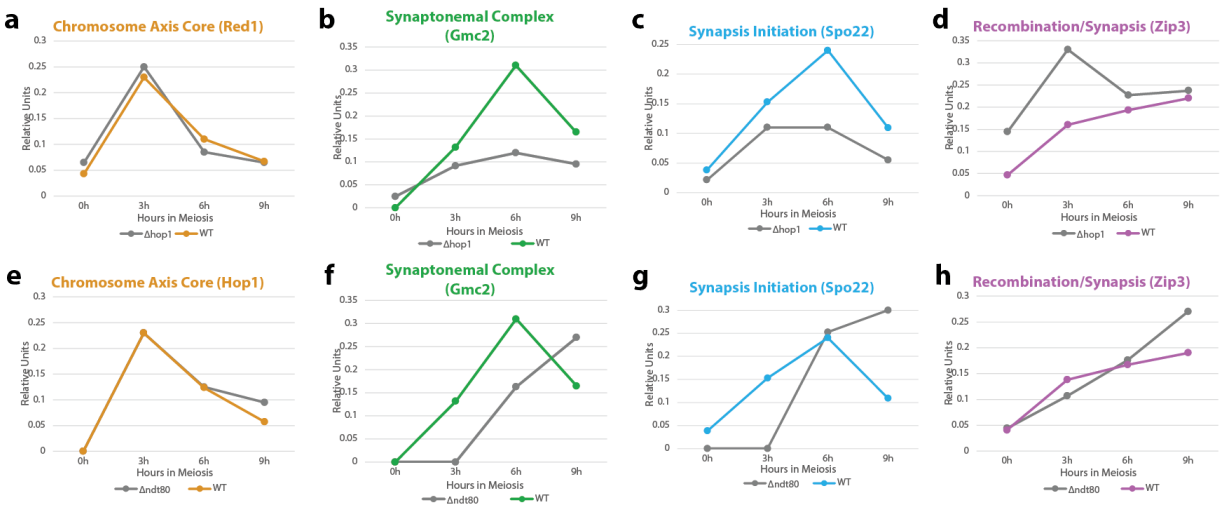

Figure 5.4: **Deletion of Key Meiotic Components.** Individual graphs of the effects of the Δhop1 (a-d) and Δndt80 (e-h) strains. Data shown were normalized to each other for comparison, units are arbitrary. **a.** No effect is seen on Red1 deposition, which is to be expected as we know Red1 localizes independently of Hop1. **b.** SC central element component Gmc2 is decreased during its peak deposition time. A similar trend was seen with Ecm11, Gmc2's known counter part. **c.** The Δhop1 strain shows a decrease in the synapsis initiation component Spo22, similar to the trend seen with Gmc2. **d.** An increase is shown at the 3h timepoint for recombination and synapsis protein Zip3. **e.** Chromosome axis HORMAD protein Hop1 is unaffected in the mutant. **f.** SC central element component Gmc2 does not disassemble, consistent with a pachytene arrest caused by Δndt80. **g.**: Synapsis initiation complex protein Spo22 also shows lack of disassembly consistent with check point arrest. **h.** Recombination and synapsis protein Zip3 shows an increase in accumulation at check point arrest.

Bibliography

1. Acharya, S., P.L. Foster, P. Brooks, and R. Fishel. 2003. The coordinated functions of the E. coli MutS and MutL proteins in mismatch repair. *Mol Cell*. 12:233-246.

2. Acquaviva, L., M. Boekhout, M.E. Karasu, K. Brick, F. Pratto, T. Li, M. van Overbeek, L. Kauppi, R.D. Camerini-Otero, M. Jasin, and S. Keeney. 2020. Ensuring meiotic DNA break formation in the mouse pseudoautosomal region. *Nature*. 582:426-431.

3. Acquaviva, L., L. Szekvolgyi, B. Dichtl, B.S. Dichtl, C. de La Roche Saint Andre, A. Nicolas, and V. Geli. 2013. The COMPASS subunit Spp1 links histone methylation to initiation of meiotic recombination. *Science*. 339:215-218.

4. Adelman, C.A., and J.H. Petrini. 2008. ZIP4H (TEX11) deficiency in the mouse impairs meiotic double strand break repair and the regulation of crossing over. *PLoS genetics*. 4:e1000042.

5. Ahuja, J.S., R. Sandhu, R. Mainpal, C. Lawson, H. Henley, P.A. Hunt, J.L. Yanowitz, and G.V. Borner. 2017. Control of meiotic pairing and recombination by chromosomally tethered 26S proteasome. *Science*. 355:408-411.

6. Albini, S.M., and G.H. Jones. 1984. Synaptonemal complex-associated centromeres and recombination nodules in plant meiocytes prepared by an improved surface-spreading technique. *Exp Cell Res*. 155:588-592.

7. Allers, T., and M. Lichten. 2001. Differential timing and control of noncrossover and crossover recombination during meiosis. *Cell*. 106:47-57.

8. Aragon, L. 2018. The Smc5/6 Complex: New and Old Functions of the Enigmatic Long-Distance Relative. *Annual Review of Genetics*. 52:89-107.

9. Aravind, L., and E.V. Koonin. 1998. The HORMA domain: a common structural denominator in mitotic checkpoints, chromosome synapsis and DNA repair. *Trends Biochem Sci*. 23:284-286.

10. Arora, K., and K.D. Corbett. 2019. The conserved XPF:ERCC1-like Zip2:Spo16 complex controls meiotic crossover formation through structure-specific DNA binding. *Nucleic Acids Res*. 47:2365-2376.

11. Baudat, F., J. Buard, C. Grey, A. Fledel-Alon, C. Ober, M. Przeworski, G. Coop, and B. de Massy. 2010. PRDM9 is a major determinant of meiotic recombination hotspots in humans and mice. *Science*. 327:836-840.

12. Beckouet, F., B. Hu, M.B. Roig, T. Sutani, M. Komata, P. Uluocak, V.L. Katis, K. Shirahige, and K. Nasmyth. 2010. An Smc3 acetylation cycle is essential for establishment of sister chromatid cohesion. *Mol Cell*. 39:689-699.

13. Bhagwat, N.R., S.N. Owens, M. Ito, J.V. Boinapalli, P. Poa, A. Ditzel, S. Kopparapu, M. Mahalawat, O.R. Davies, S.R. Collins, J.R. Johnson, N.J. Krogan, and N. Hunter. 2021. SUMO is a pervasive regulator of meiosis. *Elife*. 10:e57720.

14. Bishop, D.K., and D. Zickler. 2004. Early decision; meiotic crossover interference prior to stable strand exchange and synapsis. *Cell*. 117:9-15.

15. Biswas, U., K. Hempel, E. Llano, A. Pendas, and R. Jessberger. 2016. Distinct Roles of Meiosis-Specific Cohesin Complexes in Mammalian Spermatogenesis. *PLoS genetics*. 12:e1006389.

16. Boekhout, M., M.E. Karasu, J. Wang, L. Acquaviva, F. Pratto, K. Brick, D.Y. Eng, J. Xu, R.D. Camerini-Otero, D.J. Patel, and S. Keeney. 2019. REC114 Partner ANKRD31 Controls Number, Timing, and Location of Meiotic DNA Breaks. *Mol Cell*. 74:1053-1068 e1058.

17. Bolcun-Filas, E., Y. Costa, R. Speed, M. Taggart, R. Benavente, D.G. De Rooij, and H.J. Cooke. 2007. SYCE2 is required for synaptonemal complex assembly, double strand break repair, and homologous recombination. *J Cell Biol*. 176:741-747.

18. Bolcun-Filas, E., E. Hall, R. Speed, M. Taggart, C. Grey, B. de Massy, R. Benavente, and H.J. Cooke. 2009. Mutation of the mouse Syce1 gene disrupts synapsis and suggests a link between synaptonemal complex structural components and DNA repair. *PLoS genetics*. 5:e1000393.

19. Borde, V., N. Robine, W. Lin, S. Bonfils, V. Geli, and A. Nicolas. 2009. Histone H3 lysine 4 trimethylation marks meiotic recombination initiation sites. *The EMBO journal*. 28:99-111.

20. Borges, V., C. Lehane, L. Lopez-Serra, H. Flynn, M. Skehel, T. Rolef Ben-Shahar, and F. Uhlmann. 2010. Hos1 deacetylates Smc3 to close the cohesin acetylation cycle. *Mol Cell*. 39:677-688.

21. Borner, G.V., A. Barot, and N. Kleckner. 2008. Yeast Pch2 promotes domainal axis organization, timely recombination progression, and arrest of defective recombinosomes during meiosis. *Proceedings of the National Academy of Sciences of the United States of America*. 105:3327-3332.

22. Borner, G.V., N. Kleckner, and N. Hunter. 2004. Crossover/noncrossover differentiation, synaptonemal complex formation, and regulatory surveillance at the leptotene/zygotene transition of meiosis. *Cell*. 117:29-45.

23. Brar, G.A., M. Yassour, N. Friedman, A. Regev, N.T. Ingolia, and J.S. Weissman. 2012. High-resolution view of the yeast meiotic program revealed by ribosome profiling. *Science*. 335:552-557.

24. Cahoon, C.K., Z. Yu, Y. Wang, F. Guo, J.R. Unruh, B.D. Slaughter, and R.S. Hawley. 2017. Superresolution expansion microscopy reveals the three-dimensional organization of the Drosophila synaptonemal complex. *Proceedings of the National Academy of Sciences of the United States of America*. 114:E6857-E6866.

25. Callender, T.L., R. Laureau, L. Wan, X. Chen, R. Sandhu, S. Laljee, S. Zhou, R.T. Suhandynata, E. Prugar, W.A. Gaines, Y. Kwon, G.V. Borner, A. Nicolas, A.M. Neiman, and N.M. Hollingsworth. 2016. Mek1 Down Regulates Rad51 Activity during Yeast Meiosis by Phosphorylation of Hed1. *PLoS genetics*. 12:e1006226.

26. Capilla-Perez, L., S. Durand, A. Hurel, Q. Lian, A. Chambon, C. Taochy, V. Solier, M. Grelon, and R. Mercier. 2021. The synaptonemal complex imposes crossover interference and heterochiasmy in Arabidopsis. *Proceedings of the National Academy of Sciences of the United States of America*. 118:e2023613118.

27. Carballo, J.A., A.L. Johnson, S.G. Sedgwick, and R.S. Cha. 2008. Phosphorylation of the axial element protein Hop1 by Mec1/Tel1 ensures meiotic interhomolog recombination. *Cell*. 132:758-770.

28. Carballo, J.A., S. Panizza, M.E. Serrentino, A.L. Johnson, M. Geymonat, V. Borde, F. Klein, and R.S. Cha. 2013. Budding yeast ATM/ATR control meiotic double-strand break (DSB) levels by down-regulating Rec114, an essential component of the DSB-machinery. *PLoS genetics*. 9:e1003545.

29. Carpenter, A.T. 1975. Electron microscopy of meiosis in Drosophila melanogaster females. I. Structure, arrangement, and temporal change of the synaptonemal complex in wild-type. *Chromosoma*. 51:157-182.

30. Chambon, A., A. West, D. Vezon, C. Horlow, A. De Muyt, L. Chelysheva, A. Ronceret, A. Darbyshire, K. Osman, S. Heckmann, F.C.H. Franklin, and M. Grelon. 2018. Identification of ASYNAPTIC4, a Component of the Meiotic Chromosome Axis. *Plant Physiol*. 178:233-246.

31. Chelysheva, L., G. Gendrot, D. Vezon, M.P. Doutriaux, R. Mercier, and M. Grelon. 2007. Zip4/Spo22 is required for class I CO formation but not for synapsis completion in Arabidopsis thaliana. *PLoS genetics*. 3:e83.

32. Chen, X., R. Gaglione, T. Leong, L. Bednor, T. de Los Santos, E. Luk, M. Airola, and N.M. Hollingsworth. 2018. Mek1 coordinates meiotic progression with DNA break repair by directly phosphorylating and inhibiting the yeast pachytene exit regulator Ndt80. *PLoS genetics*. 14:e1007832.

33. Cheng, Z., G.M. Otto, E.N. Powers, A. Keskin, P. Mertins, S.A. Carr, M. Jovanovic, and G.A. Brar. 2018. Pervasive, Coordinated Protein-Level Changes Driven by Transcript Isoform Switching during Meiosis. *Cell*. 172:910-923 e916.

34. Chikashige, Y., C. Tsutsumi, M. Yamane, K. Okamasa, T. Haraguchi, and Y. Hiraoka. 2006. Meiotic proteins bqt1 and bqt2 tether telomeres to form the bouquet arrangement of chromosomes. *Cell*. 125:59-69.

35. Chu, S., J. DeRisi, M. Eisen, J. Mulholland, D. Botstein, P.O. Brown, and I. Herskowitz. 1998. The transcriptional program of sporulation in budding yeast. *Science*. 282:699-705.

36. Chua, P.R., and G.S. Roeder. 1998. Zip2, a meiosis-specific protein required for the initiation of chromosome synapsis. *Cell*. 93:349-359.

37. Chuang, C.N., Y.H. Cheng, and T.F. Wang. 2012. Mek1 stabilizes Hop1-Thr318 phosphorylation to promote interhomolog recombination and checkpoint responses during yeast meiosis. *Nucleic Acids Res*. 40:11416-11427.

38. Claeys Bouuaert, C.P., S.; Wang, J.; Oger, C.; Daccache, D.; Xie, W.; Patel, D. J.; Keeney, S. 2021. DNA-driven condensation assembles the meiotic DNA break machinery. *Nature*.

39. Clift, D., and A.L. Marston. 2011. The role of shugoshin in meiotic chromosome segregation. *Cytogenet Genome Res*. 133:234-242.

40. Cooper, T.J., K. Wardell, V. Garcia, and M.J. Neale. 2014. Homeostatic regulation of meiotic DSB formation by ATM/ATR. *Exp Cell Res*. 329:124-131.

41. Craig, J.M., and W.A. Bickmore. 1993. Chromosome bands--flavours to savour. *Bioessays*. 15:349-354.

42. Davidson, I.F., B. Bauer, D. Goetz, W. Tang, G. Wutz, and J.M. Peters. 2019. DNA loop extrusion by human cohesin. *Science*. 366:1338-1345.

43. Davies, O.R., J.D. Maman, and L. Pellegrini. 2012. Structural analysis of the human SYCE2-TEX12 complex provides molecular insights into synaptonemal complex assembly. *Open Biol*. 2:120099.

44. De Muyt, A., A. Pyatnitskaya, J. Andreani, L. Ranjha, C. Ramus, R. Laureau, A. Fernandez-Vega, D. Holoch, E. Girard, J. Govin, R. Margueron, Y. Coute, P. Cejka, R. Guerois, and V. Borde. 2018. A meiotic XPF-ERCC1-like complex recognizes joint molecule recombination intermediates to promote crossover formation. *Genes & development*. 32:283-296.

45. del Mazo, J., and L. Gil-Alberdi. 1986. Multistranded organization of the lateral elements of the synaptonemal complex in the rat and mouse. *Cytogenet Cell Genet*. 41:219-224.

46. Dereli, I., M. Stanzione, F. Olmeda, F. Papanikos, M. Baumann, S. Demir, F. Carofiglio, J. Lange, B. de Massy, W.M. Baarends, J. Turner, S. Rulands, and A. Toth. 2021. Four-pronged negative feedback of DSB machinery in meiotic DNA-break control in mice. *Nucleic Acids Res*. 49:2609-2628.

47. Ding, X., R. Xu, J. Yu, T. Xu, Y. Zhuang, and M. Han. 2007. SUN1 is required for telomere attachment to nuclear envelope and gametogenesis in mice. *Dev Cell*. 12:863-872.

48. Dixon, J.R., S. Selvaraj, F. Yue, A. Kim, Y. Li, Y. Shen, M. Hu, J.S. Liu, and B. Ren. 2012. Topological domains in mammalian genomes identified by analysis of chromatin interactions. *Nature*. 485:376-380.

49. Dobson, M.J., R.E. Pearlman, A. Karaiskakis, B. Spyropoulos, and P.B. Moens. 1994. Synaptonemal complex proteins: occurrence, epitope mapping and chromosome disjunction. *Journal of cell science*. 107:2749-2760.

50. Dong, H., and G.S. Roeder. 2000. Organization of the yeast Zip1 protein within the central region of the synaptonemal complex. *J Cell Biol*. 148:417-426.

51. Dumont, J., K. Oegema, and A. Desai. 2010. A kinetochore-independent mechanism drives anaphase chromosome separation during acentrosomal meiosis. *Nat Cell Biol*. 12:894-901.

52. Dunce, J.M., O.M. Dunne, M. Ratcliff, C. Millan, S. Madgwick, I. Uson, and O.R. Davies. 2018. Structural basis of meiotic chromosome synapsis through SYCP1 self-assembly. *Nat Struct Mol Biol*. 25:557-569.

53. Dunne, O.M., and O.R. Davies. 2019a. A molecular model for self-assembly of the synaptonemal complex protein SYCE3. *The Journal of biological chemistry*. 294:9260-9275.

54. Dunne, O.M., and O.R. Davies. 2019b. Molecular structure of human synaptonemal complex protein SYCE1. *Chromosoma*. 128:223-236.

55. Eichinger, C.S., and S. Jentsch. 2010. Synaptonemal complex formation and meiotic checkpoint signaling are linked to the lateral element protein Red1. *Proceedings of the National Academy of Sciences of the United States of America*. 107:11370-11375.

56. Falk, M., Y. Feodorova, N. Naumova, M. Imakaev, B.R. Lajoie, H. Leonhardt, B. Joffe, J. Dekker, G. Fudenberg, I. Solovei, and L.A. Mirny. 2019. Heterochromatin drives compartmentalization of inverted and conventional nuclei. *Nature*. 570:395-399.

57. Feng, J., S. Fu, X. Cao, H. Wu, J. Lu, M. Zeng, L. Liu, X. Yang, and Y. Shen. 2017. Synaptonemal complex protein 2 (SYCP2) mediates the association of the centromere with the synaptonemal complex. *Protein Cell*. 8:538-543.

58. Ferdous, M., J.D. Higgins, K. Osman, C. Lambing, E. Roitinger, K. Mechtler, S.J. Armstrong, R. Perry, M. Pradillo, N. Cunado, and F.C. Franklin. 2012. Inter-homolog

crossing-over and synapsis in *Arabidopsis* meiosis are dependent on the chromosome axis protein AtASY3. *PLoS genetics*. 8:e1002507.

59. Ferrandiz, N., C. Barroso, O. Telecan, N. Shao, H.M. Kim, S. Testori, P. Faull, P. Cutillas, A.P. Snijders, M.P. Colaiacovo, and E. Martinez-Perez. 2018. Spatiotemporal regulation of Aurora B recruitment ensures release of cohesion during *C. elegans* oocyte meiosis. *Nat Commun*. 9:834.

60. Fowler, K.R., R.W. Hyppa, G.A. Cromie, and G.R. Smith. 2018. Physical basis for long-distance communication along meiotic chromosomes. *Proceedings of the National Academy of Sciences of the United States of America*. 115:E9333-E9342.

61. Fudenberg, G., M. Imakaev, C. Lu, A. Goloborodko, N. Abdennur, and L.A. Mirny. 2016. Formation of Chromosomal Domains by Loop Extrusion. *Cell Rep*. 15:2038-2049.

62. Fujiwara, Y., Y. Horisawa-Takada, E. Inoue, N. Tani, H. Shibuya, S. Fujimura, R. Kariyazono, T. Sakata, K. Ohta, K. Araki, Y. Okada, and K.I. Ishiguro. 2020. Meiotic cohesins mediate initial loading of HORMAD1 to the chromosomes and coordinate SC formation during meiotic prophase. *PLoS genetics*. 16:e1009048.

63. Fung, J.C., B. Rockmill, M. Odell, and G.S. Roeder. 2004. Imposition of crossover interference through the nonrandom distribution of synapsis initiation complexes. *Cell*. 116:795-802.

64. Furey, T.S., and D. Haussler. 2003. Integration of the cytogenetic map with the draft human genome sequence. *Human molecular genetics*. 12:1037-1044.

65. Ganji, M., I.A. Shaltiel, S. Bisht, E. Kim, A. Kalichava, C.H. Haering, and C. Dekker. 2018. Real-time imaging of DNA loop extrusion by condensin. *Science*. 360:102-105.

66. Gao, J., and M.P. Colaiacovo. 2018. Zipping and Unzipping: Protein Modifications Regulating Synaptonemal Complex Dynamics. *Trends Genet*. 34:232-245.

67. Garcia, V., S. Gray, R.M. Allison, T.J. Cooper, and M.J. Neale. 2015. Tel1(ATM)-mediated interference suppresses clustered meiotic double-strand-break formation. *Nature*. 520:114-118.

68. Gibcus, J.H., K. Samejima, A. Goloborodko, I. Samejima, N. Naumova, J. Nuebler, M.T. Kanemaki, L. Xie, J.R. Paulson, W.C. Earnshaw, L.A. Mirny, and J. Dekker. 2018. A pathway for mitotic chromosome formation. *Science*. 359:eaao6135.

69. Gomez, H.L., N. Felipe-Medina, M. Sanchez-Martin, O.R. Davies, I. Ramos, I. Garcia-Tunon, D.G. de Rooij, I. Dereli, A. Toth, J.L. Barbero, R. Benavente, E. Llano, and A.M. Pendas. 2016. C14ORF39/SIX6OS1 is a constituent of the synaptonemal complex and is essential for mouse fertility. *Nat Commun*. 7:13298.

70. Goodyer, W., S. Kaitna, F. Couteau, J.D. Ward, S.J. Boulton, and M. Zetka. 2008. HTP-3 links DSB formation with homolog pairing and crossing over during C. elegans meiosis. *Dev Cell*. 14:263-274.

71. Gordon, S.G., L.E. Kursel, K. Xu, and O. Rog. 2021. Synaptonemal Complex dimerization regulates chromosome alignment and crossover patterning in meiosis. *PLoS genetics*. 17:e1009205.

72. Gradia, S., S. Acharya, and R. Fishel. 1997. The human mismatch recognition complex hMSH2-hMSH6 functions as a novel molecular switch. *Cell*. 91:995-1005.

73. Guiraldelli, M.F., A. Felberg, L.P. Almeida, A. Parikh, R.O. de Castro, and R.J. Pezza. 2018. SHOC1 is a ERCC4-(HhH)2-like protein, integral to the formation of crossover recombination intermediates during mammalian meiosis. *PLoS genetics*. 14:e1007381.

74. Gutierrez-Caballero, C., Y. Herran, M. Sanchez-Martin, J.A. Suja, J.L. Barbero, E. Llano, and A.M. Pendas. 2011. Identification and molecular characterization of the mammalian alpha-kleisin RAD21L. *Cell Cycle*. 10:1477-1487.

75. Gyuricza, M.R., K.B. Manheimer, V. Apte, B. Krishnan, E.F. Joyce, B.D. McKee, and K.S. McKim. 2016. Dynamic and Stable Cohesins Regulate Synaptonemal Complex Assembly and Chromosome Segregation. *Curr Biol*. 26:1688-1698.

76. Hamer, G., K. Gell, A. Kouznetsova, I. Novak, R. Benavente, and C. Hoog. 2006. Characterization of a novel meiosis-specific protein within the central element of the synaptonemal complex. *Journal of cell science*. 119:4025-4032.

77. Hamer, G., H. Wang, E. Bolcun-Filas, H.J. Cooke, R. Benavente, and C. Hoog. 2008. Progression of meiotic recombination requires structural maturation of the central element of the synaptonemal complex. *Journal of cell science*. 121:2445-2451.

78. Hassold, T., H. Hall, and P. Hunt. 2007. The origin of human aneuploidy: where we have been, where we are going. *Human molecular genetics*. 16:R203-208.

79. Hassold, T., and P. Hunt. 2001. To err (meiotically) is human: the genesis of human aneuploidy. *Nat Rev Genet*. 2:280-291.

80. Henzel, J.V., K. Nabeshima, M. Schvarzstein, B.E. Turner, A.M. Villeneuve, and K.J. Hillers. 2011. An asymmetric chromosome pair undergoes synaptic adjustment and crossover redistribution during *Caenorhabditis elegans* meiosis: implications for sex chromosome evolution. *Genetics*. 187:685-699.

81. Herran, Y., C. Gutierrez-Caballero, M. Sanchez-Martin, T. Hernandez, A. Viera, J.L. Barbero, E. de Alava, D.G. de Rooij, J.A. Suja, E. Llano, and A.M. Pendas. 2011. The cohesin subunit RAD21L functions in meiotic synapsis and exhibits sexual dimorphism in fertility. *The EMBO journal*. 30:3091-3105.

82. Herruzo, E., B. Santos, R. Freire, J.A. Carballo, and P.A. San-Segundo. 2019. Characterization of Pch2 localization determinants reveals a nucleolar-independent role in the meiotic recombination checkpoint. *Chromosoma*. 128:297-316.

83. Hollingsworth, N.M. 2010. Phosphorylation and the creation of interhomolog bias during meiosis in yeast. *Cell Cycle*. 9:436-437.

84. Hollingsworth, N.M., L. Goetsch, and B. Byers. 1990. The HOP1 gene encodes a meiosis-specific component of yeast chromosomes. *Cell*. 61:73-84.

85. Hollingsworth, N.M., and A.D. Johnson. 1993. A conditional allele of the *Saccharomyces cerevisiae* HOP1 gene is suppressed by overexpression of two other meiosis-specific genes: RED1 and REC104. *Genetics*. 133:785-797.

86. Horn, H.F., D.I. Kim, G.D. Wright, E.S. Wong, C.L. Stewart, B. Burke, and K.J. Roux. 2013. A mammalian KASH domain protein coupling meiotic chromosomes to the cytoskeleton. *J Cell Biol*. 202:1023-1039.

87. Huang, T., S. Yuan, L. Gao, M. Li, X. Yu, J. Zhan, Y. Yin, C. Liu, C. Zhang, G. Lu, W. Li, J. Liu, Z.J. Chen, and H. Liu. 2020. The histone modification reader ZCWPW1 links histone methylation to PRDM9-induced double-strand break repair. *Elife*. 9:e53459.

88. Hughes, S.E., D.E. Miller, A.L. Miller, and R.S. Hawley. 2018. Female Meiosis: Synapsis, Recombination, and Segregation in *Drosophila melanogaster*. *Genetics*. 208:875-908.

89. Humphryes, N., and A. Hochwagen. 2014. A non-sister act: recombination template choice during meiosis. *Exp Cell Res*. 329:53-60.

90. Humphryes, N., W.K. Leung, B. Argunhan, Y. Terentyev, M. Dvorackova, and H. Tsubouchi. 2013. The Ecm11-Gmc2 complex promotes synaptonemal complex formation through assembly of transverse filaments in budding yeast. *PLoS genetics*. 9:e1003194.

91. Hurlock, M.E., I. Cavka, L.E. Kursel, J. Haversat, M. Wooten, Z. Nizami, R. Turniansky, P. Hoess, J. Ries, J.G. Gall, O. Rog, S. Kohler, and Y. Kim. 2020. Identification of novel synaptonemal complex components in *C. elegans*. *J Cell Biol*. 219:e201910043.

92. Ishiguro, T., K. Tanaka, T. Sakuno, and Y. Watanabe. 2010. Shugoshin-PP2A counteracts casein-kinase-1-dependent cleavage of Rec8 by separase. *Nat Cell Biol*. 12:500-506.

93. Ivanov, D., A. Schleiffer, F. Eisenhaber, K. Mechtler, C.H. Haering, and K. Nasmyth. 2002. Eco1 is a novel acetyltransferase that can acetylate proteins involved in cohesion. *Curr Biol*. 12:323-328.

94. Jin, X., ; Fudenberg, G; Pollard, K. S. 2021. Genome-wide variability in recombination activity is associated with meiotic chromatin organization. *bioRxiv*:10.1101/2021.1101.1106.425599.

95. Johnson, D.C., M.; Cooper, T.; Claeys Bouuaert, C.; Keeney, S.; Llorente, B.; Garcia, V.; Neale, M. J. 2019. Concerted cutting by Spo11 illuminates DNA break mechanisms and initiates gap repair during meiosis. *bioRxiv*:10.1101/2019.1112.1118.881268.

96. Joshi, N., A. Barot, C. Jamison, and G.V. Borner. 2009. Pch2 links chromosome axis remodeling at future crossover sites and crossover distribution during yeast meiosis. *PLoS genetics*. 5:e1000557.

97. Joyce, E.F., M. Pedersen, S. Tiong, S.K. White-Brown, A. Paul, S.D. Campbell, and K.S. McKim. 2011. *Drosophila* ATM and ATR have distinct activities in the regulation of meiotic DNA damage and repair. *J Cell Biol*. 195:359-367.

98. Kariyazono, R., A. Oda, T. Yamada, and K. Ohta. 2019. Conserved HORMA domain-containing protein Hop1 stabilizes interaction between proteins of meiotic DNA break hotspots and chromosome axis. *Nucleic Acids Res*. 47:10166-10180.

99. Keeney, S. 2001. Mechanism and control of meiotic recombination initiation. *Curr Top Dev Biol*. 52:1-53.

100. Kim, K.P., B.M. Weiner, L. Zhang, A. Jordan, J. Dekker, and N. Kleckner. 2010. Sister cohesion and structural axis components mediate homolog bias of meiotic recombination. *Cell*. 143:924-937.

101. Kim, Y., S.C. Rosenberg, C.L. Kugel, N. Kostow, O. Rog, V. Davydov, T.Y. Su, A.F. Dernburg, and K.D. Corbett. 2014. The chromosome axis controls meiotic events through a hierarchical assembly of HORMA domain proteins. *Dev Cell*. 31:487-502.

102. Kim, Y., Z. Shi, H. Zhang, I.J. Finkelstein, and H. Yu. 2019. Human cohesin compacts DNA by loop extrusion. *Science*. 366:1345-1349.

103. Klein, F., P. Mahr, M. Galova, S.B. Buonomo, C. Michaelis, K. Nairz, and K. Nasmyth. 1999. A central role for cohesins in sister chromatid cohesion, formation of axial elements, and recombination during yeast meiosis. *Cell*. 98:91-103.

104. Köhler, S., M. Wojcik, K. Xu, and A.F. Dernburg. 2017. Superresolution microscopy reveals the three-dimensional organization of meiotic chromosome axes in intact *Caenorhabditis elegans* tissue. *Proceedings of the National Academy of Sciences of the United States of America*. 114:E4734-E4743.

105. Kolas, N.K., and P.E. Cohen. 2004. Novel and diverse functions of the DNA mismatch repair family in mammalian meiosis and recombination. *Cytogenet Genome Res*. 107:216-231.

106. Kong, M., E.E. Cutts, D. Pan, F. Beuron, T. Kaliyappan, C. Xue, E.P. Morris, A. Musacchio, A. Vannini, and E.C. Greene. 2020. Human Condensin I and II Drive Extensive ATP-Dependent Compaction of Nucleosome-Bound DNA. *Mol Cell*. 79:99-114 e119.

107. Krishnan, B., S.E. Thomas, R. Yan, H. Yamada, I.B. Zhulin, and B.D. McKee. 2014. Sisters unbound is required for meiotic centromeric cohesion in *Drosophila melanogaster*. *Genetics*. 198:947-965.

108. Kumar, R., C. Oliver, C. Brun, A.B. Juarez-Martinez, Y. Tarabay, J. Kadlec, and B. de Massy. 2018. Mouse REC114 is essential for meiotic DNA double-strand break formation and forms a complex with MEI4. *Life Sci Alliance*. 1:e201800259.

109. Lambing, C., K. Osman, K. Nuntasoontorn, A. West, J.D. Higgins, G.P. Copenhaver, J. Yang, S.J. Armstrong, K. Mechtler, E. Roitinger, and F.C. Franklin. 2015. *Arabidopsis* PCH2 Mediates Meiotic Chromosome Remodeling and Maturation of Crossovers. *PLoS genetics*. 11:e1005372.

110. Lander, E.S., L.M. Linton, B. Birren, C. Nusbaum, M.C. Zody, J. Baldwin, K. Devon, K. Dewar, M. Doyle, W. FitzHugh, R. Funke, D. Gage, K. Harris, A. Heaford, J. Howland, L. Kann, J. Lehoczky, R. LeVine, P. McEwan, K. McKernan, J. Meldrim, J.P. Mesirov, C. Miranda, W. Morris, J. Naylor, C. Raymond, M. Rosetti, R. Santos, A. Sheridan, C. Sougnez, Y. Stange-Thomann, N. Stojanovic, A. Subramanian, D. Wyman, J. Rogers, J. Sulston, R. Ainscough, S. Beck, D. Bentley, J. Burton, C. Clee, N. Carter, A. Coulson, R. Deadman, P. Deloukas, A. Dunham, I. Dunham, R. Durbin, L. French, D. Grafham, S. Gregory, T. Hubbard, S. Humphray, A. Hunt, M. Jones, C. Lloyd, A. McMurray, L. Matthews, S. Mercer, S. Milne, J.C. Mullikin, A. Mungall, R. Plumb, M. Ross, R. Shownkeen, S. Sims, R.H. Waterston, R.K. Wilson, L.W. Hillier, J.D. McPherson, M.A. Marra, E.R. Mardis, L.A. Fulton, A.T. Chinwalla, K.H. Pepin, W.R. Gish, S.L. Chissoe, M.C. Wendl, K.D. Delehaunty, T.L. Miner, A. Delehaunty, J.B. Kramer, L.L. Cook, R.S. Fulton, D.L. Johnson, P.J. Minx, S.W. Clifton, T. Hawkins, E. Branscomb, P. Predki, P. Richardson, S. Wenning, T. Slezak, N. Doggett, J.F. Cheng, A. Olsen, S. Lucas, C. Elkin, E. Uberbacher, M. Frazier, et al. 2001. Initial sequencing and analysis of the human genome. *Nature*. 409:860-921.

111. Lange, J., J. Pan, F. Cole, M.P. Thelen, M. Jasin, and S. Keeney. 2011. ATM controls meiotic double-strand-break formation. *Nature*. 479:237-240.

112. Lange, J., S. Yamada, S.E. Tischfield, J. Pan, S. Kim, X. Zhu, N.D. Socci, M. Jasin, and S. Keeney. 2016. The Landscape of Mouse Meiotic Double-Strand Break Formation, Processing, and Repair. *Cell*. 167:695-708 e616.

113. Lao, J.P., V. Cloud, C.C. Huang, J. Grubb, D. Thacker, C.Y. Lee, M.E. Dresser, N. Hunter, and D.K. Bishop. 2013. Meiotic crossover control by concerted action of Rad51-Dmc1 in homolog template bias and robust homeostatic regulation. *PLoS genetics*. 9:e1003978.

114. Lao, J.P., and N. Hunter. 2010. Trying to avoid your sister. *PLoS Biol*. 8:e1000519.

115. Lee, J., and T. Hirano. 2011. RAD21L, a novel cohesin subunit implicated in linking homologous chromosomes in mammalian meiosis. *J Cell Biol*. 192:263-276.

116. Lenzi, M.L., J. Smith, T. Snowden, M. Kim, R. Fishel, B.K. Poulos, and P.E. Cohen. 2005. Extreme heterogeneity in the molecular events leading to the establishment of chiasmata during meiosis i in human oocytes. *American journal of human genetics*. 76:112-127.

117. Li, J., G.W. Hooker, and G.S. Roeder. 2006. *Saccharomyces cerevisiae* Mer2, Mei4 and Rec114 form a complex required for meiotic double-strand break formation. *Genetics*. 173:1969-1981.

118. Li, Y., J.H.I. Haarhuis, A. Sedeno Cacciatore, R. Oldenkamp, M.S. van Ruiten, L. Willems, H. Teunissen, K.W. Muir, E. de Wit, B.D. Rowland, and D. Panne. 2020. The structural basis for cohesin-CTCF-anchored loops. *Nature*. 578:472-476.

119. Libuda, D.E., S. Uzawa, B.J. Meyer, and A.M. Villeneuve. 2013. Meiotic chromosome structures constrain and respond to designation of crossover sites. *Nature*. 502:703-706.

120. Lichten, M., and B. de Massy. 2011. The impressionistic landscape of meiotic recombination. *Cell*. 147:267-270.

121. Lieberman-Aiden, E., N.L. van Berkum, L. Williams, M. Imakaev, T. Ragoczy, A. Telling, I. Amit, B.R. Lajoie, P.J. Sabo, M.O. Dorschner, R. Sandstrom, B. Bernstein, M.A. Bender, M. Groudine, A. Gnirke, J. Stamatoyannopoulos, L.A. Mirny, E.S. Lander, and J. Dekker. 2009. Comprehensive mapping of long-range interactions reveals folding principles of the human genome. *Science*. 326:289-293.

122. Liu, J.G., L. Yuan, E. Brundell, B. Bjorkroth, B. Daneholt, and C. Hoog. 1996. Localization of the N-terminus of SCP1 to the central element of the synaptonemal complex and evidence for direct interactions between the N-termini of SCP1 molecules organized head-to-head. *Exp Cell Res*. 226:11-19.

123. Lorenz, A., J.L. Wells, D.W. Pryce, M. Novatchkova, F. Eisenhaber, R.J. McFarlane, and J. Loidl. 2004. *S. pombe* meiotic linear elements contain proteins related to synaptonemal complex components. *Journal of cell science*. 117:3343-3351.

124. Lu, J., Y. Gu, J. Feng, W. Zhou, X. Yang, and Y. Shen. 2014. Structural insight into the central element assembly of the synaptonemal complex. *Sci Rep*. 4:7059.

125. Luger, K., A.W. Mader, R.K. Richmond, D.F. Sargent, and T.J. Richmond. 1997. Crystal structure of the nucleosome core particle at 2.8 Å resolution. *Nature*. 389:251-260.

126. Lukaszewicz, A., J. Lange, S. Keeney, and M. Jasin. 2018. Control of meiotic double-strand-break formation by ATM: local and global views. *Cell Cycle*. 17:1155-1172.

127. Macaisne, N., M. Novatchkova, L. Peirera, D. Vezon, S. Jolivet, N. Froger, L. Chelysheva, M. Grelon, and R. Mercier. 2008. SHOC1, an XPF endonuclease-related protein, is essential for the formation of class I meiotic crossovers. *Curr Biol*. 18:1432-1437.

128. Macaisne, N., J. Vignard, and R. Mercier. 2011. SHOC1 and PTD form an XPF-ERCC1-like complex that is required for formation of class I crossovers. *Journal of cell science*. 124:2687-2691.

129. Maddox, P.S., K. Oegema, A. Desai, and I.M. Cheeseman. 2004. "Holo"er than thou: chromosome segregation and kinetochore function in *C. elegans*. *Chromosome Res*. 12:641-653.

130. Mahgoub, M., J. Paiano, M. Bruno, W. Wu, S. Pathuri, X. Zhang, S. Ralls, X. Cheng, A. Nussenzweig, and T.S. Macfarlan. 2020. Dual histone methyl reader ZCWPW1 facilitates repair of meiotic double strand breaks in male mice. *Elife*. 9:e53360.

131. Malavasic, M.J., and R.T. Elder. 1990. Complementary transcripts from two genes necessary for normal meiosis in the yeast *Saccharomyces cerevisiae*. *Molecular and cellular biology*. 10:2809-2819.

132. Manheim, E.A., and K.S. McKim. 2003. The Synaptonemal complex component C(2)M regulates meiotic crossing over in *Drosophila*. *Curr Biol*. 13:276-285.

133. Marston, A.L., and A. Amon. 2004. Meiosis: cell-cycle controls shuffle and deal. *Nat Rev Mol Cell Biol*. 5:983-997.

134. Martinez-Perez, E., M. Schvarzstein, C. Barroso, J. Lightfoot, A.F. Dernburg, and A.M. Villeneuve. 2008. Crossovers trigger a remodeling of meiotic chromosome axis composition that is linked to two-step loss of sister chromatid cohesion. *Genes & development*. 22:2886-2901.

135. McKim, K.S., and A. Hayashi-Hagihara. 1998. mei-W68 in Drosophila melanogaster encodes a Spo11 homolog: evidence that the mechanism for initiating meiotic recombination is conserved. *Genes & development*. 12:2932-2942.

136. Morgan, T.H. 1911. Random segregation versus coupling in Mendelian inheritance. *Science*. 34:384.

137. Morimoto, A., H. Shibuya, X. Zhu, J. Kim, K. Ishiguro, M. Han, and Y. Watanabe. 2012. A conserved KASH domain protein associates with telomeres, SUN1, and dynactin during mammalian meiosis. *J Cell Biol*. 198:165-172.

138. Moses, M.J. 1956. Chromosomal structures in crayfish spermatocytes. *J Biophys Biochem Cytol*. 2:215-218.

139. Muller. 1916. The mechanism of crossing-over. *American Naturalist*. 50:193-221.

140. Murakami, H., I. Lam, P.C. Huang, J. Song, M. van Overbeek, and S. Keeney. 2020. Multilayered mechanisms ensure that short chromosomes recombine in meiosis. *Nature*. 582:124-128.

141. Myers, S., R. Bowden, A. Tumian, R.E. Bontrop, C. Freeman, T.S. MacFie, G. McVean, and P. Donnelly. 2010. Drive against hotspot motifs in primates implicates the PRDM9 gene in meiotic recombination. *Science*. 327:876-879.

142. Nabeshima, K., A.M. Villeneuve, and M.P. Colaiacovo. 2005. Crossing over is coupled to late meiotic prophase bivalent differentiation through asymmetric disassembly of the SC. *J Cell Biol*. 168:683-689.

143. Nasmyth, K. 2001. Disseminating the genome: joining, resolving, and separating sister chromatids during mitosis and meiosis. *Annu Rev Genet*. 35:673-745.

144. Nasmyth, K. 2015. A meiotic mystery: How sister kinetochores avoid being pulled in opposite directions during the first division. *Bioessays*. 37:657-665.

145. Naumova, N., M. Imakaev, G. Fudenberg, Y. Zhan, B.R. Lajoie, L.A. Mirny, and J. Dekker. 2013. Organization of the mitotic chromosome. *Science*. 342:948-953.

146. Neyton, S., F. Lespinasse, P.B. Moens, R. Paul, P. Gaudray, V. Paquis-Flucklinger, and S. Santucci-Darmanin. 2004. Association between MSH4 (MutS homologue 4) and the DNA strand-exchange RAD51 and DMC1 proteins during mammalian meiosis. *Mol Hum Reprod*. 10:917-924.

147. Nguyen, H., S. Labella, N. Silva, V. Jantsch, and M. Zetka. 2018. C. elegans ZHP-4 is required at multiple distinct steps in the formation of crossovers and their transition to segregation competent chiasmata. *PLoS genetics*. 14:e1007776.

148. Niu, H., X. Li, E. Job, C. Park, D. Moazed, S.P. Gygi, and N.M. Hollingsworth. 2007. Mek1 kinase is regulated to suppress double-strand break repair between sister chromatids during budding yeast meiosis. *Molecular and cellular biology*. 27:5456-5467.

149. Niu, H., L. Wan, V. Busygina, Y. Kwon, J.A. Allen, X. Li, R.C. Kunz, K. Kubota, B. Wang, P. Sung, K.M. Shokat, S.P. Gygi, and N.M. Hollingsworth. 2009. Regulation of meiotic recombination via Mek1-mediated Rad54 phosphorylation. *Mol Cell*. 36:393-404.

150. Nora, E.P., A. Goloborodko, A.L. Valton, J.H. Gibcus, A. Uebersohn, N. Abdennur, J. Dekker, L.A. Mirny, and B.G. Bruneau. 2017. Targeted Degradation of CTCF Decouples Local Insulation of Chromosome Domains from Genomic Compartmentalization. *Cell*. 169:930-944 e922.

151. Novak, I., H. Wang, E. Revenkova, R. Jessberger, H. Scherthan, and C. Hoog. 2008. Cohesin Smc1beta determines meiotic chromatin axis loop organization. *J Cell Biol*. 180:83-90.

152. Novak, J.E., P.B. Ross-Macdonald, and G.S. Roeder. 2001. The budding yeast Msh4 protein functions in chromosome synapsis and the regulation of crossover distribution. *Genetics*. 158:1013-1025.

153. Oliver-Bonet, M., M. Campillo, P.J. Turek, E. Ko, and R.H. Martin. 2007. Analysis of replication protein A (RPA) in human spermatogenesis. *Mol Hum Reprod*. 13:837-844.

154. Otto, S.P., and B.A. Payseur. 2019. Crossover Interference: Shedding Light on the Evolution of Recombination. *Annu Rev Genet*. 53:19-44.

155. Page, S.L., and R.S. Hawley. 2001. c(3)G encodes a *Drosophila* synaptonemal complex protein. *Genes & development*. 15:3130-3143.

156. Page, S.L., and R.S. Hawley. 2004. The genetics and molecular biology of the synaptonemal complex. *Annu Rev Cell Dev Biol*. 20:525-558.

157. Pan, J., and S. Keeney. 2007. Molecular cartography: mapping the landscape of meiotic recombination. *PLoS Biol*. 5:e333.

158. Pan, J., M. Sasaki, R. Kniewel, H. Murakami, H.G. Blitzblau, S.E. Tischfield, X. Zhu, M.J. Neale, M. Jasin, N.D. Socci, A. Hochwagen, and S. Keeney. 2011. A hierarchical combination of factors shapes the genome-wide topography of yeast meiotic recombination initiation. *Cell*. 144:719-731.

159. Panizza, S., M.A. Mendoza, M. Berlinger, L. Huang, A. Nicolas, K. Shirahige, and F. Klein. 2011. Spo11-accessory proteins link double-strand break sites to the chromosome axis in early meiotic recombination. *Cell*. 146:372-383.

160. Papanikos, F., J.A.J. Clement, E. Testa, R. Ravindranathan, C. Grey, I. Dereli, A. Bondarieva, S. Valerio-Cabrera, M. Stanzione, A. Schleiffer, P. Jansa, D. Lustyk, J.F. Fei, I.R. Adams, J. Forejt, M. Barchi, B. de Massy, and A. Toth. 2019. Mouse ANKRD31 Regulates Spatiotemporal Patterning of Meiotic Recombination Initiation and Ensures Recombination between X and Y Sex Chromosomes. *Mol Cell*. 74:1069-1085 e1011.

161. Parvanov, E.D., P.M. Petkov, and K. Paigen. 2010. Prdm9 controls activation of mammalian recombination hotspots. *Science*. 327:835.

162. Pasierbek, P., M. Jantsch, M. Melcher, A. Schleiffer, D. Schweizer, and J. Loidl. 2001. A *Caenorhabditis elegans* cohesion protein with functions in meiotic chromosome pairing and disjunction. *Genes & development*. 15:1349-1360.

163. Patel, L., R. Kang, S.C. Rosenberg, Y. Qiu, R. Raviram, S. Chee, R. Hu, B. Ren, F. Cole, and K.D. Corbett. 2019. Dynamic reorganization of the genome shapes the recombination landscape in meiotic prophase. *Nat Struct Mol Biol*. 26:164-174.

164. Penedos, A., A.L. Johnson, E. Strong, A.S. Goldman, J.A. Carballo, and R.S. Cha. 2015. Essential and Checkpoint Functions of Budding Yeast ATM and ATR during Meiotic Prophase Are Facilitated by Differential Phosphorylation of a Meiotic Adaptor Protein, Hop1. *PloS one*. 10:e0134297.

165. Perry, J., N. Kleckner, and G.V. Borner. 2005. Bioinformatic analyses implicate the collaborating meiotic crossover/chiasma proteins Zip2, Zip3, and Spo22/Zip4 in ubiquitin labeling. *Proceedings of the National Academy of Sciences of the United States of America*. 102:17594-17599.

166. Phillips, C.M., and A.F. Dernburg. 2006. A family of zinc-finger proteins is required for chromosome-specific pairing and synapsis during meiosis in *C. elegans*. *Dev Cell*. 11:817-829.

167. Phillips, C.M., X. Meng, L. Zhang, J.H. Chretien, F.D. Urnov, and A.F. Dernburg. 2009. Identification of chromosome sequence motifs that mediate meiotic pairing and synapsis in *C. elegans*. *Nat Cell Biol*. 11:934-942.

168. Phillips, C.M., C. Wong, N. Bhalla, P.M. Carlton, P. Weiser, P.M. Meneely, and A.F. Dernburg. 2005. HIM-8 binds to the X chromosome pairing center and mediates chromosome-specific meiotic synapsis. *Cell*. 123:1051-1063.

169. Prakash, K., D. Fournier, S. Redl, G. Best, M. Borsos, V.K. Tiwari, K. Tachibana-Konwalski, R.F. Ketting, S.H. Parekh, C. Cremer, and U.J. Birk. 2015. Superresolution imaging reveals structurally distinct periodic patterns of chromatin along pachytene chromosomes. *Proceedings of the National Academy of Sciences of the United States of America*. 112:14635-14640.

170. Prieto, I., J.A. Suja, N. Pezzi, L. Kremer, A.C. Martinez, J.S. Rufas, and J.L. Barbero. 2001. Mammalian STAG3 is a cohesin specific to sister chromatid arms in meiosis I. *Nat Cell Biol*. 3:761-766.

171. Prugar, E., C. Burnett, X. Chen, and N.M. Hollingsworth. 2017. Coordination of Double Strand Break Repair and Meiotic Progression in Yeast by a Mek1-Ndt80 Negative Feedback Loop. *Genetics*. 206:497-512.

172. Pyatnitskaya, A., V. Borde, and A. De Muyt. 2019. Crossing and zipping: molecular duties of the ZMM proteins in meiosis. *Chromosoma*. 128:181-198.

173. Rando, O.J. 2012. Combinatorial complexity in chromatin structure and function: revisiting the histone code. *Curr Opin Genet Dev*. 22:148-155.

174. Rao, H.B., H. Qiao, S.K. Bhatt, L.R. Bailey, H.D. Tran, S.L. Bourne, W. Qiu, A. Deshpande, A.N. Sharma, C.J. Beebout, R.J. Pezza, and N. Hunter. 2017a. A SUMO-ubiquitin relay recruits proteasomes to chromosome axes to regulate meiotic recombination. *Science*. 355:403-407.

175. Rao, S.S., M.H. Huntley, N.C. Durand, E.K. Stamenova, I.D. Bochkov, J.T. Robinson, A.L. Sanborn, I. Machol, A.D. Omer, E.S. Lander, and E.L. Aiden. 2014. A 3D map of the human genome at kilobase resolution reveals principles of chromatin looping. *Cell*. 159:1665-1680.

176. Rao, S.S.P., S.C. Huang, B. Glenn St Hilaire, J.M. Engreitz, E.M. Perez, K.R. Kieffer-Kwon, A.L. Sanborn, S.E. Johnstone, G.D. Bascom, I.D. Bochkov, X. Huang, M.S. Shamim, J. Shin, D. Turner, Z. Ye, A.D. Omer, J.T. Robinson, T. Schlick, B.E. Bernstein, R. Casellas, E.S. Lander, and E.L. Aiden. 2017b. Cohesin Loss Eliminates All Loop Domains. *Cell*. 171:305-320 e324.

177. Revenkova, E., M. Eijpe, C. Heyting, B. Gross, and R. Jessberger. 2001. Novel meiosis-specific isoform of mammalian SMC1. *Molecular and cellular biology*. 21:6984-6998.

178. Revenkova, E., M. Eijpe, C. Heyting, C.A. Hodges, P.A. Hunt, B. Liebe, H. Scherthan, and R. Jessberger. 2004. Cohesin SMC1 beta is required for meiotic chromosome dynamics, sister chromatid cohesion and DNA recombination. *Nat Cell Biol*. 6:555-562.

179. Rockmill, B., and G.S. Roeder. 1990. Meiosis in asynaptic yeast. *Genetics*. 126:563-574.

180. Rockmill, B., M. Sym, H. Scherthan, and G.S. Roeder. 1995. Roles for two RecA homologs in promoting meiotic chromosome synapsis. *Genes & development*. 9:2684-2695.

181. Rog, O., and A.F. Dernburg. 2015. Direct Visualization Reveals Kinetics of Meiotic Chromosome Synapsis. *Cell Rep*. 10:1639-1645.

182. Rog, O., S. Köhler, and A.F. Dernburg. 2017. The synaptonemal complex has liquid crystalline properties and spatially regulates meiotic recombination factors. *Elife*. 6:e21455.

183. Roig, I., J.A. Dowdle, A. Toth, D.G. de Rooij, M. Jasin, and S. Keeney. 2010. Mouse TRIP13/PCH2 is required for recombination and normal higher-order chromosome structure during meiosis. *PLoS genetics*. 6:e1001062.

184. Rosenberg, S.C., and K.D. Corbett. 2015. The multifaceted roles of the HORMA domain in cellular signaling. *J Cell Biol*. 211:745-755.

185. Rousova, D.F., S. K.; Reichle, H.; Weir, J. R. 2020. Mer2 binds directly to both nucleosomes and axial proteins as the keystone of meiotic recombination. *bioRxiv*:10.1101/2020.1107.1130.228908.

186. San-Segundo, P.A., and G.S. Roeder. 1999. Pch2 links chromatin silencing to meiotic checkpoint control. *Cell*. 97:313-324.

187. Sanchez, R., and M.M. Zhou. 2011. The PHD finger: a versatile epigenome reader. *Trends Biochem Sci*. 36:364-372.

188. Sanchez-Saez, F., H.L. Gomez, O.M. Dunne, C. Gallego-Paramo, N. Felipe-Medina, M. Sanchez-Martin, E. Llano, A.M. Pendas, and O.R. Davies. 2020. Meiotic chromosome synapsis depends on multivalent SYCE1-SIX6OS1 interactions that are disrupted in cases of human infertility. *Sci Adv*. 6:eabb1660.

189. Santucci-Darmanin, S., D. Walpita, F. Lespinasse, C. Desnuelle, T. Ashley, and V. Paquis-Flucklinger. 2000. MSH4 acts in conjunction with MLH1 during mammalian meiosis. *FASEB J*. 14:1539-1547.

190. Sarangapani, K.K., E. Duro, Y. Deng, L. Alves Fde, Q. Ye, K.N. Opoku, S. Ceto, J. Rappsilber, K.D. Corbett, S. Biggins, A.L. Marston, and C.L. Asbury. 2014. Sister kinetochores are mechanically fused during meiosis I in yeast. *Science*. 346:248-251.

191. Sato, A., B. Isaac, C.M. Phillips, R. Rillo, P.M. Carlton, D.J. Wynne, R.A. Kasad, and A.F. Dernburg. 2009. Cytoskeletal forces span the nuclear envelope to coordinate meiotic chromosome pairing and synapsis. *Cell*. 139:907-919.

192. Schalbetter, S.A., G. Fudenberg, J. Baxter, K.S. Pollard, and M.J. Neale. 2019. Principles of meiotic chromosome assembly revealed in *S. cerevisiae*. *Nat Commun*. 10:4795.

193. Schild-Prufert, K., T.T. Saito, S. Smolikov, Y. Gu, M. Hincapie, D.E. Hill, M. Vidal, K. McDonald, and M.P. Colaiacovo. 2011. Organization of the synaptonemal complex during meiosis in *Caenorhabditis elegans*. *Genetics*. 189:411-421.

194. Schmekel, K., R.L. Meuwissen, A.J. Dietrich, A.C. Vink, J. van Marle, H. van Veen, and C. Heyting. 1996. Organization of SCP1 protein molecules within synaptonemal complexes of the rat. *Exp Cell Res*. 226:20-30.

195. Schramm, S., J. Fraune, R. Naumann, A. Hernandez-Hernandez, C. Hoog, H.J. Cooke, M. Alsheimer, and R. Benavente. 2011. A novel mouse synaptonemal complex protein is essential for loading of central element proteins, recombination, and fertility. *PLoS genetics*. 7:e1002088.

196. Severson, A.F., L. Ling, V. van Zuylen, and B.J. Meyer. 2009. The axial element protein HTP-3 promotes cohesin loading and meiotic axis assembly in *C. elegans* to implement the meiotic program of chromosome segregation. *Genes & development*. 23:1763-1778.

197. Shen, Y., D. Tang, K. Wang, M. Wang, J. Huang, W. Luo, Q. Luo, L. Hong, M. Li, and Z. Cheng. 2012. ZIP4 in homologous chromosome synapsis and crossover formation in rice meiosis. *Journal of cell science*. 125:2581-2591.

198. Shi, Z., H. Gao, X.C. Bai, and H. Yu. 2020. Cryo-EM structure of the human cohesin-NIPBL-DNA complex. *Science*. 368:1454-1459.

199. Shin, Y.H., Y. Choi, S.U. Erdin, S.A. Yatsenko, M. Kloc, F. Yang, P.J. Wang, M.L. Meistrich, and A. Rajkovic. 2010. Hormad1 mutation disrupts synaptonemal complex formation, recombination, and chromosome segregation in mammalian meiosis. *PLoS genetics*. 6:e1001190.

200. Shinohara, M., S.D. Oh, N. Hunter, and A. Shinohara. 2008. Crossover assurance and crossover interference are distinctly regulated by the ZMM proteins during yeast meiosis. *Nature genetics*. 40:299-309.

201. Simonis, M., P. Klous, E. Splinter, Y. Moshkin, R. Willemsen, E. de Wit, B. van Steensel, and W. de Laat. 2006. Nuclear organization of active and inactive chromatin domains uncovered by chromosome conformation capture-on-chip (4C). *Nature genetics*. 38:1348-1354.

202. Skibbens, R.V., L.B. Corson, D. Koshland, and P. Hieter. 1999. Ctf7p is essential for sister chromatid cohesion and links mitotic chromosome structure to the DNA replication machinery. *Genes & development*. 13:307-319.

203. Smith, A.V., and G.S. Roeder. 1997. The yeast Red1 protein localizes to the cores of meiotic chromosomes. *J Cell Biol*. 136:957-967.

204. Snowden, T., S. Acharya, C. Butz, M. Berardini, and R. Fishel. 2004. hMSH4-hMSH5 recognizes Holliday Junctions and forms a meiosis-specific sliding clamp that embraces homologous chromosomes. *Mol Cell*. 15:437-451.

205. Snowden, T., K.S. Shim, C. Schmutte, S. Acharya, and R. Fishel. 2008. hMSH4-hMSH5 adenosine nucleotide processing and interactions with homologous recombination machinery. *The Journal of biological chemistry*. 283:145-154.

206. Sommermeyer, V., C. Beneut, E. Chaplais, M.E. Serrentino, and V. Borde. 2013. Spp1, a member of the Set1 Complex, promotes meiotic DSB formation in promoters by tethering histone H3K4 methylation sites to chromosome axes. *Mol Cell*. 49:43-54.

207. Spindler, M.C., S. Filbeck, C. Stigloher, and R. Benavente. 2019. Quantitative basis of meiotic chromosome synapsis analyzed by electron tomography. *Sci Rep*. 9:16102.

208. Stanzione, M., M. Baumann, F. Papanikos, I. Dereli, J. Lange, A. Ramlal, D. Trankner, H. Shibuya, B. de Massy, Y. Watanabe, M. Jasin, S. Keeney, and A. Toth. 2016. Meiotic DNA break formation requires the unsynapsed chromosome axis-binding protein IHO1 (CCDC36) in mice. *Nat Cell Biol*. 18:1208-1220.

209. Strahl, B.D., and C.D. Allis. 2000. The language of covalent histone modifications. *Nature*. 403:41-45.

210. Sturtevant, A.H. 1913. The linear arrangement of six sex-linked factors in *Drosophila*, as shown by their mode of association. *Journal of Experimental Zoology*. 14:43-59.

211. Subramanian, V.V., and A. Hochwagen. 2014. The meiotic checkpoint network: step-by-step through meiotic prophase. *Cold Spring Harb Perspect Biol*. 6:a016675.

212. Subramanian, V.V., A.J. MacQueen, G. Vader, M. Shinohara, A. Sanchez, V. Borde, A. Shinohara, and A. Hochwagen. 2016. Chromosome Synapsis Alleviates Mek1-Dependent Suppression of Meiotic DNA Repair. *PLoS Biol*. 14:e1002369.

213. Suhandynata, R., J. Liang, C.P. Albuquerque, H. Zhou, and N.M. Hollingsworth. 2014. A method for sporulating budding yeast cells that allows for unbiased identification of kinase substrates using stable isotope labeling by amino acids in cell culture. *G3 (Bethesda)*. 4:2125-2135.

214. Sun, X., L. Huang, T.E. Markowitz, H.G. Blitzblau, D. Chen, F. Klein, and A. Hochwagen. 2015. Transcription dynamically patterns the meiotic chromosome-axis interface. *Elife*. 4:e07424.

215. Sym, M., J.A. Engebrecht, and G.S. Roeder. 1993. ZIP1 is a synaptonemal complex protein required for meiotic chromosome synapsis. *Cell*. 72:365-378.

216. Syrjanen, J.L., L. Pellegrini, and O.R. Davies. 2014. A molecular model for the role of SYCP3 in meiotic chromosome organisation. *Elife*. 3:e02963.

217. Terakawa, T., S. Bisht, J.M. Eeftens, C. Dekker, C.H. Haering, and E.C. Greene. 2017. The condensin complex is a mechanochemical motor that translocates along DNA. *Science*. 358:672-676.

218. Toth, A., R. Ciosk, F. Uhlmann, M. Galova, A. Schleiffer, and K. Nasmyth. 1999. Yeast cohesin complex requires a conserved protein, Eco1p(Ctf7), to establish cohesion between sister chromatids during DNA replication. *Genes & development*. 13:320-333.

219. Tromer, E.C., J.J.E. van Hooff, G. Kops, and B. Snel. 2019. Mosaic origin of the eukaryotic kinetochore. *Proceedings of the National Academy of Sciences of the United States of America*. 116:12873-12882.

220. Tromer, E.C., T.A. Wemyss, R.F. Waller, and B. Akiyoshi. 2021. Repurposing of Synaptonemal Complex Proteins for Kinetochores in Kinetoplastida. *bioRxiv*:10.1101/2021.1102.1106.430040.

221. Tsai, B., W. Liu, D. Dong, K. Shi, L. Chen, and N. Gao. 2020. Phase separation of Mer2 organizes the meiotic loop-axis structure during meiosis I. *bioRxiv*:10.1101/2020.1112.1115.422856.

222. Tsubouchi, T., H. Zhao, and G.S. Roeder. 2006. The meiosis-specific zip4 protein regulates crossover distribution by promoting synaptonemal complex formation together with zip2. *Dev Cell*. 10:809-819.

223. Tung, K.S., E.J. Hong, and G.S. Roeder. 2000. The pachytene checkpoint prevents accumulation and phosphorylation of the meiosis-specific transcription factor Ndt80. *Proceedings of the National Academy of Sciences of the United States of America*. 97:12187-12192.

224. Ur, S., C. Milano, A. Hochwagen, and K.D. Corbett. 2021. A central domain of *S. cerevisiae* Hop1 mediates Rec8-independent meiotic chromosome axis assembly. *bioRxiv*.

225. van Heemst, D., and C. Heyting. 2000. Sister chromatid cohesion and recombination in meiosis. *Chromosoma*. 109:10-26.

226. Vara, C., A. Paytuvi-Gallart, Y. Cuartero, F. Le Dily, F. Garcia, J. Salva-Castro, H.L. Gomez, E. Julia, C. Moutinho, R. Aiese Cigliano, W. Sanseverino, O. Fornas, A.M. Pendas, H. Heyn, P.D. Waters, M.A. Marti-Renom, and A. Ruiz-Herrera. 2019. Three-Dimensional Genomic Structure and Cohesin Occupancy Correlate with Transcriptional Activity during Spermatogenesis. *Cell Rep*. 28:352-367 e359.

227. Voelkel-Meiman, K., S.S. Moustafa, P. Lefrancois, A.M. Villeneuve, and A.J. MacQueen. 2012. Full-length synaptonemal complex grows continuously during meiotic prophase in budding yeast. *PLoS genetics*. 8:e1002993.

228. Voelkel-Meiman, K., L.F. Taylor, P. Mukherjee, N. Humphryes, H. Tsubouchi, and A.J. Macqueen. 2013. SUMO localizes to the central element of synaptonemal complex and is required for the full synapsis of meiotic chromosomes in budding yeast. *PLoS genetics*. 9:e1003837.

229. Wan, L., T. de los Santos, C. Zhang, K. Shokat, and N.M. Hollingsworth. 2004. Mek1 kinase activity functions downstream of RED1 in the regulation of meiotic double strand break repair in budding yeast. *Mol Biol Cell*. 15:11-23.

230. Watts, F.Z., and E. Hoffmann. 2011. SUMO meets meiosis: an encounter at the synaptonemal complex: SUMO chains and sumoylated proteins suggest that heterogeneous and complex interactions lie at the centre of the synaptonemal complex. *Bioessays*. 33:529-537.

231. Webber, H.A., L. Howard, and S.E. Bickel. 2004. The cohesion protein ORD is required for homologue bias during meiotic recombination. *J Cell Biol*. 164:819-829.

232. Wells, D., E. Bitoun, D. Moralli, G. Zhang, A. Hinch, J. Jankowska, P. Donnelly, C. Green, and S.R. Myers. 2020. ZCWPW1 is recruited to recombination hotspots by PRDM9 and is essential for meiotic double strand break repair. *Elife*. 9:e53392.

233. West, A.M., S.C. Rosenberg, S.N. Ur, M.K. Lehmer, Q. Ye, G. Hagemann, I. Caballero, I. Uson, A.J. MacQueen, F. Herzog, and K.D. Corbett. 2019. A conserved filamentous assembly underlies the structure of the meiotic chromosome axis. *Elife*. 8:e40372.

234. West, A.M.V., E.A. Komives, and K.D. Corbett. 2018. Conformational dynamics of the Hop1 HORMA domain reveal a common mechanism with the spindle checkpoint protein Mad2. *Nucleic Acids Res*. 46:279-292.

235. Wijeratne, A.J., C. Chen, W. Zhang, L. Timofejeva, and H. Ma. 2006. The *Arabidopsis thaliana* PARTING DANCERS gene encoding a novel protein is required for normal meiotic homologous recombination. *Mol Biol Cell*. 17:1331-1343.

236. Winters, T., F. McNicoll, and R. Jessberger. 2014. Meiotic cohesin STAG3 is required for chromosome axis formation and sister chromatid cohesion. *The EMBO journal*. 33:1256-1270.

237. Woglar, A., K. Yamaya, B. Roelens, A. Boettiger, S. Kohler, and A.M. Villeneuve. 2020. Quantitative cytogenetics reveals molecular stoichiometry and longitudinal organization of meiotic chromosome axes and loops. *PLoS Biol*. 18:e3000817.

238. Wojtasz, L., K. Daniel, I. Roig, E. Bolcun-Filas, H. Xu, V. Boonsanay, C.R. Eckmann, H.J. Cooke, M. Jasin, S. Keeney, M.J. McKay, and A. Toth. 2009. Mouse HORMAD1 and HORMAD2, two conserved meiotic chromosomal proteins, are depleted from synapsed chromosome axes with the help of TRIP13 AAA-ATPase. *PLoS genetics*. 5:e1000702.

239. Woltering, D., B. Baumgartner, S. Bagchi, B. Larkin, J. Loidl, T. de los Santos, and N.M. Hollingsworth. 2000. Meiotic segregation, synapsis, and recombination checkpoint

functions require physical interaction between the chromosomal proteins Red1p and Hop1p. *Molecular and cellular biology*. 20:6646-6658.

240. Xie, C., C. He, Y. Jiang, H. Yu, L. Cheng, G. Nshogoza, M.S. Ala, C. Tian, J. Wu, Y. Shi, and F. Li. 2018. Structural insights into the recognition of phosphorylated Hop1 by Mek1. *Acta Crystallogr D Struct Biol*. 74:1027-1038.

241. Xu, H., Z. Tong, Q. Ye, T. Sun, Z. Hong, L. Zhang, A. Bortnick, S. Cho, P. Beuzer, J. Axelrod, Q. Hu, M. Wang, S.M. Evans, C. Murre, L.F. Lu, S. Sun, K.D. Corbett, and H. Cang. 2019. Molecular organization of mammalian meiotic chromosome axis revealed by expansion STORM microscopy. *Proceedings of the National Academy of Sciences of the United States of America*. 116:18423-18428.

242. Xu, L., M. Ajimura, R. Padmore, C. Klein, and N. Kleckner. 1995. NDT80, a meiosis-specific gene required for exit from pachytene in Saccharomyces cerevisiae. *Molecular and cellular biology*. 15:6572-6581.

243. Yan, R., and B.D. McKee. 2013. The cohesion protein SOLO associates with SMC1 and is required for synapsis, recombination, homolog bias and cohesion and pairing of centromeres in *Drosophila* meiosis. *PLoS genetics*. 9:e1003637.

244. Yang, C., B. Hu, S.M. Portheine, P. Chuenban, and A. Schnittger. 2020. State changes of the HORMA protein ASY1 are mediated by an interplay between its closure motif and PCH2. *Nucleic Acids Res*. 48:11521-11535.

245. Yang, F., R. De La Fuente, N.A. Leu, C. Baumann, K.J. McLaughlin, and P.J. Wang. 2006. Mouse SYCP2 is required for synaptonemal complex assembly and chromosomal synapsis during male meiosis. *J Cell Biol*. 173:497-507.

246. Yatskevich, S., J. Rhodes, and K. Nasmyth. 2019. Organization of Chromosomal DNA by SMC Complexes. *Annu Rev Genet*. 53:445-482.

247. Ye, Q., D.H. Kim, I. Dereli, S.C. Rosenberg, G. Hagemann, F. Herzog, A. Toth, D.W. Cleveland, and K.D. Corbett. 2017. The AAA+ ATPase TRIP13 remodels HORMA domains through N-terminal engagement and unfolding. *The EMBO journal*. 36:2419-2434.

248. Ye, Q., S.C. Rosenberg, A. Moeller, J.A. Speir, T.Y. Su, and K.D. Corbett. 2015. TRIP13 is a protein-remodeling AAA+ ATPase that catalyzes MAD2 conformation switching. *Elife*. 4:e07367.

249. Yu, Y., ; Li, S.; Ser, Z.; Sanyal, T.; Choi, K.; Wan, B.; Sali, A.; Kentsis, A.; Patel, D. J.; Zhao, X. 2021. Integrative analysis reveals unique features of the Smc5/6 complex. *bioRxiv*:10.1101/2020.1112.1131.424863.

250. Yuan, L., J.G. Liu, M.R. Hoja, J. Wilbertz, K. Nordqvist, and C. Hoog. 2002. Female germ cell aneuploidy and embryo death in mice lacking the meiosis-specific protein SCP3. *Science*. 296:1115-1118.

251. Yuan, L., J.G. Liu, J. Zhao, E. Brundell, B. Daneholt, and C. Hoog. 2000. The murine SCP3 gene is required for synaptonemal complex assembly, chromosome synapsis, and male fertility. *Mol Cell*. 5:73-83.

252. Zhang, L., K.P. Kim, N.E. Kleckner, and A. Storlazzi. 2011. Meiotic double-strand breaks occur once per pair of (sister) chromatids and, via Mec1/ATR and Tel1/ATM, once per quartet of chromatids. *Proceedings of the National Academy of Sciences of the United States of America*. 108:20036-20041.

253. Zhang, L., S. Kohler, R. Rillo-Bohn, and A.F. Dernburg. 2018a. A compartmentalized signaling network mediates crossover control in meiosis. *Elife*. 7:e30789.

254. Zhang, Q., S.Y. Ji, K. Busayavalasa, and C. Yu. 2019. SPO16 binds SHOC1 to promote homologous recombination and crossing-over in meiotic prophase I. *Sci Adv*. 5:eaau9780.

255. Zhang, Q., J. Shao, H.Y. Fan, and C. Yu. 2018b. Evolutionarily-conserved MZIP2 is essential for crossover formation in mammalian meiosis. *Commun Biol*. 1:147.

256. Zhang, Z., S. Xie, R. Wang, S. Guo, Q. Zhao, H. Nie, Y. Liu, F. Zhang, M. Chen, L. Liu, X. Meng, M. Liu, L. Zhao, M.P. Colaiacovo, J. Zhou, and J. Gao. 2020. Multivalent weak interactions between assembly units drive synaptonemal complex formation. *J Cell Biol*. 219:e201910086.

257. Zickler, D., and N. Kleckner. 1999. Meiotic chromosomes: integrating structure and function. *Annu Rev Genet*. 33:603-754.

258. Zickler, D., and N. Kleckner. 2015. Recombination, Pairing, and Synapsis of Homologs during Meiosis. *Cold Spring Harb Perspect Biol*. 7:a016626.

259. Zickler, D., and N. Kleckner. 2016. A few of our favorite things: Pairing, the bouquet, crossover interference and evolution of meiosis. *Semin Cell Dev Biol*. 54:135-148.

260. Zickler, D., P.J. Moreau, A.D. Huynh, and A.M. Slezec. 1992. Correlation between pairing initiation sites, recombination nodules and meiotic recombination in *Sordaria macrospora*. *Genetics*. 132:135-148.

261. Zwettler, F.U., M.C. Spindler, S. Reinhard, T. Klein, A. Kurz, R. Benavente, and M. Sauer. 2020. Tracking down the molecular architecture of the synaptonemal complex by expansion microscopy. *Nat Commun*. 11:3222.